www.coinweb.no

SINTEF Building and Infrastructure

Sindre Sandbakk, Terje Kanstad (NTNU), Øyvind Bjøntegaard (NPRA), Lucie Vandewalle (KUL) and Benoit Parmentier (BBRI)

International Round Robin Testing of Circular FRC slabs

Reporting and Evaluation of Test Results from Norway and Belgium

COIN Project report 23 - 2010

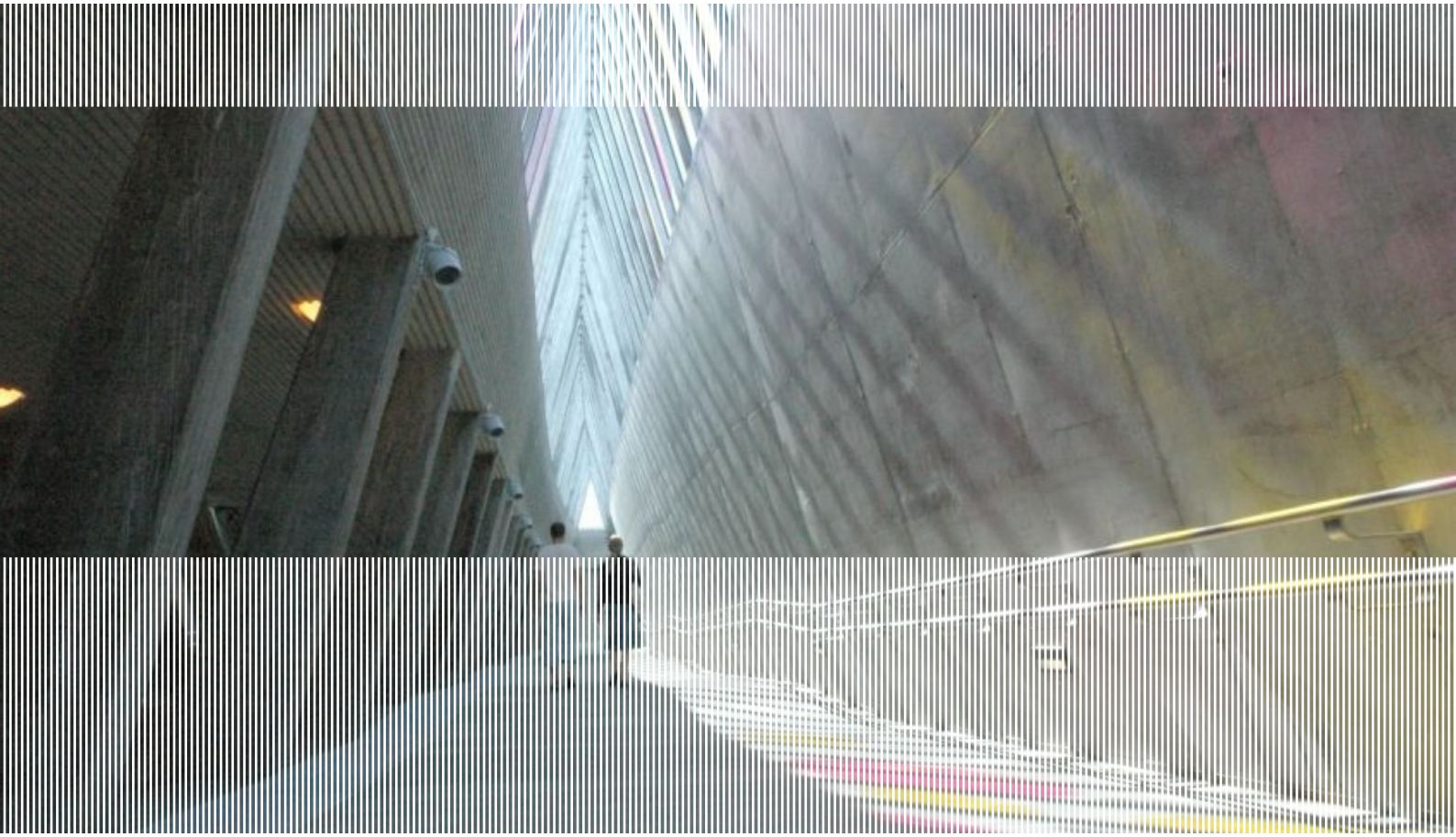

SINTEF

SINTEF Building and Infrastructure

Sindre Sandbakk, Terje Kanstad (NTNU), Øyvind Bjøntegaard (NPRA),
Lucie Vandewalle (KUL) and Benoit Parmentier (BBRI)

International Round Robin Testing of Circular FRC slabs

Reporting and Evaluation of Test Results from Norway and Belgium

FA 2.2 High tensile strength allround concrete

SP 2.2.4 Test methods

COIN Project report 23 – 2010

COIN Project report no 23
Sindre Sandbakk, Terje Kanstad (NTNU), Øyvind Bjøntegaard (NPRA), Lucie Vandewalle (KUL)
and Benoit Parmentier (BBRI)
International Round Robin Testing of Circular FRC slabs
Reporting and Evaluation of Test Results from Norway and Belgium
FA 2.2 High tensile strength allround concrete
SP 2.2.4 Test methods

Keywords:
Fibre, test methods

Project no.: 3D005920

Photo, cover: Sinsen underground station, Oslo. Vetle Houg

ISSN 1891–1978 (online)
ISBN 978-82-536-1172-3 (pdf)
ISBN 978-82-536-1173-0 (printed)

17 copies printed by AIT Oslo
Content: 100 g Scandia
Cover: 240 g Trucard

Address: Forskningsveien 3 B
POBox 124 Blindern
N-0314 OSLO
Tel: +47 22 96 55 55
Fax: +47 22 69 94 38 and 22 96 55 08

www.sintef.no/byggforsk
www.coinweb.no

Cooperation partners / Consortium Concrete Innovation Centre (COIN)

Aker Solutions
Contact: Jan-Diederik Advocaat
Email: jan-diederik.advocaat@akersolutions.com
Tel: +47 67595050

Saint Gobain Weber
Contact: Geir Norden
Email: geir.norden@saint-gobain.com
Tel: +47 22887700

Norcem AS
Contact: Terje Rønning
Email: terje.ronning@norcem.no
Tel: +47 35572000

NTNU
Contact: Terje Kanstad
Email: terje.kanstad@ntnu.no
Tel: +47 73594700

Rescon Mapei AS
Contact: Trond Hagerud
Email: trond.hagerud@resconmapei.no
Tel: +47 69972000

SINTEF Building and Infrastructure
Contact: Tor Arne Hammer
Email: tor.hammer@sintef.no
Tel: +47 73596856

Skanska Norge AS
Contact: Sverre Smeplass
Email: sverre.smeplass@skanska.no
Tel: +47 40013660

Spenncon AS
Contact: Ingrid Dahl Hovland
Email: ingrid.dahl.hovland@spenncon.no
Tel: +47 67573900

Norwegian Public Roads Administration
Contact: Kjersti K. Dunham
Email: kjersti.kvalheim.dunham@vegvesen.no
Tel: +47 22073940

Unicon AS
Contact: Stein Tosterud
Email: stto@unicon.no
Tel: +47 22309035

Veidekke Entreprenør ASA
Contact: Christine Hauck
Email: christine.hauck@veidekke.no
Tel: +47 21055000

Preface

This study has been carried out within COIN - Concrete Innovation Centre - one of presently 14 Centres for Research based Innovation (CRI), which is an initiative by the Research Council of Norway. The main objective for the CRIs is to enhance the capability of the business sector to innovate by focusing on long-term research based on forging close alliances between research-intensive enterprises and prominent research groups.

The vision of COIN is creation of more attractive concrete buildings and constructions. Attractiveness implies aesthetics, functionality, sustainability, energy efficiency, indoor climate, industrialized construction, improved work environment, and cost efficiency during the whole service life. The primary goal is to fulfil this vision by bringing the development a major leap forward by more fundamental understanding of the mechanisms in order to develop advanced materials, efficient construction techniques and new design concepts combined with more environmentally friendly material production.

The corporate partners are leading multinational companies in the cement and building industry and the aim of COIN is to increase their value creation and strengthen their research activities in Norway. Our over-all ambition is to establish COIN as the display window for concrete innovation in Europe.

About 25 researchers from SINTEF (host), the Norwegian University of Science and Technology - NTNU (research partner) and industry partners, 15 - 20 PhD-students, 5 - 10 MSc-students every year and a number of international guest researchers, work on presently eight projects in three focus areas:

- Environmentally friendly concrete
- Economically competitive construction
- Aesthetic and technical performance

COIN has presently a budget of NOK 200 mill over 8 years (from 2007), and is financed by the Research Council of Norway (approx. 40 %), industrial partners (approx 45 %) and by SINTEF Building and Infrastructure and NTNU (in all approx 15 %).

For more information, see www.coinweb.no

Tor Arne Hammer
Centre Manager

Summary

Background
A round robin test program to evaluate whether the ASTM-procedure are able to produce consistent results for nominally identical panels tested at different laboratories with different measuring systems has been carried out. The tests are performed at four different laboratories.

The four laboratories are:

- Catholic University of Leuven (KUL)
- Belgian Building Research Institute (BBRI)
- Norwegian University of Science and Technology (NTNU) together with SINTEF Building and Infrastructure
- Norwegian Public Roads Administration (NPRA)

In total 96 round concrete panels are tested according to ASTM C 1550. The test program consists of 6 different concretes, involving steel fibre reinforced concrete, synthetic fibre reinforced concrete and concrete without fibres. Details of the fibres and fibre dosages are as follows:

- Blanco concrete without fibres
- Synthetic fibre reinforced concrete with fibre content equal to 4,5 kg/m^3
- Synthetic fibre reinforced concrete with fibre content equal to 9 kg/m^3
- Metallic fibre reinforced concrete with fibre content equal to 20 kg/m^3
- Metallic fibre reinforced concrete with fibre content equal to 40 kg/m^3
- Metallic fibre reinforced concrete with fibre content equal to 60 kg/m^3

From every series, four panels were tested at each laboratory. To avoid variation in results due to differences in calculation method, the results from every laboratory are calculated by the same person. All calculations are done at NTNU/SINTEF.

Calculation
In general, the calculations are performed according to the description in ASTM C 1550, which means to calculate the absorbed energy up to 40mm of deflection. In addition, the absorbed energy up to a deflection of 5mm, 10mm and 20mm is calculated. At BBRI and KUL, there were mounted LVDT's to measure not only the deflection but also the crack opening. Another subject that is investigated is the maximum load, and the corresponding deflection.

In general, there will always be differences in the results when tests are performed at different laboratories. And further, it will always be differences in the results when test are performed several times at one lab as well. To investigate whether these differences are real, or just an expected variation, statistical calculation may be performed. In this test program, a statistical calculation based on a two sample Welch t-test is performed to compare the results from one laboratory with the results from another laboratory. This means that all laboratories are compared with each other. In the statistical calculation, the $\alpha/2$ is set to be 0.025, which means that the results from the statistical calculation are at the 95% significance level.

Main findings
Even though the energy absorption seems to be dependent on where the panels are tested, the statistical calculation shows that all panels with identical fibre content may be considered to be within one series. This means that the ASTM-procedure in fact is able to produce consistent results for nominally identical panels tested at different laboratories with different measuring systems.

Regarding maximum load and corresponding deflection, it seems like both are dependent on the fibre type and the fibre dosage. Furthermore, it seems like the different laboratories do not necessarily gives equal results. This subject is not properly discussed because it is not within the scope of this report.

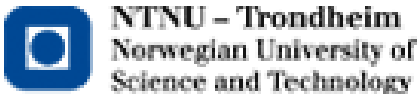

Table of contents

1 Introduction

This report summarizes the results from a round robin test program carried out by Catholic University of Leuven (KUL), Belgian Building Research Institute (BBRI), Norwegian University of Science and Technology (NTNU) (in collaboration with SINTEF Building and Infrastructure[1]) and Norwegian Public Roads Administration (NPRA). The test program involves testing of round panels (with diameter 800 mm and thickness 75 mm) made of fibre reinforced concrete. All panels have been tested according to ASTM C 1550 [ASTM C 1550].

The test program consists of 6 different concretes, involving steel fibre reinforced concrete, synthetic fibre reinforced concrete and concrete without fibres. Details of the fibres and fibre dosages are as follows:

- 0 kg/m^3. Blanco concrete, marked with B
- 4,5 kg/m^3 synthetic fibre, marked with SF4,5
- 9 kg/m^3 synthetic fibre, marked with SF9
- 20 kg/m^3 metallic fibre, marked with MF20
- 40 kg/m^3 metallic fibre, marked with MF40
- 60 kg/m^3 metallic fibre, marked with MF60

For every concrete type 16 panels were cast, and 4 panels of each concrete type were distributed to the laboratories:

1. Catholic University of Leuven (KUL), marked with KUL
2. Belgian Building Research Institute (BBRI), marked with BBRI
3. Norwegian University of Science and Technology (NTNU) together with SINTEF Building and Infrastructure, marked with NTNU
4. Norwegian Public Roads Administration (NPRA), marked with NPRA

The panels with metallic fibres were cast at KUL, while the panels with synthetic fibres and the blanco panels were cast at BBRI. In total (6x4x4=) 96 panels were cast. The fibres used were:

- Synthetic fibres: Chryso S50
  - Mix of polypropylene and polyethylene
  - Tensile strength: 600MPa
  - E-modulus: 5 000MPa
  - Length: 50mm
- Metallic fibres: TABIX 1/50
  - Undulated steel
  - Tensile Strength: 1100MPa
  - E-modulus: 200 000MPa
  - Length: 50mm
  - Aspect ratio: 50

[1] The work in Trondheim has been done as collaboration between NTNU and SINTEF Building and Infrastructure.

All panels are named PT – fibre type and dosage-x-y

- PT means Plate Test
- Fibre type and dosage describes the type and dosage of fibre, B, SF4,5, SF9, MF20, MF40 and MF60
- x is the series number and describes at which laboratory the test are performed, 1, 2, 3 and 4 are associated with KUL, BBRI, NTNU and NPRA respectively.
- y is the plate number within the same series, from 1 to 4.

The objective of this work is to evaluate whether the ASTM-procedure are able to produce consistent results for nominally identical panels tested at different laboratories with different measuring systems.

The energy absorption (EABS) from every test is calculated by the same person to ensure that the results are treated in similar way. All calculations are done at NTNU/SINTEF.

1.1 Concrete composition

The concrete panels were cast at KUL and BBRI. The blanco- and SF- panels were cast at BBRI, while the MF- panels were cast at KUL.

The concrete composition is shown in Table 1

Table 1 Concrete composition

	Type	[kg/m^3]
Cement	CEM I 52.5 N	310.00
Sand[1]	0/4	577.5
Sand[1]	0/5	192.5
Gravel	4/15	1155
Water	w/c=0.55	170.50
Fibres	Synthetic/Metallic	0 / S4.5 / S9 / M20 / M40 / M60
Superplasticizer	Sika gold 20	2.5
[1]2 different fractions of sand was used in order to achieve a suitable grading curve		

The slump values were only reported from BBRI and they were rather low, 12mm, 25mm and 9mm for the concrete without fibre (blanco), the SF4.5 concrete and SF9 concrete respectively. The casting process appeared to be successful, despite the low slump values.

The compressive strengths were only tested for the concrete with various MF-content. The compressive strengths were:

- MF20: 59MPa
- MF40: 65MPa
- MF60: 62MPa

1.2 Description of the test procedure

The round panels are placed on the three supports with the moulded face pointed down, as showed in Figure 1. In order to allow rotation during the test, the support consist of the supporting cylinder, a metal ball (Ø 16 mm) and a steel plate (40 x 50 mm^2) with a spherical seat as described in paragraph 6.2 of the ASTM C1550 standard.

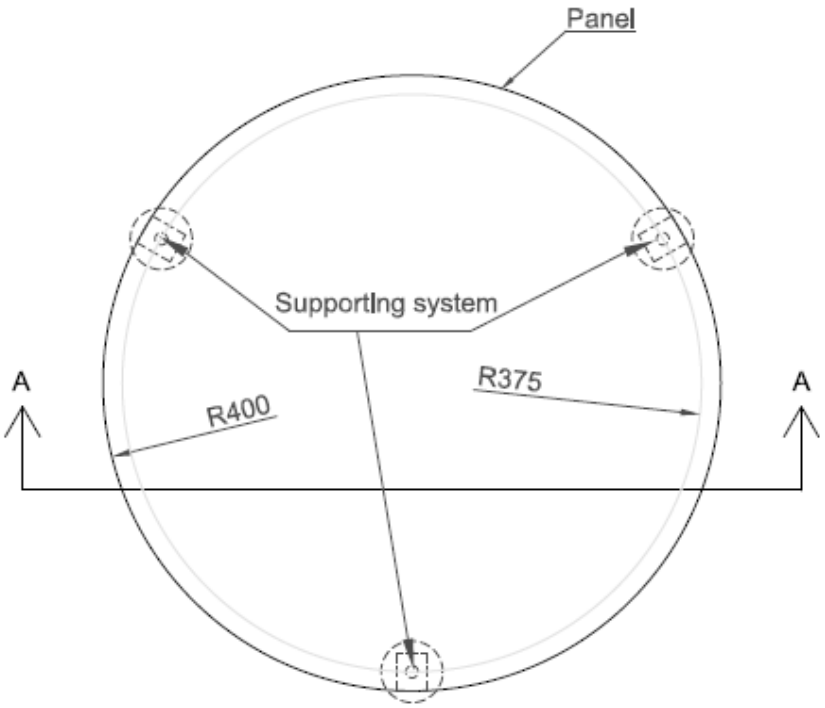

Figure 1 Plan view of the concrete panel including the supporting system

The load and corresponding deflection are recorded. The deflection was measured in two ways; the displacement of the load piston, and the deflection of the panel. This is showed in Figure 2.

The deflection of the panel was measured directly at the tensile surface of the panel, at the panel's centre, and can be considered to be the true deflection, as long as the supporting points do not deform and there is no crushing of the concrete.

The displacement of the piston was measured because if a crack appears at the centre of the panel, the measurement from the panel deflection may be useless. The displacement of the load piston was measured (some place) at the test machine, and includes load train deformation.

The deflection measurement was done somewhat different at the different labs. At KUL, BBRI and NPRA the deflection measurement was done by LVDT, while at NTNU it was done by a laser. The design of the LVDT measurement at KUL and BBRI results in that when a crack appears at the centre of the panel, the measurement may be useless because the LVDT may slip into the crack.

At NPRA and NTNU the deflection was measured beyond the deflection at which cracking occurred. At NPRA this was possible by use of a disc on the top of the LVDT. This disc can rotate along with the rotation of the panels, as well as bridging over the cracks. At NTNU the deflection was measured by a laser. At the tension side of the panels, a thin flexible sheet of plastic was attached. This plastic sheet prevented the laser to "be lost" in the cracks.

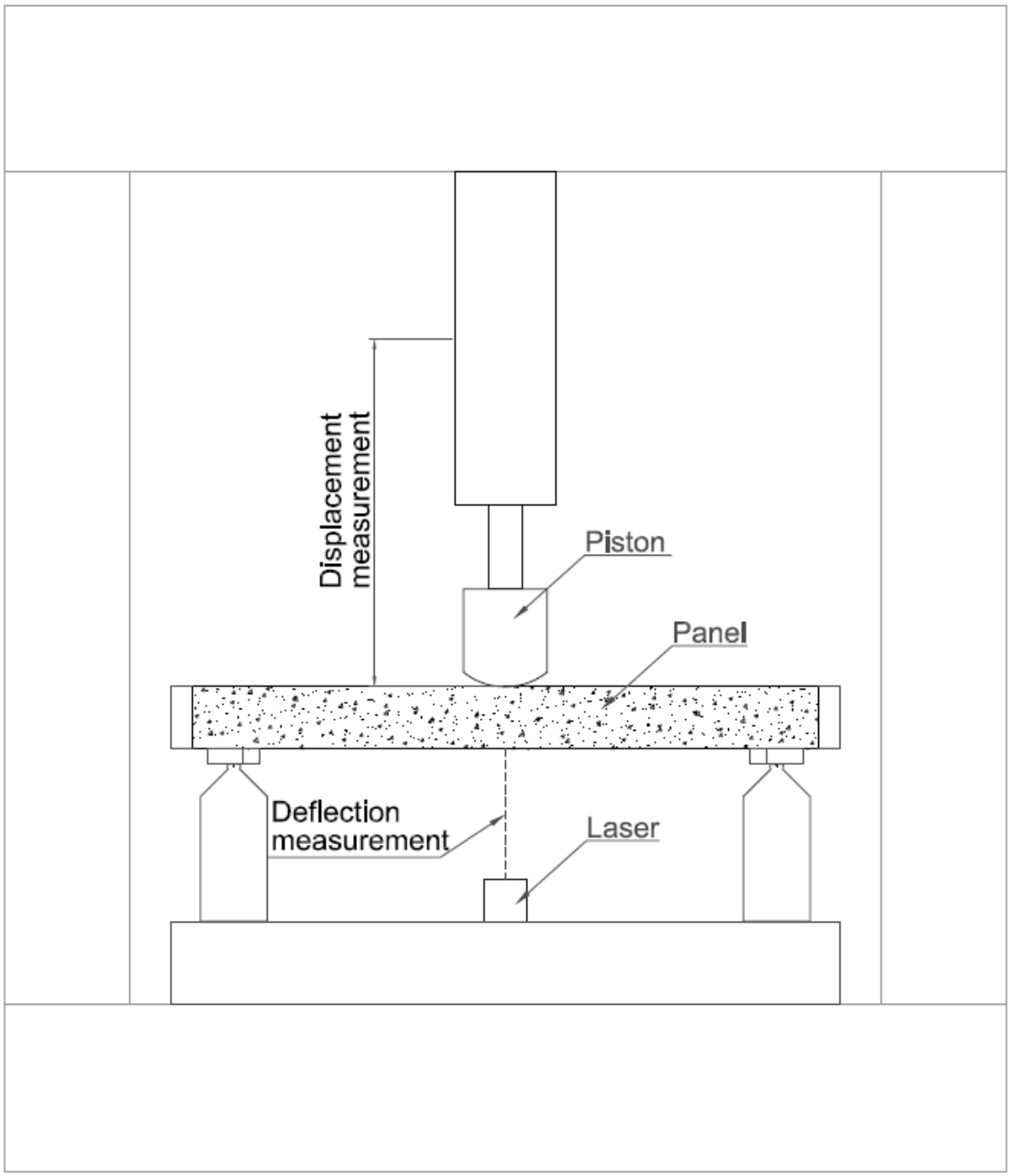

Figure 2 Sketch of the test system (section A-A from Figure 1)

The diameter of the panels was measured three times, and the thickness of the panels was measured ten times (three times in each crack and also in the centre).

The tests were carried out displacement controlled, with a rate of displacement equal to 4 mm/min up to a central displacement of at least 45 mm.

At KUL, BBRI and NTNU the displacement of the load cell was used to control the rate of displacement, while at NPRA the deflection of the panel was used.

1.3 Description of the calculation

The calculation of energy absorption includes several steps. All steps are in agreement with ASTM C 1550, and the equations are copied from ASTM C 1550.

1. The load-deflection record measured with LVDT are adjusted in order to remove the non-linear part at the start of the measurement and to intersect origin.
2. The load-displacement record measured with the piston are adjusted in order to remove the non-linear part at the start of the measurement and to intersect origin.
3. The adjusted load-deflection relationship exclusive of the load train deformation is calculated.
4. The measured EABS, *W'*, is calculated
5. The corrected EABS, *W*, is calculated by taking into account the average diameter and average thickness.

In sub-chapter 1.3.1 and 1.3.2, when it is written *load-deflection* it means that the deflection is measured with LVDT. When it is written *load-displacement* it means that the displacement is measured with the piston.

As mentioned in chapter 1.2, at NTNU and NPRA the deflection was measured beyond the deflection at which cracking occurred. This made it possible to use the "true" deflection directly. Nevertheless, the same calculation process is used for every panel to eliminate as many variables as possible. The effect of using only the LVDT-record to calculate EABS are showed in chapter 2.5.

1.3.1 Adjustment of load-deflection record

Figure 3 shows a typical load-deflection curve. The linear adjustment is based on the load and corresponding deflection at 30% and 80% of peak load. The range between 30% and 80% is chosen of two reasons:

1. The relationship between load and deflection is linear up to a given percent of peak load. An upper limit of 80% of peak load is considered to be within the linear range. Normally a load level of 80% of the peak load is considered to be beyond the linear range, but the relationship is checked for all 96 panels and all of them have a load-deflection relationship similar to PT-MF20-3-1 shown in Figure 3.
2. For some panels a small extraneous deformation arose. The reason may be dust or small sand particles between the concrete panel and the transfer plates, or crushing of concrete at the transfer plates. In any case, using 30% of peak load excludes non-linear relationship in the beginning of the test.

a

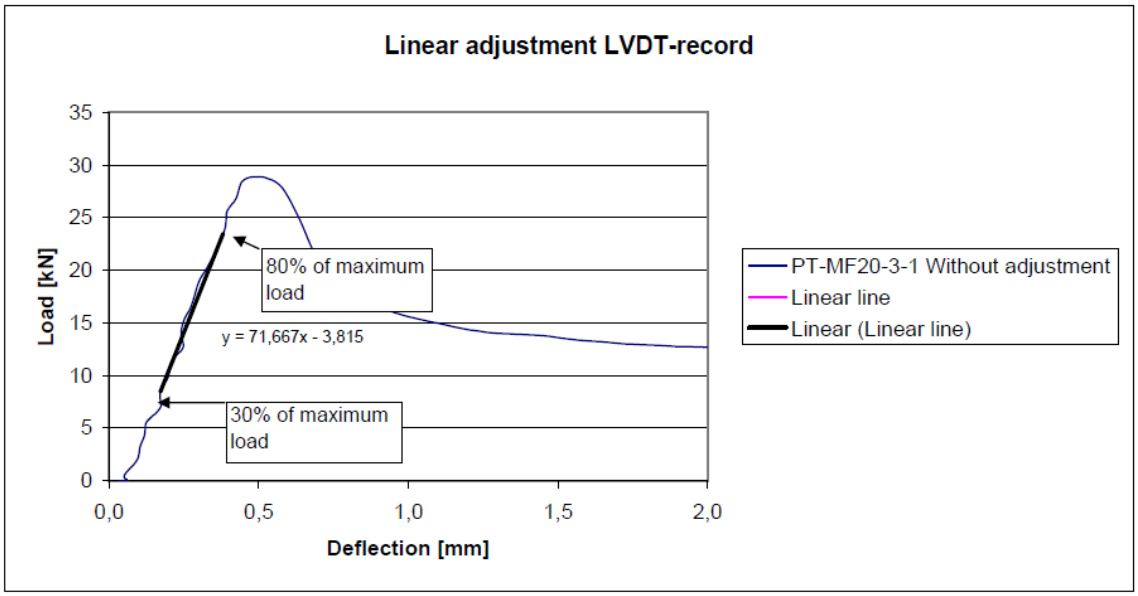

b

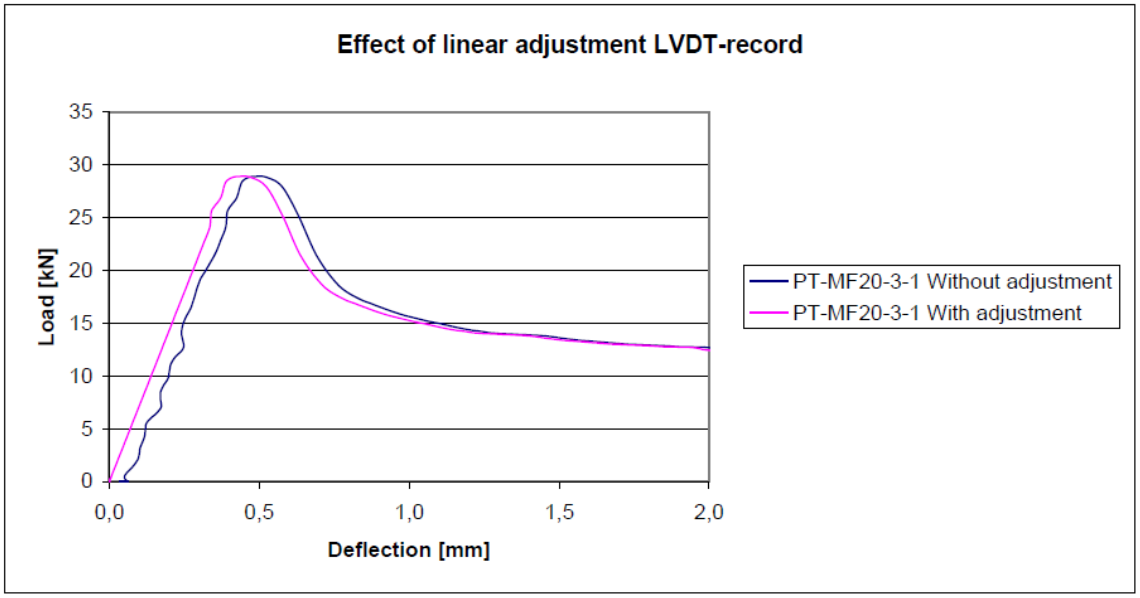

Figure 3 Adjustment of the load-deflection record (at NTNU) measured with LASER

As seen in Figure 3a, the load-deflection curve does not cross origin. The offset occurs because of two reasons:

1. The load-deflection relationship may be non-linear at small deflections because of extraneous deformation.
2. The deflection record is not rest to zero before start of testing.

The offset in Figure 3a is because the deflection record is not reset to zero before start of testing.

The mathematic function of the linear part between 30-80% of peak load is shown in the figure. The offset between the measured and net deflection (X_0) is determined by calculating

at which x-value the linear line intersect the X-axis. The load-deflection curve is then shifted horizontally with X_0, so that the curve goes through origin.

Figure 3b shows the effect of linear adjustment including horizontal translation for a typical load-deflection curve.

For the majority of the panels, the offset could have been corrected simply by reset the deflection measurement when the load was 0. But again, it is chosen to do all calculation the same way.

1.3.2 Adjustment of load-displacement record

The adjustment of the load-deformation record is done the same way as explained above. The only difference is that the horizontal translation may be larger, and that the non-linear range in the beginning of the test may be more pronounced. Figure 4 shows a typical load-deformation curve.

a

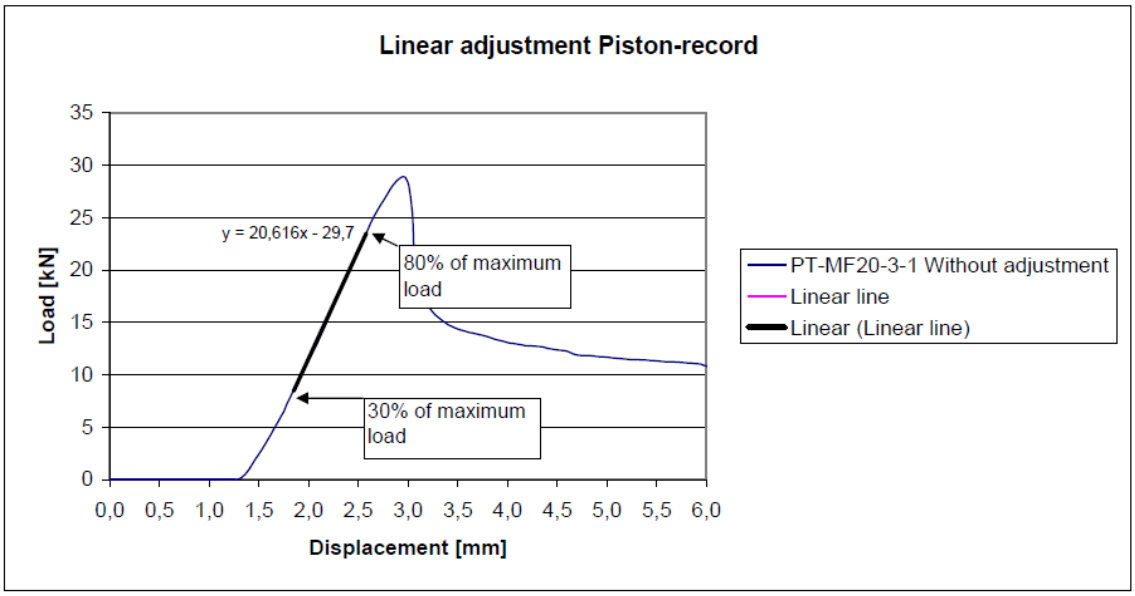

b

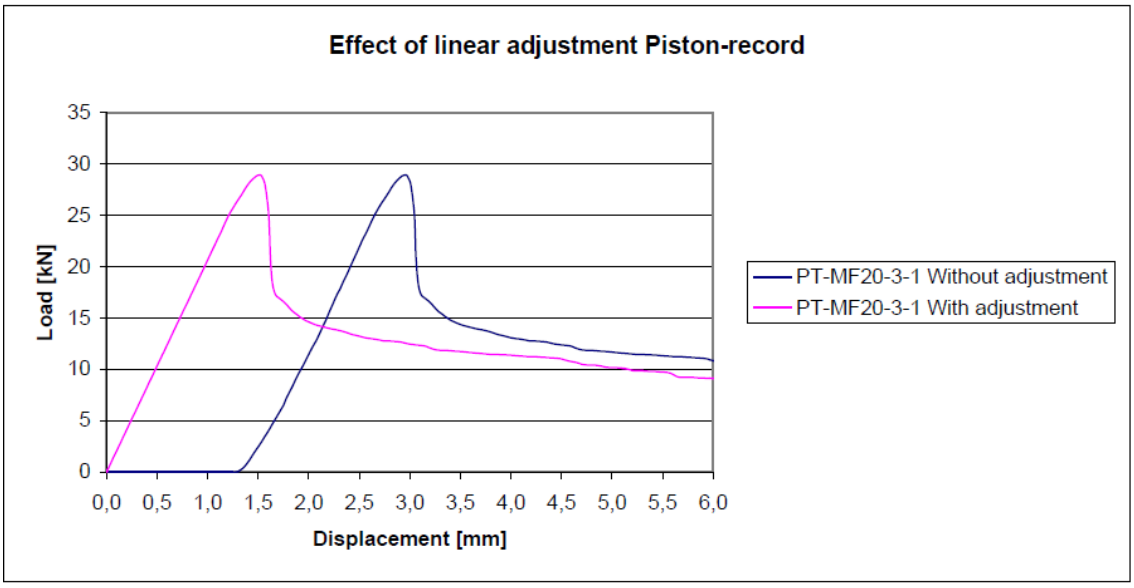

Figure 4 Adjustment of the load-displacement record (at NTNU) measured with the piston

The reason why the non-linear range in the beginning is more pronounced (than for the load-deflection record) is because of the deformation of the load train and crushing of the concrete around the load point. (Crushing of concrete around the supports would give the same non-linear range in both cases.) As for the load-deflection record, the reason why the displacement measurement is not zero at zero load is because the displacement record was not reset to zero.

1.3.3 Calculation of deflection exclusive load train deformation

Figure 5 shows the adjusted load-deflection curve when the deflection/displacement is measured by LVDT and the piston, and also the deflection exclusive the load train deformation (marked ASTM) as calculated as described in ASTM C 1550.

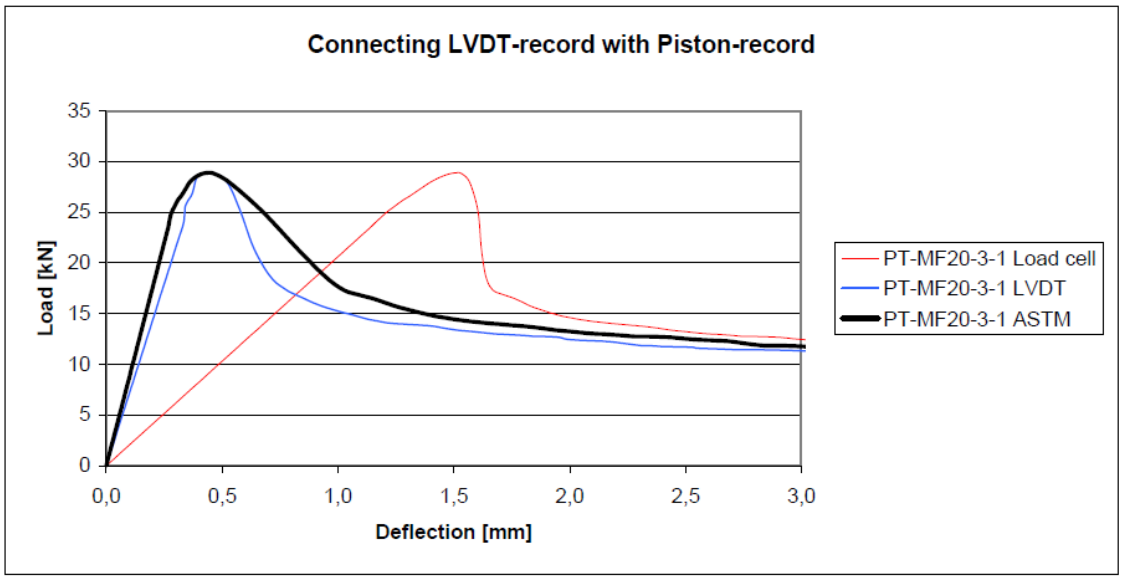

Figure 5 Connecting piston- and LVDT- measurements (NTNU-panel)

In Figure 5 the curve marked:

- PT-MF20-3-1 Load cell is the adjusted load-displacement curve.
- PT-MF20-3-1 LVDT is the adjusted load-deflection curve.
- PT-MF20-3-1 ASTM is the calculated load-deflection curve. This curve is used for EABS calculations.

The deflection exclusive load train deformation, δ, is calculated by the following equation [ASTM C 1550]

$$\delta = \delta_m - P \cdot C_{LT} \quad (1)$$

where

δ_m is the adjusted displacement of the piston [mm]
P is the load corresponding to δ_m [kN]
C_{LT} is the compliance of the load train [mm/kN]

The compliance of the load train is the difference between the apparent compliance of the specimen when deformation of the load train is included and the true compliance of the specimen [ASTM C 1550].

$$C_{LT} = C_{app} - C_{spec} \quad (2)$$

where

C_{app} is the apparent compliance of the specimen inclusive of load train deformation
C_{spec} is the true compliance of the specimen.

and

$$C_{app(spec)} = \frac{\Delta_{app(spec)}}{P_{Max}} \quad (3)$$

To calculate C_{app} and C_{spec} the deformation, Δ_{app}, or deflection, Δ_{spec}, at peak load, P_{Max}, is used. This is the explanation why the ASTM curve and the LVDT curve do not coincide

before peak load in Figure 5. If C_{app} and C_{spec} had been calculated based on the deformation, Δ_{app}, or deflection, Δ_{spec}, at 80% of peak load, the ASTM curve and the LVDT curve would coincide up to 80% of peak load. But then the load train deformation from 80% to 100% of peak load would not be adjusted for. Another parameter that influences whether the ASTM curve and the LVDT curve coincide is whether the load-deflection curve and load-deformation curve are still linear from 80% to 100% of peak load. In any case, the area between the ASTM curve and the LVDT curve, and thereby the effect of the calculated EABS is practically zero.

In the following, when it is written *load-deflection*, it means that the deflection is corrected according to the calculations above, and that the deflection is considered to be the true deflection.

1.3.4 Calculation of measured EABS, *W'*

The measured EABS, *W'*, is calculated as the area under the load-deflection curve between the origin and a deflection of 40mm. This is done by numerical integration according to the following equation:

$$W' = \sum_{i=0}^{i=x} \left(\delta_{i+1} - \delta_i\right) \frac{P_i + P_{i+1}}{2} \tag{4}$$

where

δ_x is the specified central deflection at which the capacity to absorb energy is measured, in mm.

In addition, the contribution for every 5 mm is calculated.

1.3.5 Calculation of corrected EABS, *W*

The measured EABS is corrected with regard to variation in diameter, *d*, and thickness, *t*, according to the following equation [ASTM C 1550]:

$$W = W' \left(\frac{t_0}{t}\right)^{\beta} \left(\frac{d_0}{d}\right) \tag{5}$$

where:

$$\beta = 2{,}0 - \frac{\delta_x - 0{,}5}{80} \tag{6}$$

and:

t_0 is the average thickness of the specimen, in mm.
d_0 is the average diameter of the specimen, in mm.
t is the intended thickness of the specimen, 75mm
d is the intended diameter of the specimen, 800mm

In the following, when it is written *EABS*, it means the corrected EABS. Further, when it is written W_X it means the corrected EABS measured up to *X*mm deflection.

2 Energy absorption

2.1 Results summarized lab by lab

In Table 2 to Table 33, *Wx* is the corrected energy absorption, EABS, up to *X* mm deflection.

2.1.1 Panels tested at KUL

Table 2 to Table 7 summarizes the results for the panels tested at KUL. For each concrete type, 4 panels are tested.

Table 2 KUL B-series

PT-B-1-	P_{Max} [kN]	W_5 [J]	W_{10} [J]	W_{20} [J]	W_{40} [J]
1	25,48	23	23	23	23
2	25,22	23	23	23	23
3	26,15	21	21	21	21
4	20,65	20	20	20	20
Mean value	**24,4**	**22**	**22**	**22**	**22**
CoV [%]	10	7	7	7	7

Table 3 KUL MF20-series

PT-MF20-1-	P_{Max} [kN]	W_5 [J]	W_{10} [J]	W_{20} [J]	W_{40} [J]
1	26,70	67	101	137	170
2	22,39	53	88	135	174
3	27,60	73	113	159	195
4	24,18	59	85	115	139
Mean value	**25,2**	**63**	**97**	**137**	**169**
CoV [%]	9	14	13	13	14

Table 4 KUL MF40-series

PT-MF40-1-	P_{Max} [kN]	W_5 [J]	W_{10} [J]	W_{20} [J]	W_{40} [J]
1	27,08	90	151	223	278
2	28,21	73	114	162	208
3	31,48	81	134	193	235
4	29,76	98	167	237	299
Mean value	**29,1**	**86**	**142**	**204**	**255**
CoV [%]	7	13	16	17	16

Table 5 KUL MF60-series

PT-MF60-1-	P_{Max} [kN]	W_5 [J]	W_{10} [J]	W_{20} [J]	W_{40} [J]
1	26,83	88	152	227	199
2	27,43	96	168	257	330
3	29,83	107	180	265	343
4	27,50	108	189	290	380
Mean value	**27,9**	**100**	**172**	**260**	**338**
CoV [%]	5	9	9	10	10

Table 6 KUL SF4.5-series

PT-SF4.5-1-	P_{Max} [kN]	W_5 [J]	W_{10} [J]	W_{20} [J]	W_{40} [J]
1[1]	25,04	47	82	132	186
2[1]	26,13	49	91	157	226
3[1]	24,36	44	75	127	181
4	27,46	50	93	162	239
Mean value	**25,7**	**47**	**85**	**145**	**208**
CoV [%]	5	6	10	12	14
[1] LVDT-record is missing, calculations include load-train deformation					

Table 7 KUL SF9-series

PT-SF9-1-	P_{Max} [kN]	W_5 [J]	W_{10} [J]	W_{20} [J]	W_{40} [J]
1	26,82	66	127	207	277
2	28,84	75	142	235	321
3	27,24	72	141	242	347
4	29,30	77	153	259	365
Mean value	**28,1**	**73**	**141**	**236**	**327**
CoV [%]	4	7	8	9	12

2.1.2 Panels tested at BBRI

Table 8 to Table 13 summarizes the results for the panels tested at BBRI. For each concrete type, 4 panels are tested. The following panels were not tested up to 40 mm deflection:

- PT-MF20-2-1. EABS up to 25 mm deflection
- PT-MF20-2-2. EABS up to 30 mm deflection
- PT-MF20-2-3. EABS up to 35 mm deflection
- PT-MF20-2-4. EABS up to 30 mm deflection
- PT-MF40-2-2. EABS up to 30 mm deflection
- PT-SF4.5-2-4. EABS up to 35 mm deflection
- PT-SF9-2-4. EABS up to 30 mm deflection

Table 8 BBRI B-series

PT-B-2-	P_{Max} [kN]	W_5 [J]	W_{10} [J]	W_{20} [J]	W_{40} [J]
1	25,84	18	18	18	18
2	29,00	22	22	22	22
3	27,48	25	25	25	25
4	23,66	23	23	23	23
Mean value	**26,5**	**22**	**22**	**22**	**22**
CoV [%]	9	14	14	14	14

Table 9 BBRI MF20-series

PT-MF20-2-	P_{Max} [kN]	W_5 [J]	W_{10} [J]	W_{20} [J]	W_{40} [J]
1	29,07	65	89	112	-
2	25,16	63	93	126	-
3	25,70	67	110	159	-
4	28,87	71	104	137	-
Mean value	**27,2**	**67**	**99**	**133**	-
CoV [%]	8	5	10	15	-

Table 10 BBRI MF40-series

PT-MF40-2-	P_{Max} [kN]	W_5 [J]	W_{10} [J]	W_{20} [J]	W_{40} [J]
1	29,53	78	129	188	240
2	32,96	98	161	241	-
3	29,58	95	153	217	280
4	30,23	104	177	268	347
Mean value	**30,6**	**94**	**155**	**229**	**289**
CoV [%]	5	12	13	14	19

Table 11 BBRI MF60-series

PT-MF60-2-	P_{Max} [kN]	W_5 [J]	W_{10} [J]	W_{20} [J]	W_{40} [J]
1	30,74	110	193	300	409
2	30,32	122	208	304	387
3	25,75	114	192	282	364
4	27,12	108	181	265	339
Mean value	**28,5**	**114**	**193**	**288**	**374**
CoV [%]	9	5	6	6	8

Table 12 BBRI SF4.5-series

PT-SF4.5-2-	P_{Max} [kN]	W_5 [J]	W_{10} [J]	W_{20} [J]	W_{40} [J]
1	29,01	60	105	178	257
2	34,77	65	116	197	291
3	26,60	51	91	154	223
4	28,76	54	94	161	-
Mean value	**29,8**	**57**	**101**	**173**	**257**
CoV [%]	12	11	11	11	13

Table 13 BBRI SF9-series

PT-SF9-2-	P_{Max} [kN]	W_5 [J]	W_{10} [J]	W_{20} [J]	W_{40} [J]
1	26,73	72	139	245	373
2	28,51	85	175	322	486
3	36,70	84	148	235	315
4	31,28	98	186	252	-
Mean value	**30,8**	**85**	**162**	**226**	**391**
CoV [%]	14	12	14	14	22

2.1.3 Panels tested at NTNU

Table 14 to Table 19 summarizes the results for the panels tested at NTNU. For each concrete type, 4 panels are tested. One of the 4 panels without fibres is discarded because it failed in a beam-like mode with only one single crack across the panel.

Table 14 NTNU B-series

PT-B-3-	P_{Max} [kN]	W_5 [J]	W_{10} [J]	W_{20} [J]	W_{40} [J]
1	27,27	27	27	27	27
2	29,81	29	30	30	30
3[1]	19,62	21	22	22	22
4[2]	7,26	9	9	9	9
Mean value	**25,6**	**26**	**26**	**26**	**26**
CoV [%]	21	15	16	16	16
[1]The panel had considerable less P_{Max} than the other panels, but it cracked like expected – not discarded [2]The panel had one crack before testing. Failed in a beam-like mode – discarded.					

Table 15 NTNU MF20-series

PT-MF20-3-	P_{Max} [kN]	W_5 [J]	W_{10} [J]	W_{20} [J]	W_{40} [J]
1	28,87	72	110	157	204
2	31,69	67	101	140	178
3	26,73	74	118	172	218
4	30,91	75	112	149	175
Mean value	**29,6**	**72**	**110**	**155**	**193**
CoV [%]	8	5	6	9	11

Table 16 NTNU MF40-series

PT-MF40-3-	P_{Max} [kN]	W_5 [J]	W_{10} [J]	W_{20} [J]	W_{40} [J]
1	34,08	105	172	232	280
2	30,90	95	157	231	303
3	34,07	105	172	251	324
4	33,46	102	170	247	315
Mean value	**33,1**	**102**	**168**	**240**	**305**
CoV [%]	5	5	4	4	6

Table 17 NTNU MF60-series

PT-MF60-3-	P_{Max} [kN]	W_5 [J]	W_{10} [J]	W_{20} [J]	W_{40} [J]
1	33,95	131	218	323	403
2	29,57	110	183	277	359
3	30,77	126	216	332	448
4	32,15	125	210	313	409
Mean value	**31,6**	**123**	**207**	**311**	**405**
CoV [%]	6	8	8	8	9

Table 18 NTNU SF4.5-series

PT-SF4.5-3-	P_{Max} [kN]	W_5 [J]	W_{10} [J]	W_{20} [J]	W_{40} [J]
1	30,14	55	96	165	245
2	33,78	57	102	179	271
3	31,97	55	93	146	197
4	31,22	67	122	200	272
Mean value	**31,8**	**59**	**103**	**172**	**246**
CoV [%]	5	10	12	13	14

Table 19 NTNU SF9-series

PT-SF9-3-	P_{Max} [kN]	W_5 [J]	W_{10} [J]	W_{20} [J]	W_{40} [J]
1	32,79	93	181	301	405
2	30,66	80	151	253	353
3	29,83	77	148	255	365
4	28,74	78	151	271	402
Mean value	**30,5**	**82**	**158**	**270**	**381**
CoV [%]	6	9	10	8	7

2.1.4 Panels tested at NPRA

Table 20 to Table 25 summarizes the results for the panels tested at NPRA. For each concrete type, 4 panels are tested. Panel PT-SF4.5-4-3 was not tested up to 40 mm deflection. EABS for PT-SF4.5-4-3 is calculated up to 35 mm deflection. (The LVDT-record passed 40 mm, but the piston-record did not)

Table 20 NPRA B-series

PT-B-4-	P_{Max} [kN]	W_5 [J]	W_{10} [J]	W_{20} [J]	W_{40} [J]
1	27,81	28	28	28	28
2	27,12	25	25	25	25
3	33,97	30	30	30	31
4	25,01	22	22	22	22
Mean value	**28,5**	**26**	**26**	**26**	**26**
CoV [%]	14	14	14	14	15

Table 21 NPRA MF20-series

PT-MF20-4-	P_{Max} [kN]	W_5 [J]	W_{10} [J]	W_{20} [J]	W_{40} [J]
1	28,37	71	111	154	189
2	25,85	57	88	124	151
3	25,86	67	103	149	198
4	31,18	61	92	129	163
Mean value	**27,8**	**64**	**99**	**139**	**175**
CoV [%]	9	10	11	11	13

Table 22 NPRA MF40-series

PT-MF40-4-	P_{Max} [kN]	W_5 [J]	W_{10} [J]	W_{20} [J]	W_{40} [J]
1	32,26	97	154	230	299
2	31,66	102	169	255	334
3	30,53	95	153	220	284
4	34,80	107	172	253	333
Mean value	**32,3**	**100**	**162**	**240**	**313**
CoV [%]	6	5	6	7	8

Table 23 NPRA MF60-series

PT-MF60-4-	P_{Max} [kN]	W_5 [J]	W_{10} [J]	W_{20} [J]	W_{40} [J]
1	33,53	125	200	298	398
2	32,62	118	205	306	395
3	29,21	108	180	265	340
4	30,71	102	177	270	355
Mean value	**31,5**	**112**	**190**	**285**	**372**
CoV [%]	6	7	7	7	8

Table 24 NPRA SF4.5-series

PT-SF4.5-4-	P_{Max} [kN]	W_5 [J]	W_{10} [J]	W_{20} [J]	W_{40} [J]
1	29,44	56	95	151	209
2	35,60	59	108	180	261
3	35,72	62	108	177	236[1]
4	30,75	62	112	196	291
Mean value	**32,9**	**60**	**106**	**176**	**254[2]**
CoV [%]	10	5	7	10	13[3]

[1]The value is W_{35}
[2] Panel 3 is not used for calculation
[3] CoV for W_{35}

Table 25 NPRA SF9-series

PT-SF9-4-	P_{Max} [kN]	W_5 [J]	W_{10} [J]	W_{20} [J]	W_{40} [J]
1	29,05	72	135	225	314
2	34,46	80	153	260	378
3	32,02	76	146	244	332
4	34,23	88	168	283	393
Mean value	**32,4**	**79**	**150**	**253**	**354**
CoV [%]	8	8	9	10	11

2.2 Results summarized lab by lab

In Table 26 to Table 31 the mean values for each lab are presented. Whether it is correct or not to calculate the average values and CoV of all panels as if they are in one series is evaluated in chapter 4.

The calculated mean values for each concrete type are the mean values for every panel, not the mean values of the average for each lab. The CoV is calculated the same way.

Generally the calculation is made for every fifth millimetre of deflection, and the EABS vs deflection diagrams are made of smoothed lines between the points. For the Blanco results, the diagrams are made of straight lines between the points, resulting in that the Blanco-curves are not exactly correct. The EABS at 5mm deflection, W_5, is correct, but the Blanco-panels reached the final EABS at less deflection.

Table 26 and Figure 6 show the results from the Blanco-series.

Table 26 Mean values blanco series

Blanco	P_{Max} [kN]	W_5 [J]	W_{10} [J]	W_{20} [J]	W_{40} [J]
KUL	24,3	22	22	22	22
BBRI	26,5	22	22	22	22
NTNU	25,6	26	26	26	26
NPRA	28,5	26	26	26	26
Mean value	**26,3**	**24**	**24**	**24**	**24**
CoV [%]	14	15	16	16	16

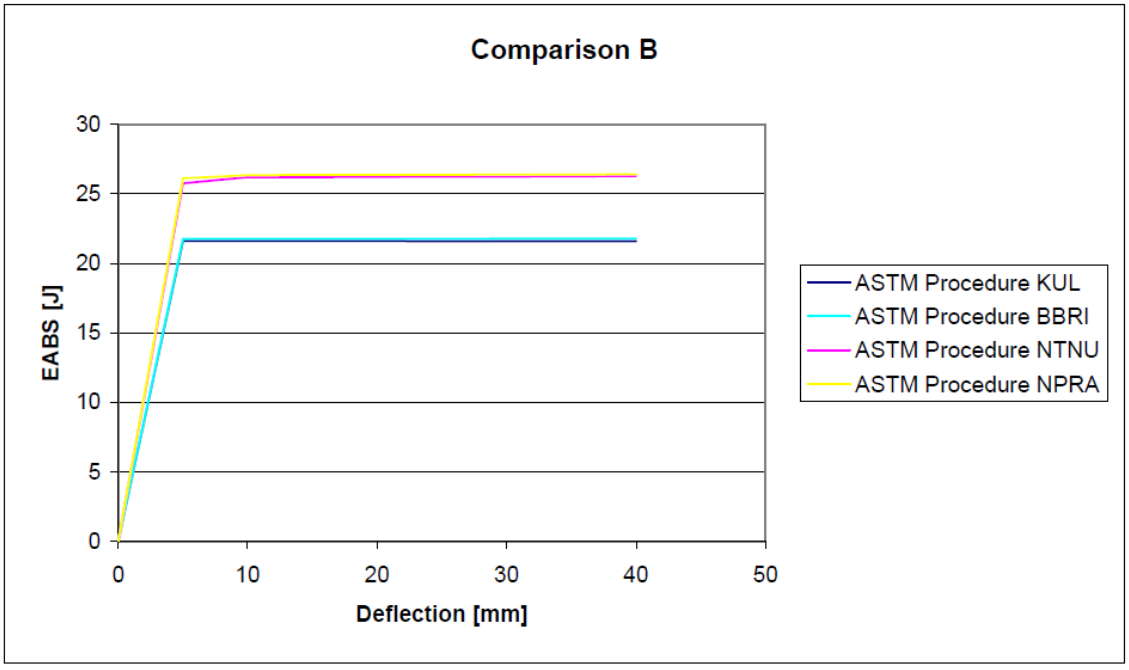

Figure 6 Mean values B-series

Table 27 and Figure 7 show the results from the MF20-series.

Table 27 Mean values MF20-series

MF20	P_{Max} [kN]	W_5 [J]	W_{10} [J]	W_{20} [J]	W_{40} [J]
KUL	25,2	63	97	137	169
BBRI	27,2	67	99	133	-
NTNU	29,6	72	110	155	193
NPRA	27,8	64	99	139	175
Mean value	**27,4**	**66**	**101**	**141**	**179**
CoV [%]	8	10	11	12	13

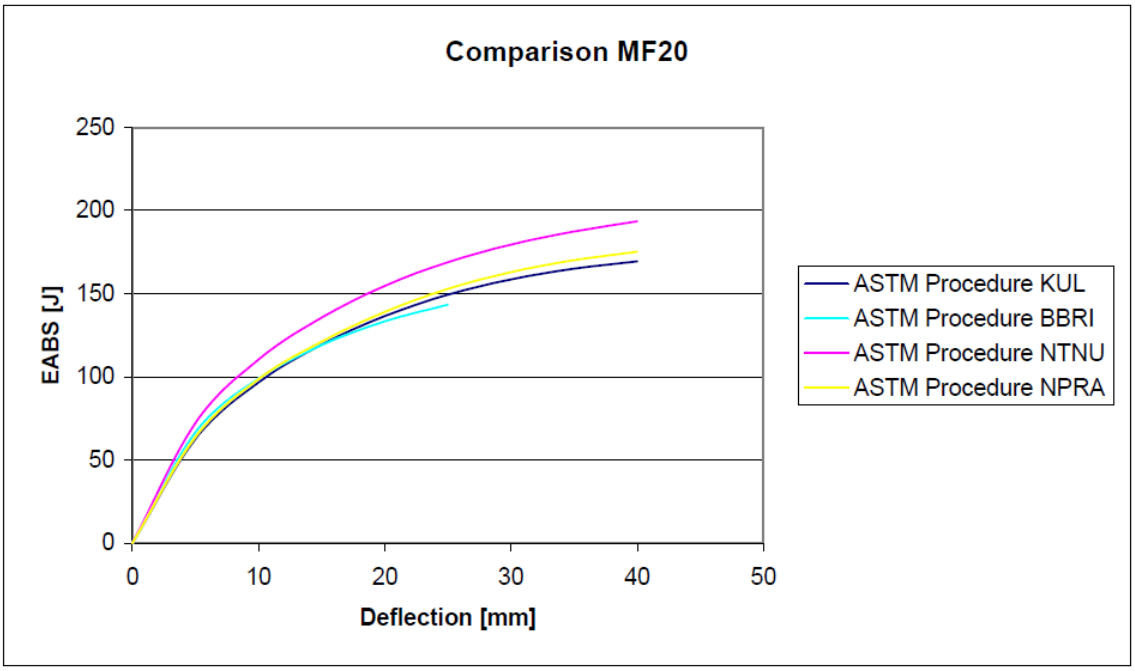

Figure 7 Mean values MF20-series

Table 28 and Figure 8 show the results from the MF40-series.

Table 28 Mean values MF40-series

MF40	P_{Max} [kN]	W_5 [J]	W_{10} [J]	W_{20} [J]	W_{40} [J]
KUL	29,1	86	142	204	255
BBRI	30,6	94	155	229	289
NTNU	33,1	102	168	240	305
NPRA	32,3	100	162	240	313
Mean value	**31,3**	**95**	**157**	**228**	**291**
CoV [%]	7	11	11	12	14

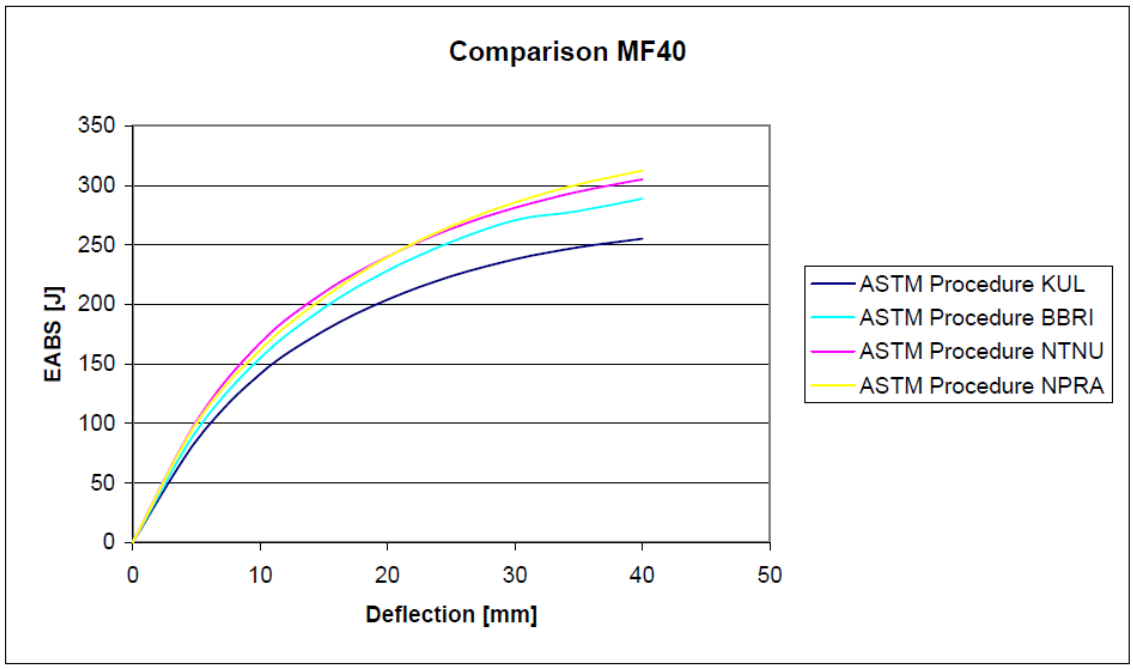

Figure 8 Mean values MF40-series

Table 29 and Figure 9 show the results from the MF60-series.

Table 29 Mean values MF60-series

MF60	P_{Max} [kN]	W_5 [J]	W_{10} [J]	W_{20} [J]	W_{40} [J]
KUL	27,9	100	172	260	338
BBRI	28,5	114	193	288	374
NTNU	31,6	123	207	311	405
NPRA	31,5	112	190	285	372
Mean value	**29,9**	**112**	**191**	**286**	**372**
CoV [%]	8	10	10	10	10

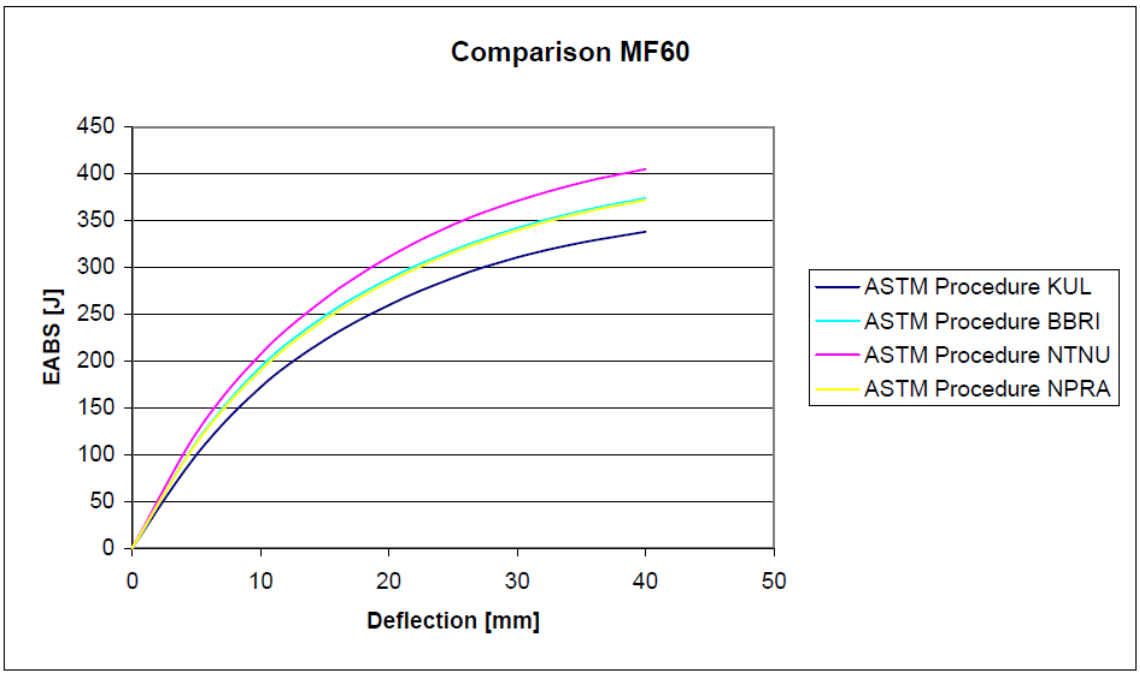

Figure 9 Mean values MF60-series

Table 30 and Figure 10 show the results from the SF4.5-series.

Table 30 Mean values SF4.5-series

SF4.5	P_{Max} [kN]	W_5 [J]	W_{10} [J]	W_{20} [J]	W_{40} [J]
KUL	25,7	47	85	145	208
BBRI	29,8	57	101	173	257
NTNU	31,8	59	103	172	246
NPRA	32,9	60	106	176	254
Mean value	**30,0**	**56**	**99**	**167**	**239**
CoV [%]	12	12	12	13	15

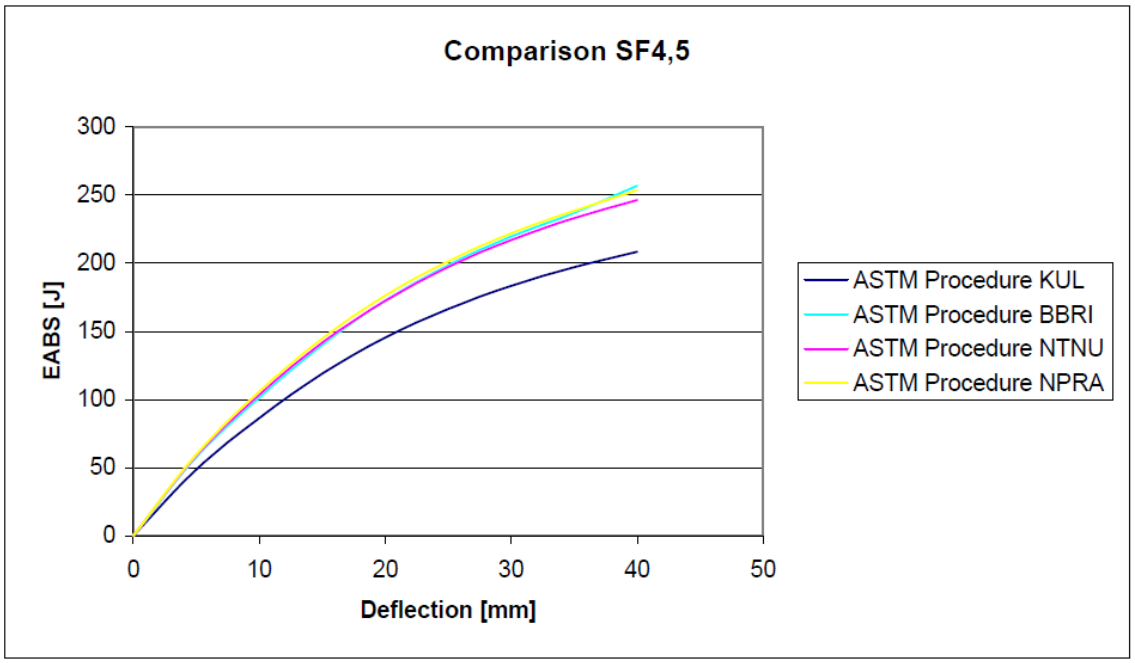

Figure 10 Mean values SF4.5-series

Table 31 and Figure 11 show the results from the SF9-series.

Table 31 Mean values SF9-series

SF9	P_{Max} [kN]	W_5 [J]	W_{10} [J]	W_{20} [J]	W_{40} [J]
KUL	28,1	73	141	236	327
BBRI	30,8	85	162	275	391
NTNU	30,5	82	158	270	381
NPRA	32,4	79	150	253	354
Mean value	**30,4**	**80**	**153**	**258**	**362**
CoV [%]	10	10	11	12	14

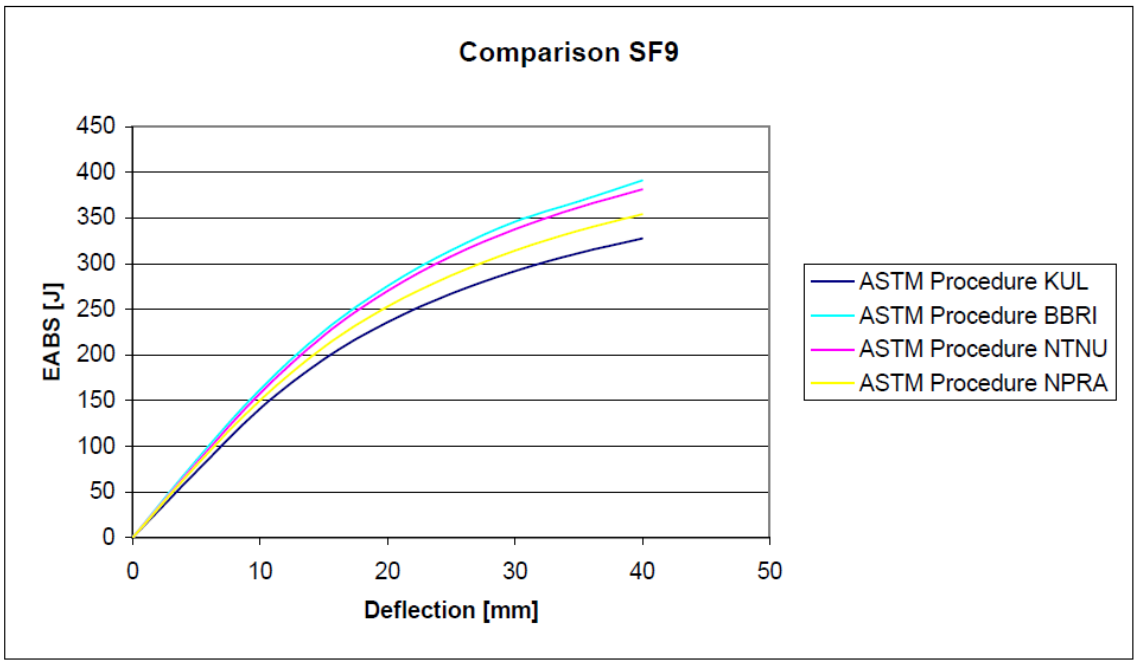

Figure 11 Mean values SF9-series

2.3 Results summarized according to concrete type

In Table 32 the mean values for each concrete type is summarized (the bold numbers from Table 26 to Table 31), and the correspondingly coefficient of variation is showed in Table 33. (The calculated values for every panel are shown in Table 3 to Table 25.) Whether it is correct or not to calculate the average values and CoV of all panels as if they are in one series is evaluated in chapter 4.

Table 32 Mean values summarized according to concrete type

Concrete type	P_{Max} [kN]	W_5 [J]	W_{10} [J]	W_{20} [J]	W_{40} [J]
Blanco	26,3 (15)	24 (15)	24 (15)	24 (15)	24 (15)
MF20	27,4	66	101	141	179 (12)
MF40	31,3	95	157	228	291 (15)
MF60	29,9	112	191	286	372
SF4.5	30,0	56	99	167	239 (14)
SF9	30,4	80	153	258	362 (15)
The number in parenthesis is the number of panels used to calculate the mean values, if no parenthesis, the number of panels is 16.					

Table 33 Coefficient of variation every panels

Concrete type	CoV P_{Max} [%]	CoV W_{40} [%]
Blanco (23/23)[1]	14	16
MF20 (24/20)[1]	8	13
MF40 (24/23)[1]	7	14
MF60 (24/24)[1]	8	10
SF4.5 (24/22)[1]	12	15
SF9 (24/23)[1]	10	14
[1](X/Y): X is the number of panels used to calculate CoV for P_{Max} Y is the number of panels used to calculate CoV for W_{40}		

In Table 34 the CoV for W_{40} is summarized. The table shows the CoV for every concrete type at every lab.

Table 34 Coefficient of variation summarized lab by lab

Concrete type	CoV W_{40} [%]			
	KUL	BBRI	NTNU	NPRA
Blanco	8	14	16[2]	15
MF20	14	14[1]	11	13
MF40	16	19[2]	6	8
MF60	10	8	9	8
SF4.5	14	13[2]	14	13[3]
SF9	12	22[2]	7	11
[1]CoV for W_{30} [2]Only 3 panels [3]CoV for W_{35}				

The Blanco-results for deflection larger than a few millimetres may be considered meaningless, because the panels collapse at small deflections. Nevertheless, the results are shown simply to show that the deviation is not related to the fibres, but to the concrete itself. Actually, it seems like the CoV of W_{40} decreases when the fibre dosage increases.

In Figure 12 the accumulated EABS (a) and the contribution to EABS pr 5mm deflection (b) for the 6 different concrete types are shown. Once again, be aware of the statistical calculation shown in chapter 4.

a

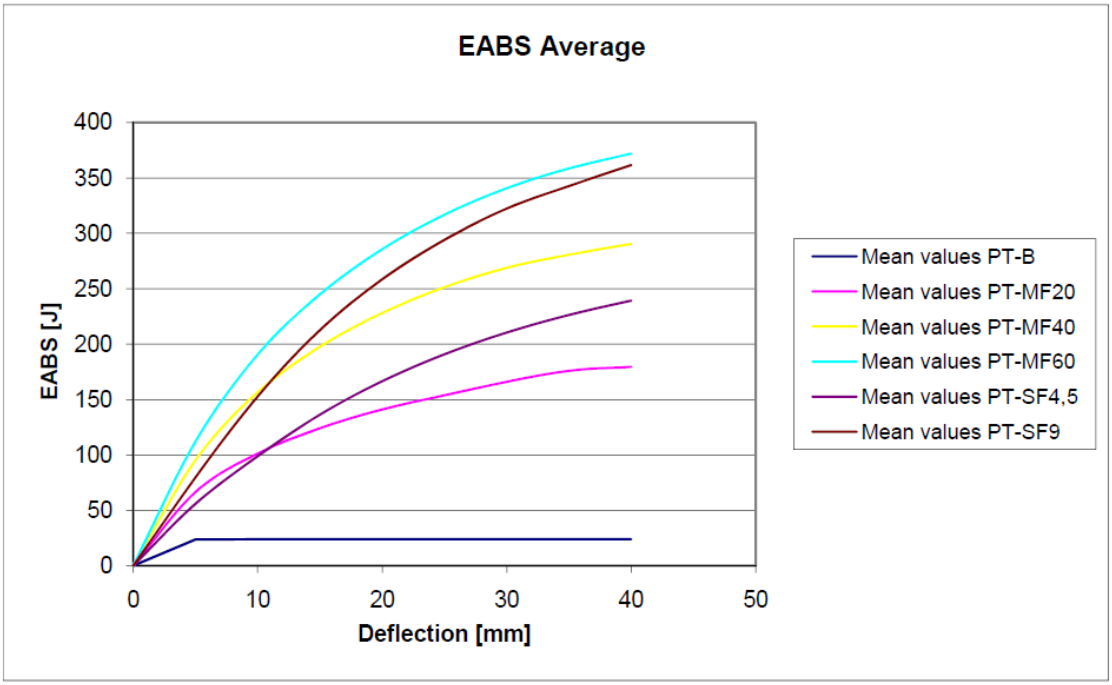

b

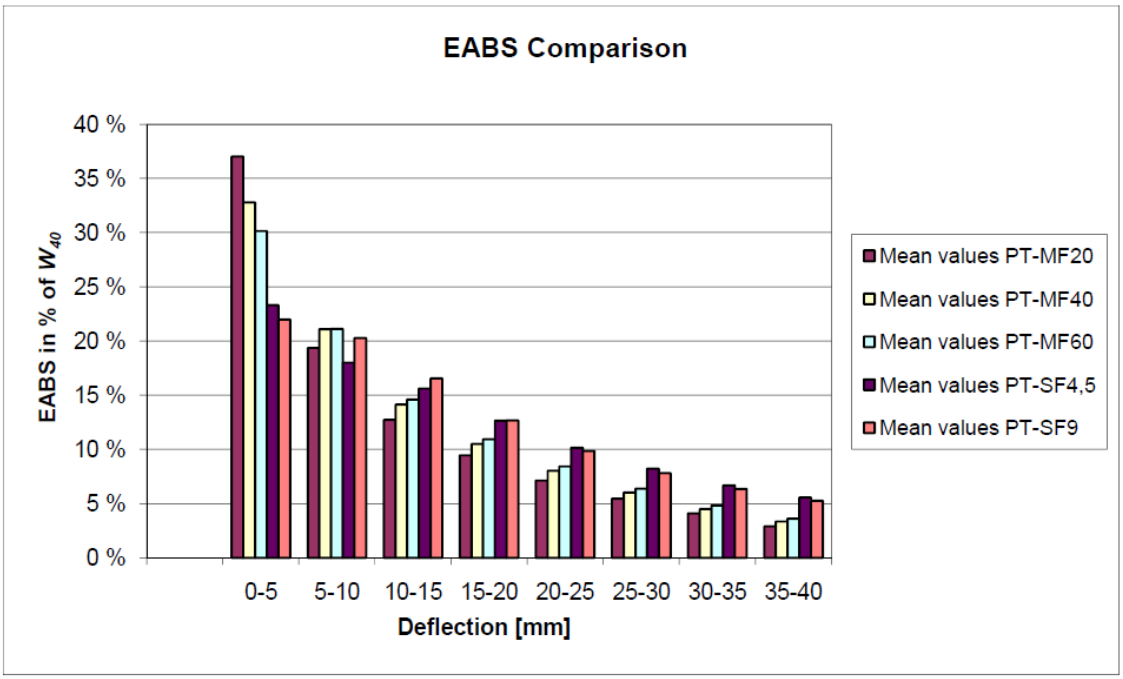

Figure 12 Mean values all panels, a) Accumulated values, b) Contribution per 5 mm deflection in % of W_{40} for the belonging series

In Figure 12b the Blanco-results are not shown simply because there is no increase in EABS after a few millimetres. From Figure 12b the main findings are:

- For the MF-panels, 30-37% of W_{40} is reached at 5mm deflection.

- For the SF-panels, approximately 27% of W_{40} is reached at 5mm deflection.
- Large deflections are favourable for SF-panels compared to MF-panels.

2.4 The effect of using only the piston-record as deflection measurement

To see in which way measuring deflection only with the piston influences the measured EABS, the EABS is calculated with piston displacement as the only deflection measurement. Also for this calculation the deflection-curve are made linear up to 80 % of peak load, as explained in chapter 1.3.2.

The results from these calculations are shown in Table 35 for the panels tested at NTNU and in Table 36 for the panels tested at NPRA.

Table 35 EABS when only Piston-record is used for calculation, NTNU

Concrete type	P_{Max} [kN]		W_5 [J]		W_{10} [J]		W_{20} [J]		W_{40} [J]	
	A*	B*	A*	B*	A*	B*	A*	B*	A*	B*
Blanco	25,6	25,6	26	26	26	26	26	26	26	26
MF20	29,6	29,6	72	70	110	110	155	154	193	193
MF40	33,1	33,1	102	97	168	166	240	240	305	305
MF60	31,6	31,6	123	109	207	201	311	309	405	405
SF4.5	31,8	31,8	59	57	103	102	172	172	246	246
SF9	30,5	30,5	82	77	158	154	270	269	381	381
* A: Values when laser-record and piston-record are connected as described in chapter 1.3.3 B: Values when only Piston-record is used										

Table 36 EABS when only Piston-record is used for calculation, NPRA

Concrete type	P_{Max} [kN]		W_5 [J]		W_{10} [J]		W_{20} [J]		W_{40} [J]	
	A*	B*	A*	B*	A*	B*	A*	B*	A*	B*
Blanco	28,5	28,5	26	26	26	26	26	26	26	26
MF20	27,8	27,8	64	63	99	98	139	139	175	175
MF40	32,3	32,3	100	97	162	161	240	239	313	312
MF60	31,5	31,5	112	104	190	187	285	284	372	372
SF4.5	32,9	32,9	60	59	106	105	176	176	254	251
SF9	32,4	32,4	79	77	150	148	253	252	354	354
* A: Values when laser-record and piston-record are coupled B: Values when only Piston-record is used										

As seen in Table 35 and Table 36, the calculated W_{40} is more or less the same. This is actually not surprisingly, because the only difference between the two deflection values is the strain of the load train, and the strain is proportional to the load. At 40mm displacement the applied load is less than 5kN, which means that the influence on the displacement measurement is practically zero. (If the radius of the load train is 6.7mm, the length is 300mm, E-modulus equal to 210 000 MPa and the load equal to 5 kN, the strain in the load train results in a contraction of the load train of approximate 0.05 mm). Another factor that may influence the results is the uncertainty of the load measurement. In general, results when the load is small are less precise than when the load is larger, and the incorrectness is depending on the maximum capacity of the hydraulic jack.

If the deflection at which cracking occurs, or the EABS up to cracking, is of interest, it is important to measure the deflection at the tensile surface of the specimen.

Table 37 and Table 38 show the central deflection at peak load and EABS up to peak load for NTNU and NPRA, respectively. For all panels, the peak load corresponds to the deflection at which cracking occurs.

Table 37 EABS up to peak load, NTNU

Concrete type	Deflection at peak load [mm]		EABS up to peak load [J]	
	A*	B*	A*	B*
Blanco	0.30	1.24	5.9	17.3
MF20	0.45	1.74	10.4	28.3
MF40	0.53	1.63	11.8	30.0
MF60	0.50	2.44	10.2	41.9
SF4.5	0.41	1.41	9.4	22.7
SF9	0.49	1.51	9.7	24.4
* A: Values when laser-record and piston-record are coupled B: Values when only Piston-record is used				

Table 38 EABS up to peak load NPRA

Concrete type	Deflection at peak load [mm]		EABS up to peak load [J]	
	A*	B*	A*	B*
Blanco	0.61	1.16	9.7	17.7
MF20	0.63	1.27	10.5	19.6
MF40	0.74	1.46	14.3	25.7
MF60	0.74	1.93	14.1	32.2
SF4.5	0.58	1.36	10.5	24.3
SF9	0.68	1.36	12.9	23.9
* A: Values when laser-record and piston-record are coupled B: Values when only Piston-record is used				

As seen from Table 37 and Table 38, the deflection at cracking and the EABS up to peak load are overestimated if only the piston-record is used. When looking at the load-deflection curve this is quite obvious, an example of a load-deflection curve is shown in Figure 5. Because the EABS is the area between the load-deflection curve and the X-axis, the EABS will increase when the deflection at peak load increases.

2.5 The effect of using only the LVDT-record as deflection measurement

At NPRA and NTNU the deflection is measured with the LVDT beyond the deflection at which cracking occurs. At NPRA this has been possible by use of a disc on the top of the LVDT. This disc can rotate along with the rotation of the panels, as well as bridging over the cracks. At NTNU the deflection is measured by a laser. At the tension side of the panels, a thin flexible sheet of plastic is attached. This plastic sheet prevents the laser to “be lost” in the cracks.

The effect of using only the LVDT/laser-record as deflection measurement is shown in Table 39 and Table 40.

Table 39 Mean values for the panels tested at NTNU, only deflection measurement by laser

Concrete type	P_{Max} [kN]		W_5 [J]		W_{10} [J]		W_{20} [J]		W_{40} [J]	
	A*	B*	A*	B*	A*	B*	A*	B*	A*	B*
Blanco	25,6	25,6	26	17	26	17	26	17	26	17
MF20	29,6	29,6	72	65	110	100	155	142	193	178
MF40	33,1	33,1	102	98	168	162	240	235	305	300
MF60	31,6	31,6	123	119	207	200	311	303	405	397
SF4.5	31,8	31,8	59	53	103	97	172	162	246	233
SF9	30,5	30,5	82	79	158	155	270	262	381	368
* A: Values when laser-record and piston-record are coupled B: Values when only laser-record are used										

Table 40 Mean values for the panels tested at NPRA, only deflection measurement by LVDT

Concrete type	P_{Max} [kN]		W_5 [J]		W_{10} [J]		W_{20} [J]		W_{40} [J]	
	A*	B*	A*	B*	A*	B*	A*	B*	A*	B*
Blanco	28,5	28,5	26	22	26	22	26	22	26	22
MF20	27,8	27,8	64	62	99	96	139	137	175	174
MF40	32,3	32,3	100	100	162	164	240	245	313	322
MF60	31,5	31,5	112	111	190	190	285	287	372	381
SF4.5	32,9	32,9	60	57	106	103	176	173	254	250
SF9	32,4	32,4	79	78	150	150	253	253	354	357
* A: Values when LVDT-record and piston-record are coupled B: Values when only LVDT-record are used										

As seen in Table 39, for the panels tested at NTNU the procedure with coupling the piston measurement and the laser measurement overestimates the EABS for all concrete types and at all deflection levels. For the NPRA-panels the relationship is not as clear as for the NTNU-panels. As seen in Table 40, the W_5 is overestimated when the LVDT-record and the piston-record are coupled for all concrete types. But when the deflection is increased to 40 mm, the relationship is not that clear. W_{40} for the SF9-, MF60- and MF40-concrete seems to be underestimated when the deflection measurements are coupled.

There seams to be two reasons why A and B in and Table 40 do not give the same results:

1. The compliance of the load train is not the same when the load decreases as when the load increases.
2. The deflection-record is not necessarily the same when the record are made at the upper side and at the under side of the panel.

Compliance of the load train

The difference in load train compliance can be seen in Figure 13. Even though the *LVDT-curve* and the C*oupled-curve* are identical up to peak-load, there is a small difference after peak load. (The compliance of the load train is calculated with the load-deflection values at zero load and peak load, as described in chapter 1.3.3.) If the compliance of the load train is the same when the load decreases, the *LVDT-curve* and the *Coupled-curve* would be identical also when unloading. This effect is important when the deflections are small, and can explain why W_5 in general is higher both for the panels tested at NTNU and NPRA. When the deflection is larger, the load level is less; hence the contraction in the load train is reduced and the results would be more or less the same even though the compliance of the load train is different at unloading.

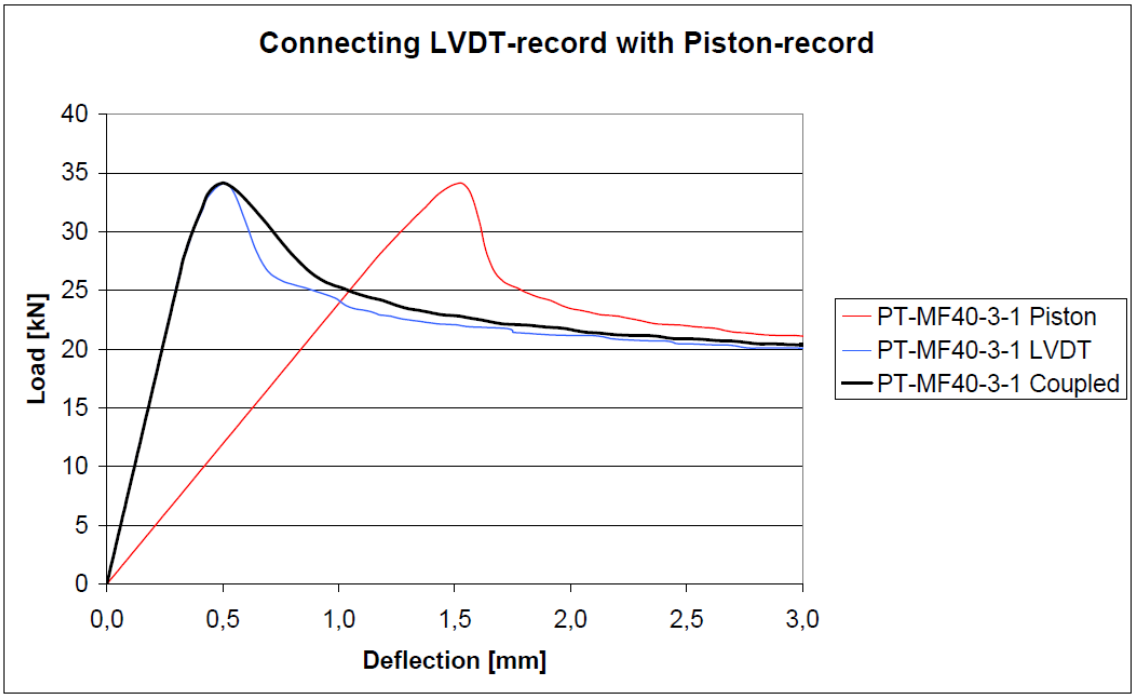

Figure 13 Difference in load-deflection curve

Difference in measured deflection at the upper side and the under side of the panel
It can be shown by geometrical calculation that for a perfect panel with smooth surfaces, and where the cracks occurs halfway between the supports, the deflection will be almost the same when measured at the upper side of the panel as when measured at the under side of the panel. (40.00 mm at the under side corresponds to 39.97 mm at the upper side according to the calculation in Appendix 1).

But, of course, none of the panels are perfect, which means that it is impossible to neglect this effect. If the Piston-record gives less deflection than the LVDT-record at the same load, the result will be that the EABS for the Piston-record will be less than the EABS for the LVDT-record, because the load is decreasing with increasing deflection. In Table 41 the load at 40 mm deflection is summarized for the panels tested at NTNU and NPRA.

Table 41 Load at 40 mm deflection, panels tested at NTNU and NPRA

	NTNU Load at 40 mm deflection [kN]		NPRA Load at 40 mm deflection [kN]	
	Coupled	Laser-record	Coupled	LVDT-record
MF20	1,04	0,93	0,92	0,94
MF40	1,76	1,77	2,04	2,16
MF60	2,43	2,52	2,50	2,78
SF4.5	2,47	2,35	2,76	2,83
SF9	3,56	3,41	3,45	3,56

From the values in Table 41 it is clear that for the panels tested at NPRA the load at 40 mm deflection is higher for the LVDT-record than the coupled-record, which will result in higher contribution to W_{40} when EABS is calculated with the LVDT-record than when the EABS is calculated with the coupled-record.

For the panels tested at NTNU the laser-record gives higher load at 40 mm deflection than the coupled-record for the MF60-panels. For the MF40-panels the load are approximate the same, while for the other panels the coupled-record gives higher load at 40 mm deflection than the laser-record.

Summarized
The difference in compliance when the load increases and the load decreases seems to be larger at NTNU than at NPRA. This can be seen in Table 39 and Table 40, which shows that the difference in W_5 is larger for the panels tested at NTNU than the panels tested at NPRA. In general, the difference in compliance results in higher W_5 when the coupled-record is used as deflection than when the LVDT- or laser-record are used.

Whether the deflection is measured at the upper side of the panel or at the under side of the panel will affect the calculated EABS, even though compliance is the same when the load increases and the load decreases. It is not possible to know beforehand which of the two deflection measurement methods described in ASTM C 1550 that will give the highest W_{40}. This is because it is not possible to know which method that will give largest deflection (or highest load at a given deflection).

The results from the calculations in this chapter show that even though ASTM C 1550 describes that both the LVDT-record and the coupled-record may be used for EABS calculation, the results are dependent on which method that is used.

2.6 The effect of making the load-deflection curve linear

2.6.1 LVDT-/laser-record

The EABS are calculated with and without linear adjustment for all panels tested at NPRA and NTNU. Even though the LVDT-/laser-record are not made linear, it is shifted to the left if necessary to intersect origin.

There is no significant effect on the EABS with regard to making the laser-/LVDT-record linear up to 80% of peak load. If there is any effect, the difference in results is some tenth of a joule.

2.6.2 Piston-record

The EABS are calculated as in chapter 2.6.1. This check is made for some panels only. For the NTNU-panels, the EABS is calculated with and without linear adjustment for the piston-record for the panels in the B-series, MF40-series and SF9-series. For the KUL-panels the EABS is calculated for the MF20-series. For the BBRI-panels, the calculation is made for the MF60-series.

Like the LVDT-/laser-record, there is no significant effect of making the piston-record linear on the W_{40}. If there is any effect, the difference in results is some tenth of a joule. At less deflection, the difference is a little bit larger, but still only maximum 2 joule.

3 Control of crack widths

At KUL and BBRI LVDT's were mounted to measure the crack widths in addition to the deflection on some panels.

At KUL the crack widths are measured at all four panels in the MF40-series and the SF9-series. At BBRI the crack widths are measured at two panels in all series, except the Blanco-series, where crack widths were measured at only one panel.

The results are showed in diagrams, with the deflection calculated according to chapter 1.3.3. In addition to the crack widths, the load-deflection relationship is shown in the same diagrams.

For the BBRI-results, the deflection in the crack- deflection curve is simply the LVDT-record. The reason for this is that the data logging system had different frequency for the Piston-record and the LVDT-record, which makes it difficult to relate one set of deflections with another one. The deflection in the load-deflection curve is the deflection according to chapter 1.3.3.

If the panels cracks in three equally sized segments and the support is in the middle of each segment, all three cracks should have equal crack widths. Further, if there is no radial or tangential strain in the concrete (no influence of friction between the support and the concrete), the three segments will rotate as rigid bodies, and the crack openings along every crack will be equal. The relationship between crack openings and deflection will then be linear.

On the other side, if the friction between the support and the concrete is sufficient, the concrete will obtain a radial strain resulting in larger crack openings near the centre of the panel relative to the end of the panel. The relationship between crack openings and deflection will in this case not be linear, but the crack opening rate will increase with increasing deflection because the load, and thereby the effect of friction, is reducing with increasing deflection.

3.1 Comparison of crack openings

3.1.1 KUL panels

Figure 14 to Figure 21 shows the relationship between crack openings, deflection and load for the panels tested at KUL. The first four figures show the results for the MF40-panels, while the last four figures show the results for the SF9-panels.

General comment to Figure 14 to Figure 21:
It seems like there has been some problem with the LVDT that was mounted at crack 1. For all panels, the crack width record has stopped at a crack width between 10 mm and 15mm, except for SF-1-2, where the crack width record is equal to zero during the whole test.

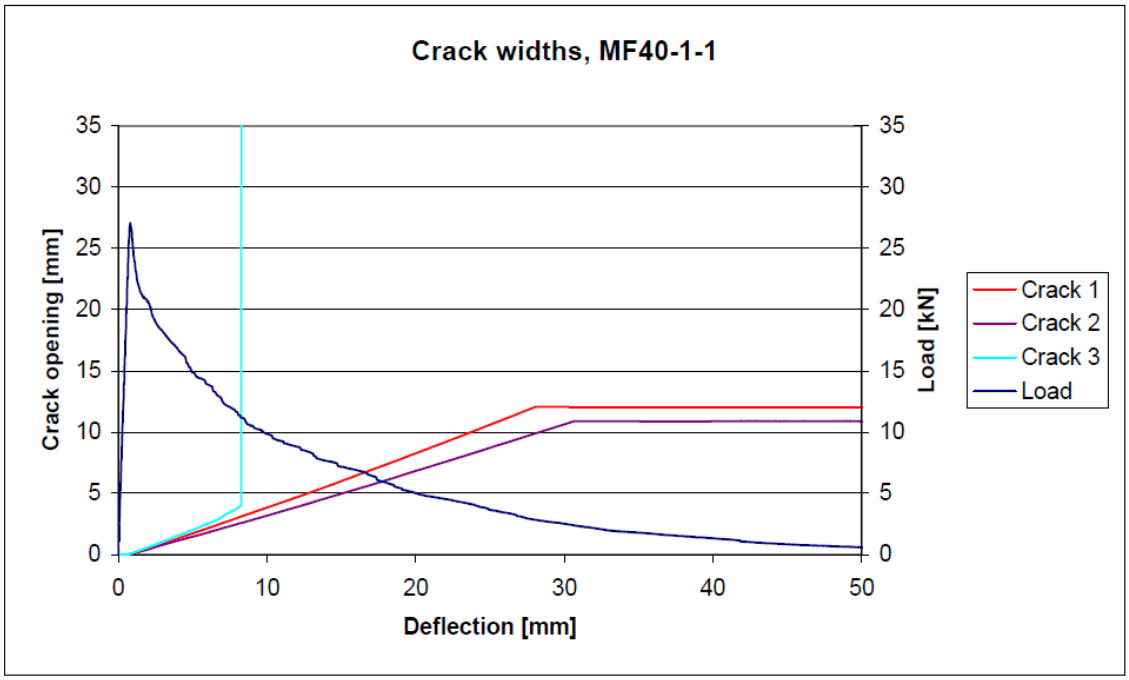

Figure 14 Crack openings MF40-1-1

Comments:

- The measurement in crack 3 seems to be lost of some reason after approximate 8 mm deflection, probably due to the limitation of the LVDT.
- The measurement in crack 1 and crack 2 seems to be lost of some reason after approximate 30 mm, probably due to the limitation of the LVDT. It is unlikely that the crack growth really stopped at deflection equal to approximate 30 mm.
- The crack width in crack 1 and crack 2 seems to approximate the same.

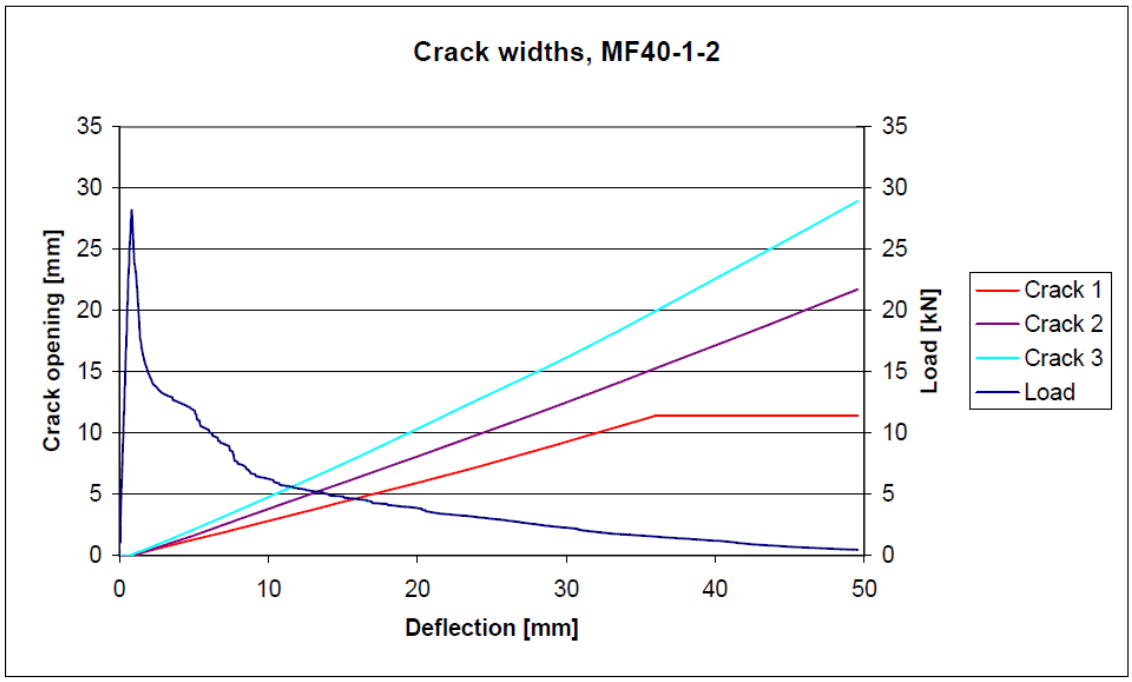

Figure 15 Crack openings MF40-1-2

Comments:

- It seems like crack 3 was the major crack, and that all cracks increased in width during the test. (It is not likely that crack growth in crack 1 really stopped after approximate 35 mm deflection).

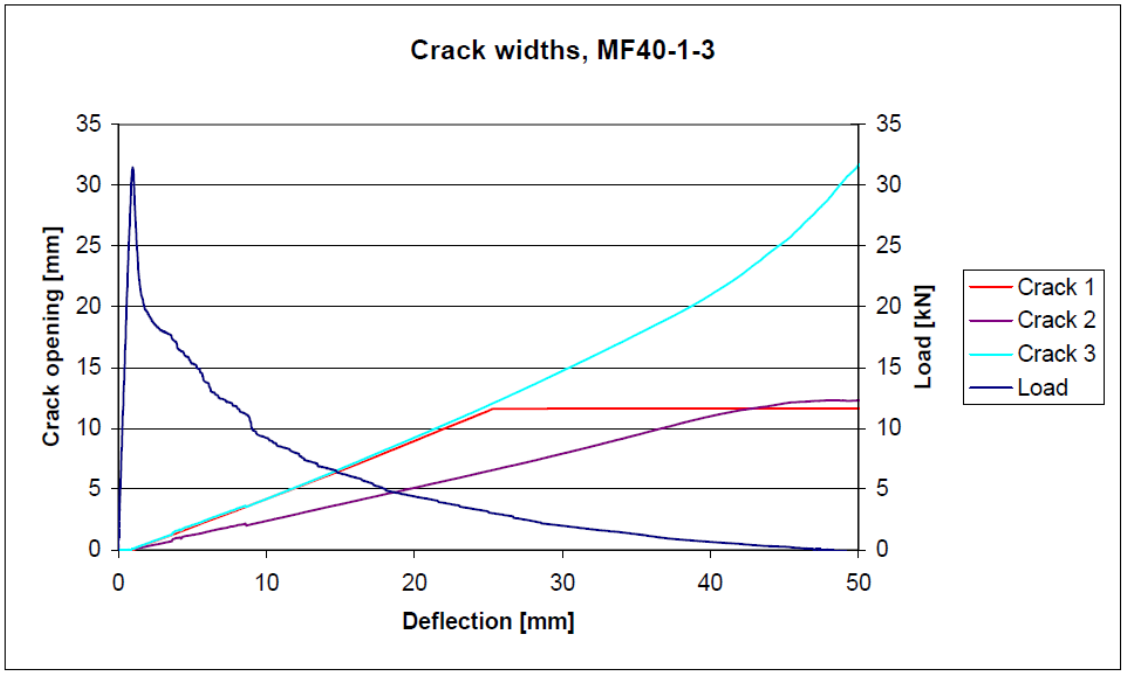

Figure 16 Crack openings MF40-1-3

Comments:

- It seems like crack 1 and crack 3 was the major cracks. The crack growth in crack 2 was less during the whole test.

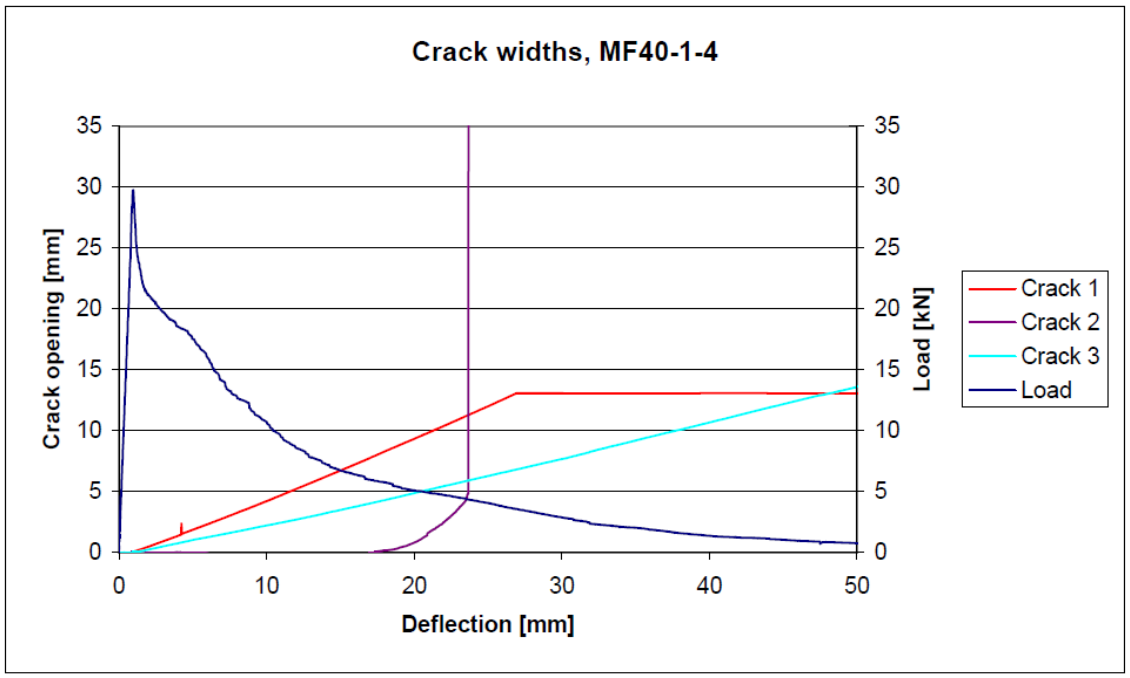

Figure 17 Crack openings MF40-1-4

Comments:

- It seems like crack 1 was the major crack. The apparent behaviour of crack 2 is most likely due to measuring technical problem, and not the real crack growth.

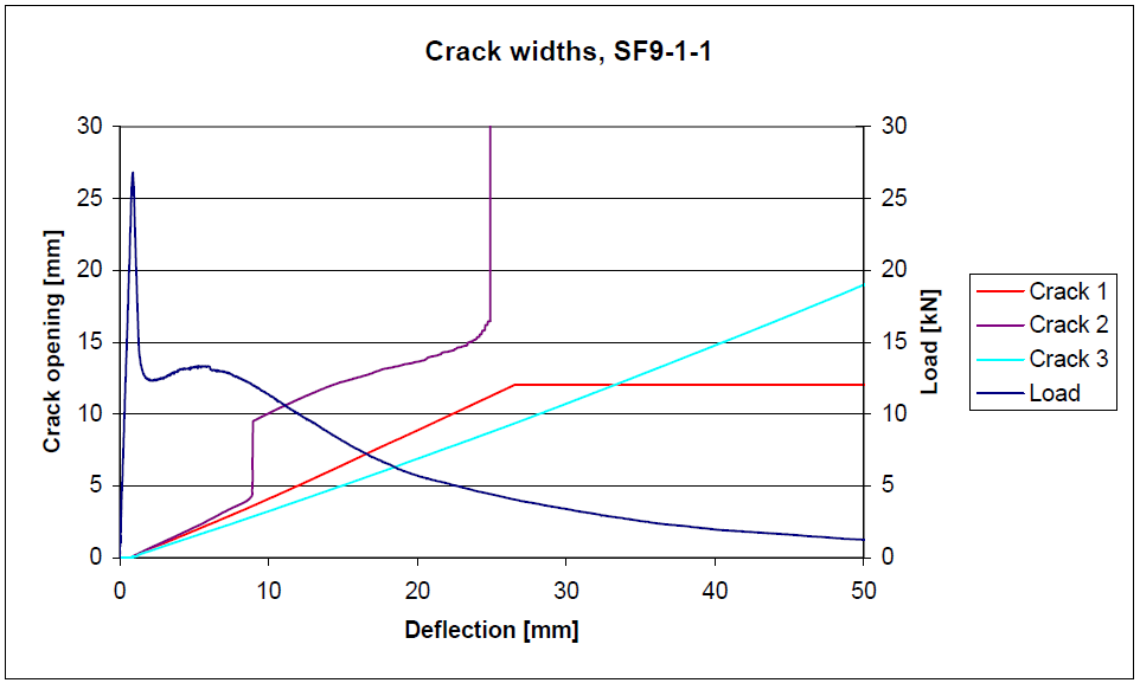

Figure 18 Crack openings SF9-1-1

Comments:

- Once again, there seems to be some technical problem with the crack growth measuring. It is difficult to analyze the result.

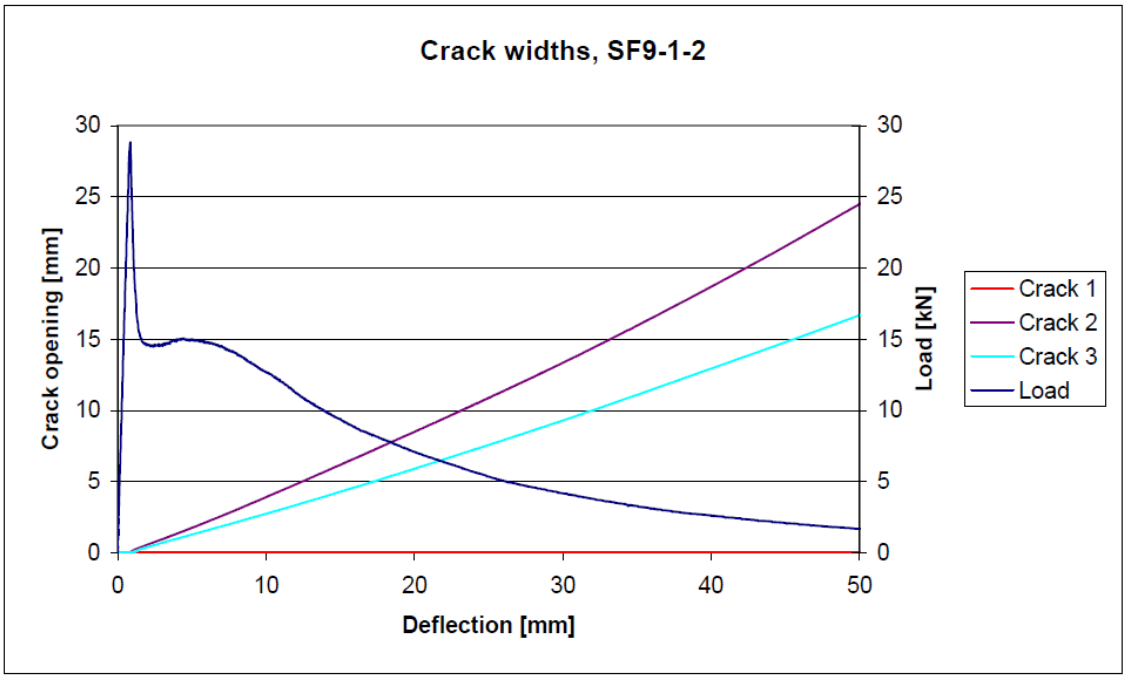

Figure 19 Crack openings SF9-1-2

Comments:

- It seems like crack 2 was the major crack.
- There are two possible explanations of the LCDT-record in crack 1
    1. Beam like failure, resulting in no crack where the LVDT was mounted
    2. The LVDT-record in crack 1 is untrustworthy.

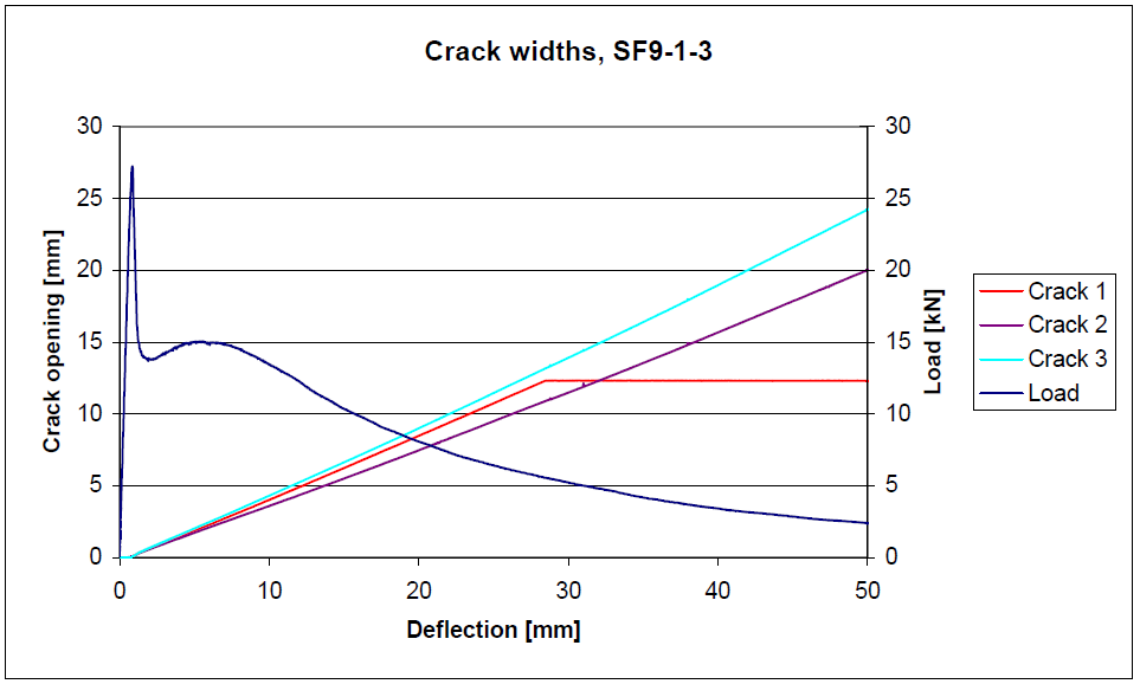

Figure 20 Crack openings SF9-1-3

Comments:

- It seems like the crack growth in all three cracks was more or less the same during the test.

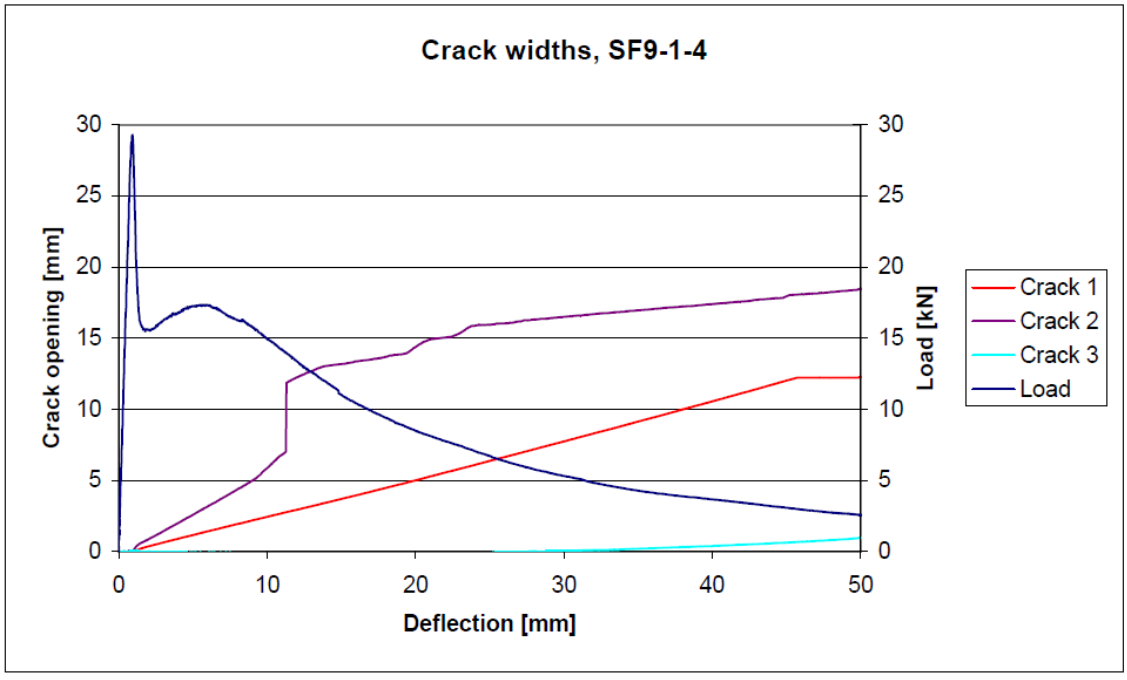

Figure 21 Crack openings SF9-1-4

Comments:

- The LVDT-record from crack 1 and crack 3 is untrustworthy.

3.1.2 BBRI panels

Figure 22 to Figure 32 show the relationship between crack openings, deflection and load for the panels tested at BBRI.

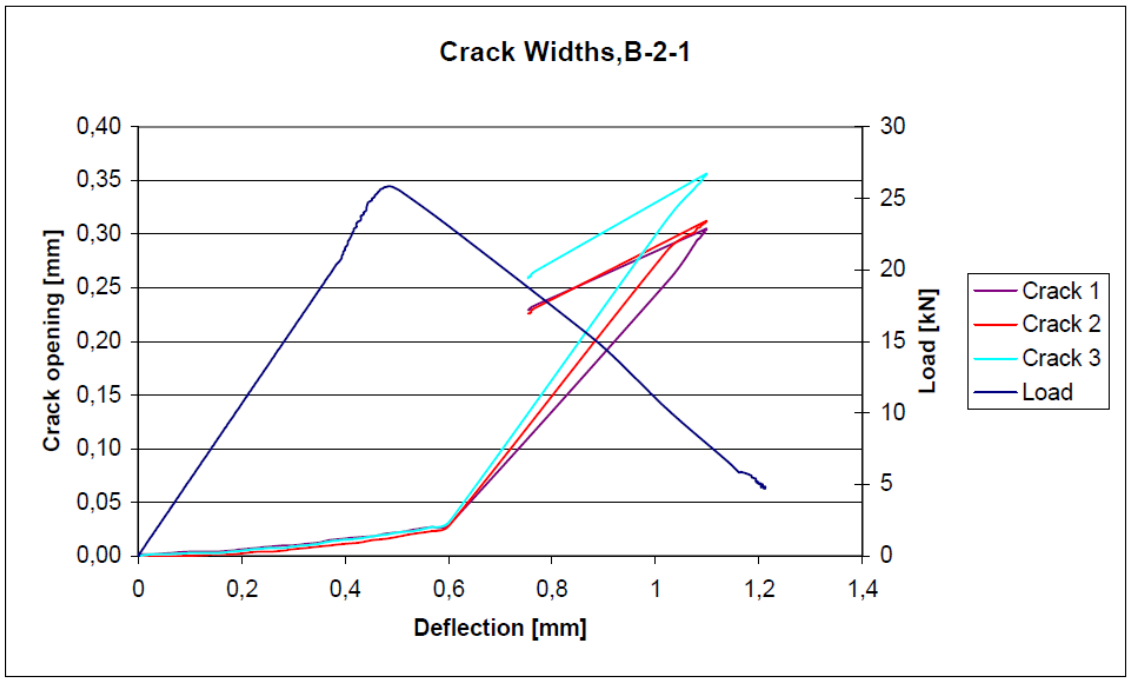

Figure 22 Crack openings B-2-1

Comments:

- For the panel without reinforcement, it seems like all three cracks have the same crack growth.
- The rapid increase in crack growths starts at approximately 0.6mm deflection, while the deflection at maximum load is approximately 0.5mm. One possible explanation for this is that the panel did not collapse once the ultimate load was reached, and that the crack "slowly" propagated upwards the panel.

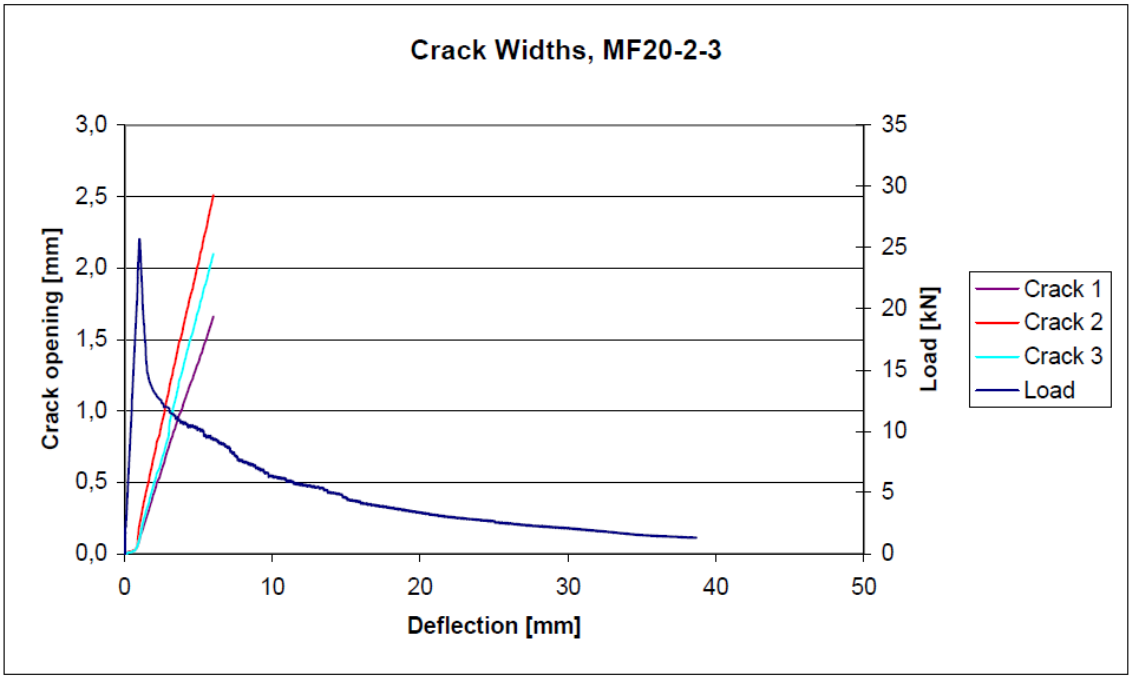

Figure 23 Crack openings MF20-2-3

Comments:

- The LVDT-record has stopped at approximate 8 mm deflection.

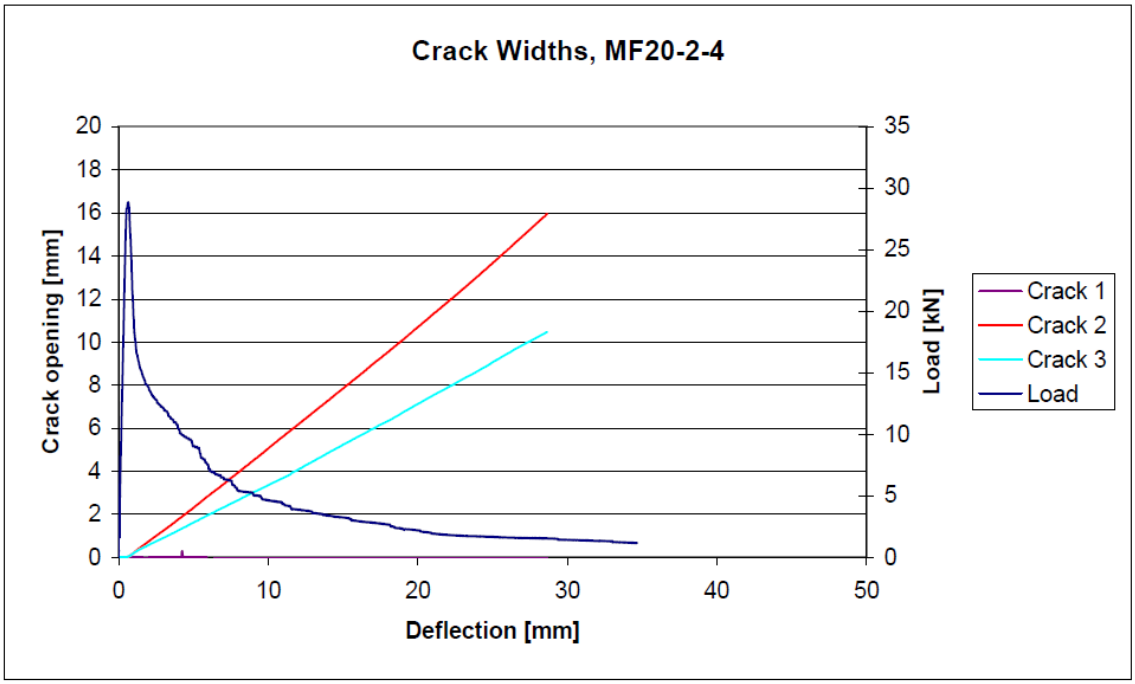

Figure 24 Crack openings MF20-2-4

Comments:

- The crack opening in crack 1 is zero during the whole test. The explanation is either that the specimen failed in a beam-like mode, or that the LVDT-record is not trustworthy.

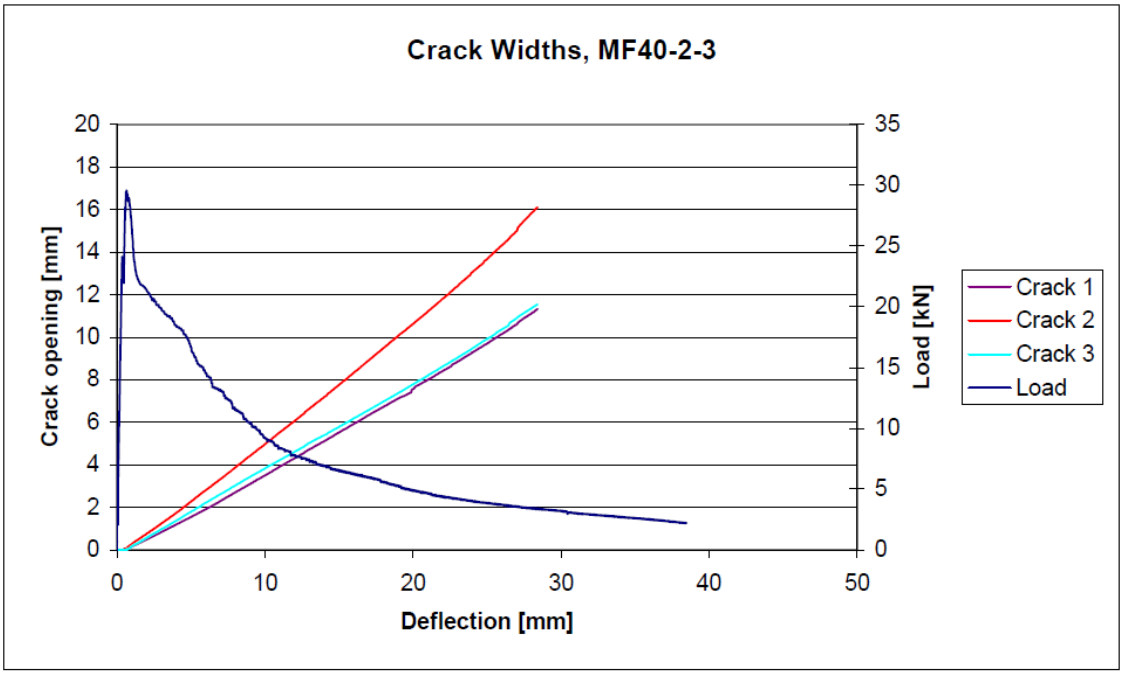

Figure 25 Crack openings MF40-2-3

Comments:

- Crack 2 seems to be the major crack, while crack 2 and crack 3 have equal crack growth.

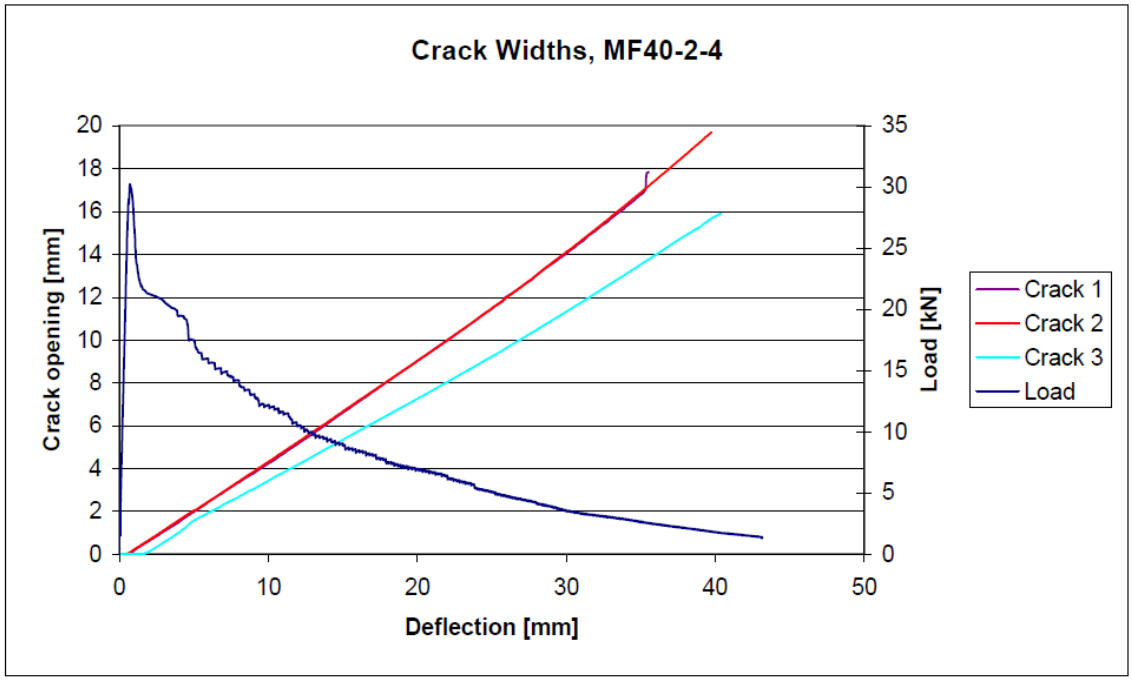

Figure 26 Crack openings MF40-2-4

Comments:

- Crack 1 and crack 2 have equal crack growth.
- It seems like crack 3 is starting to grow later than the other cracks, but this is most likely not correct. The explanation may be that the LVDT was not placed within its measuring range before the test started.

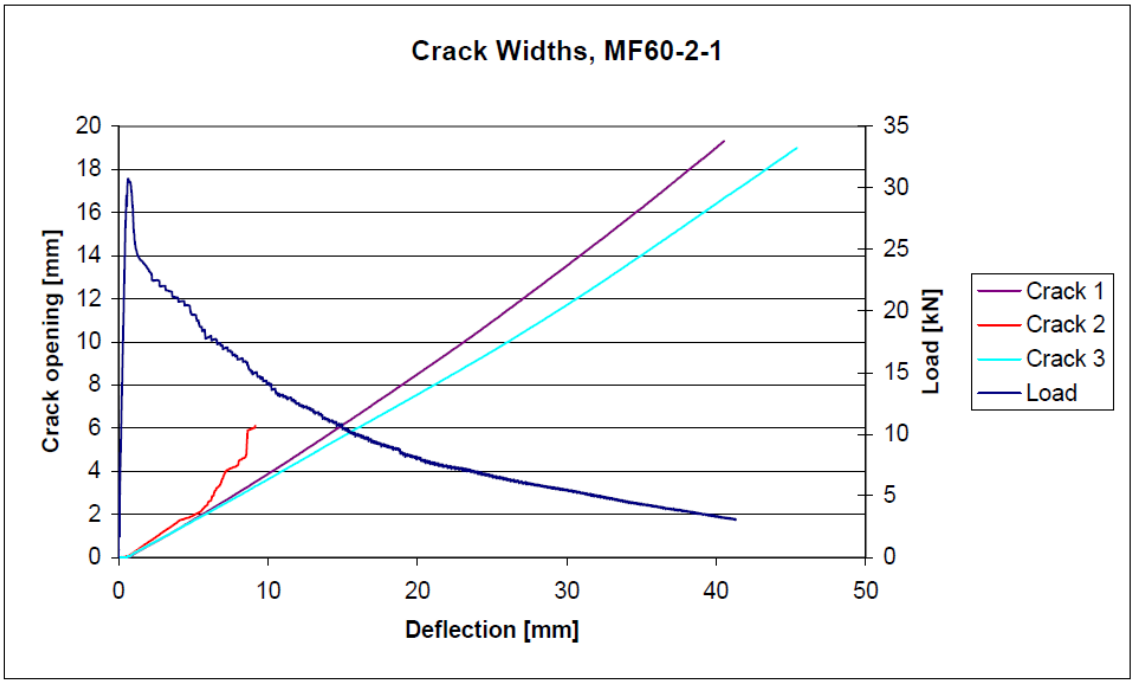

Figure 27 Crack openings MF60-2-1

Comments:

- The LVDT-record from crack 2 has stopped for some reason.

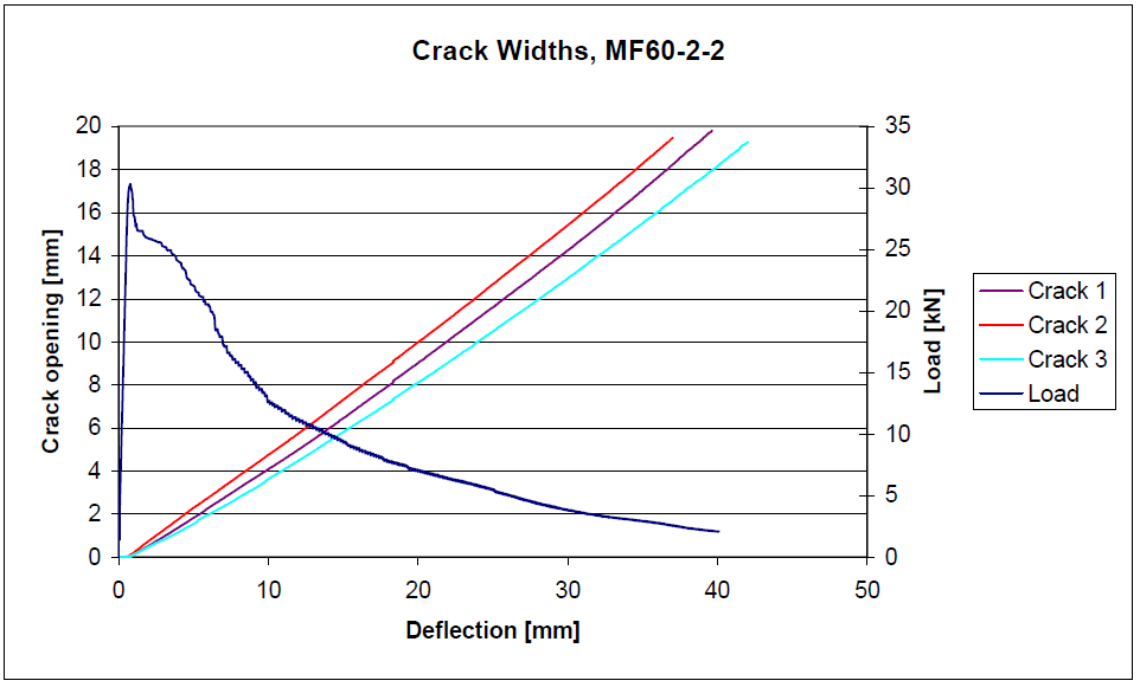

Figure 28 Crack openings MF60-2-2

Comments:

- All three cracks are more or less equal.

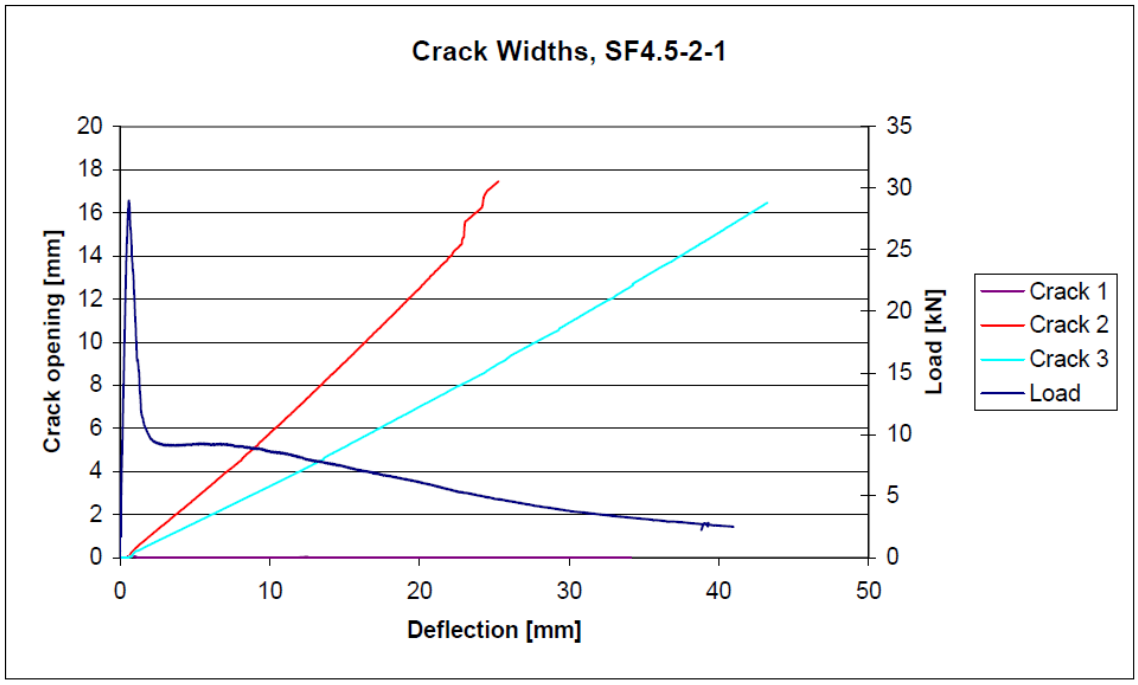

Figure 29 Crack openings SF4.5-2-1

Comments:

- It seems like crack 2 is the major crack.
- As for MF20-2-4, the LVDT-record from crack 1 is most likely not trustworthy.

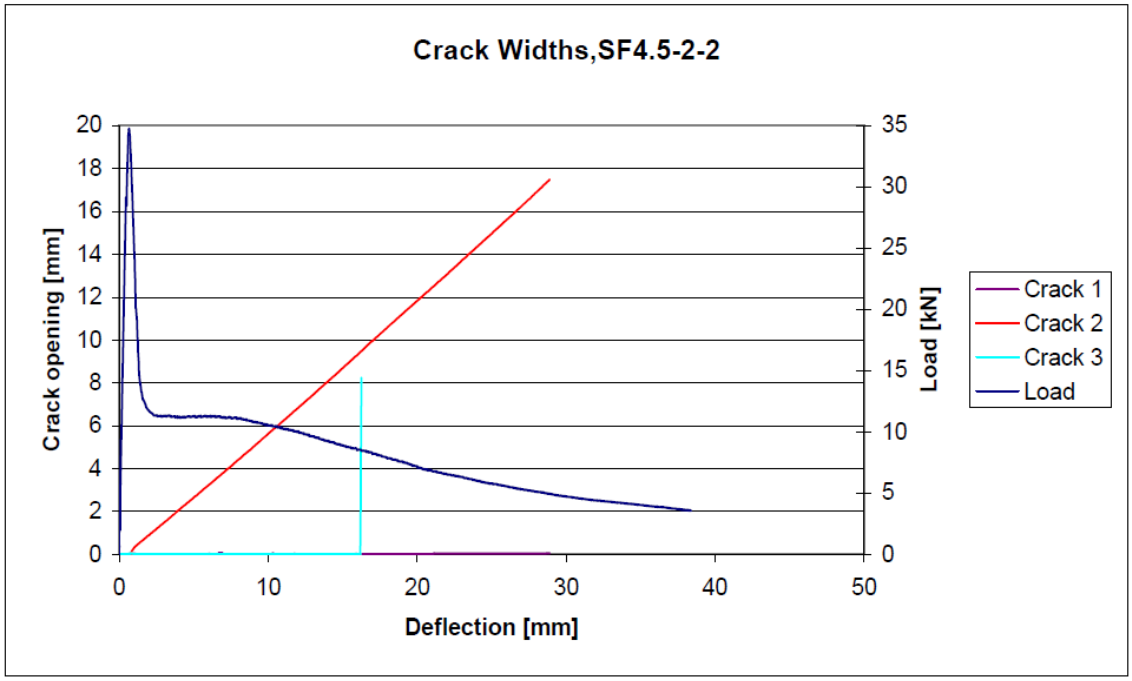

Figure 30 Crack openings SF4.5-2-2

Comments:

- The LVDT-record from crack 1 and crack 3 is not trustworthy.

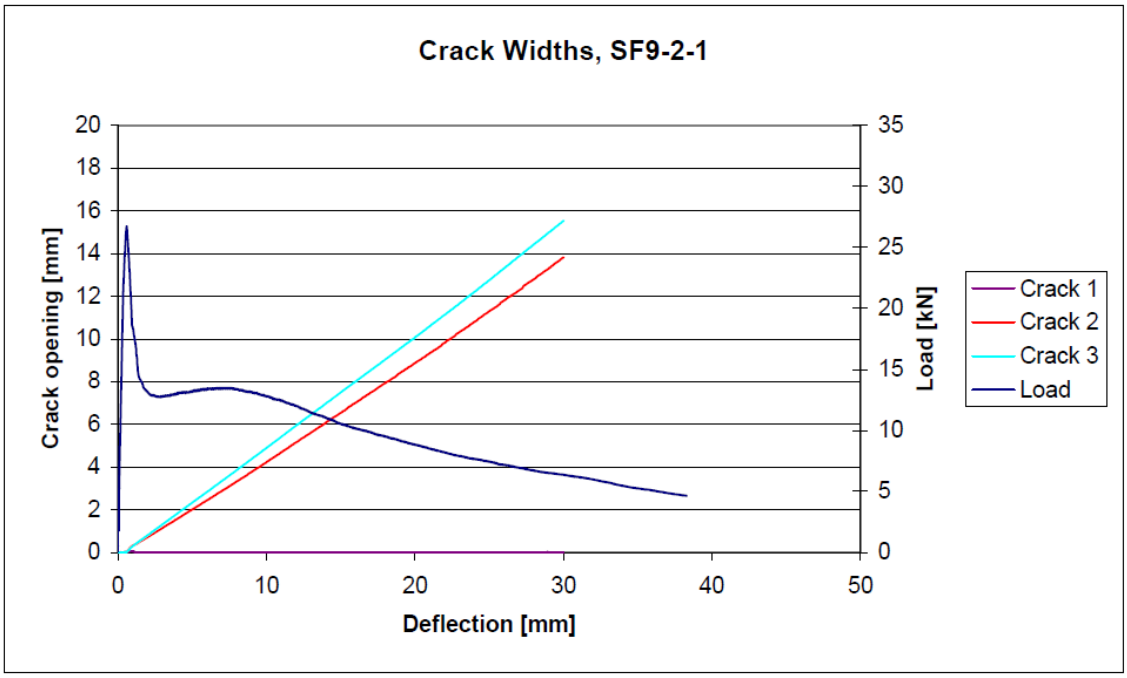

Figure 31 Crack openings SF9-2-1

Comments:

- The LVDT-record from crack 1 is not trustworthy.
- The crack growth in crack 2 and crack 3 is more or less equal.

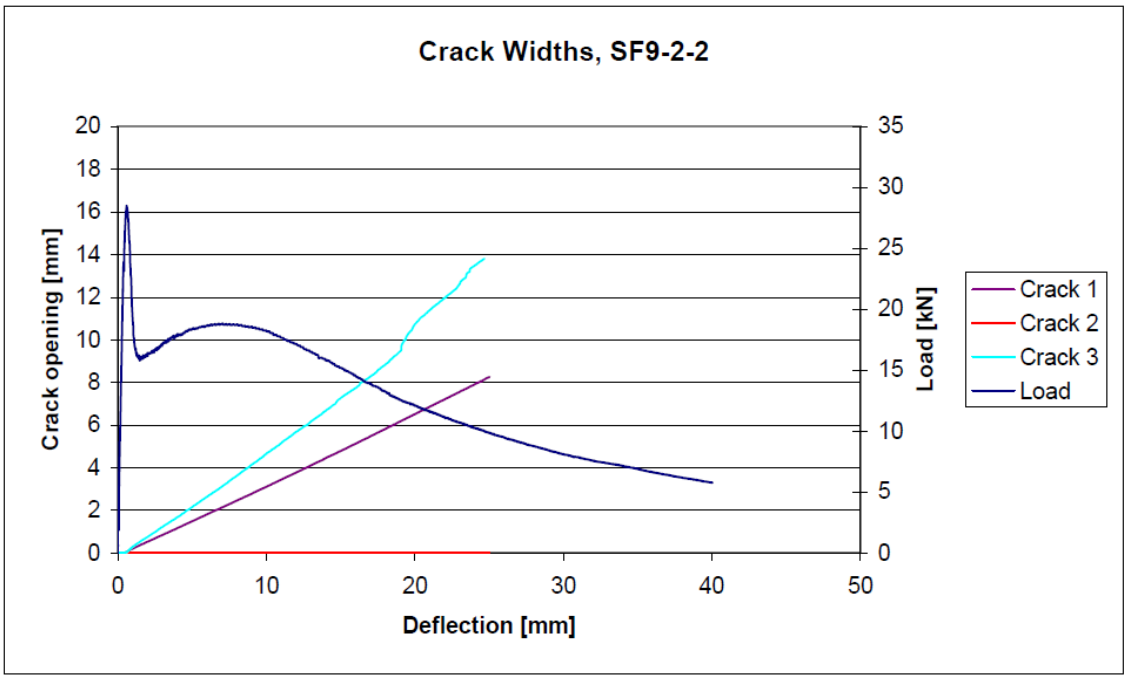

Figure 32 Crack openings SF9-2-2

Comments:

- The LVDT-record from crack 2 is not trustworthy.
- Crack 3 seems to be the major crack.

3.1.3 Crack openings summarized

As seen from Figure 14 to Figure 32, the crack growth is not necessarily the same in all three cracks. The simplest explanation of this is that the panels did not crack in three equally sized segments. Another important finding is that the relationship between crack opening and deflection is not linear. The crack growth is increasing with increasing deflection (for all reliable crack opening measurements), which indicates that the panels are influenced by friction between the support and the concrete.

3.2 Comparison of crack opening along one crack

3.2.1 KUL panels

Figure 33 to Figure 40 show the crack opening measured three places along one crack for the KUL-panels.

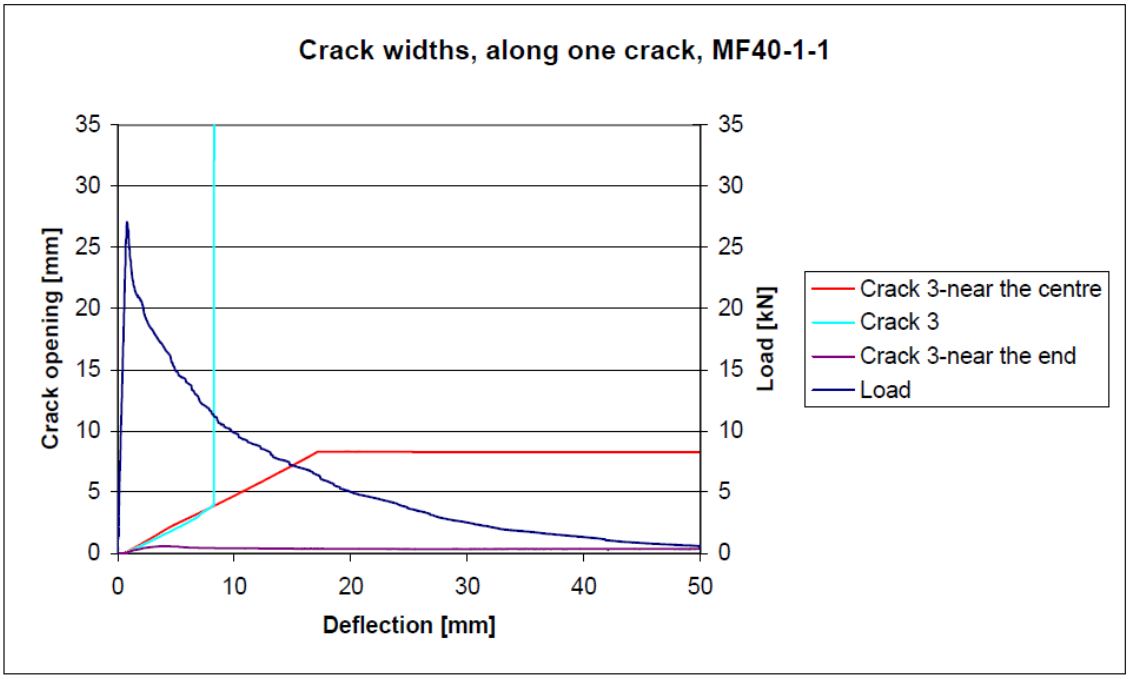

Figure 33 Crack opening along one crack, panel MF40-1-1

Comment:

- The LVDT-record from the LVDT near the centre and the LVDT near the end of the panel is untrustworthy.

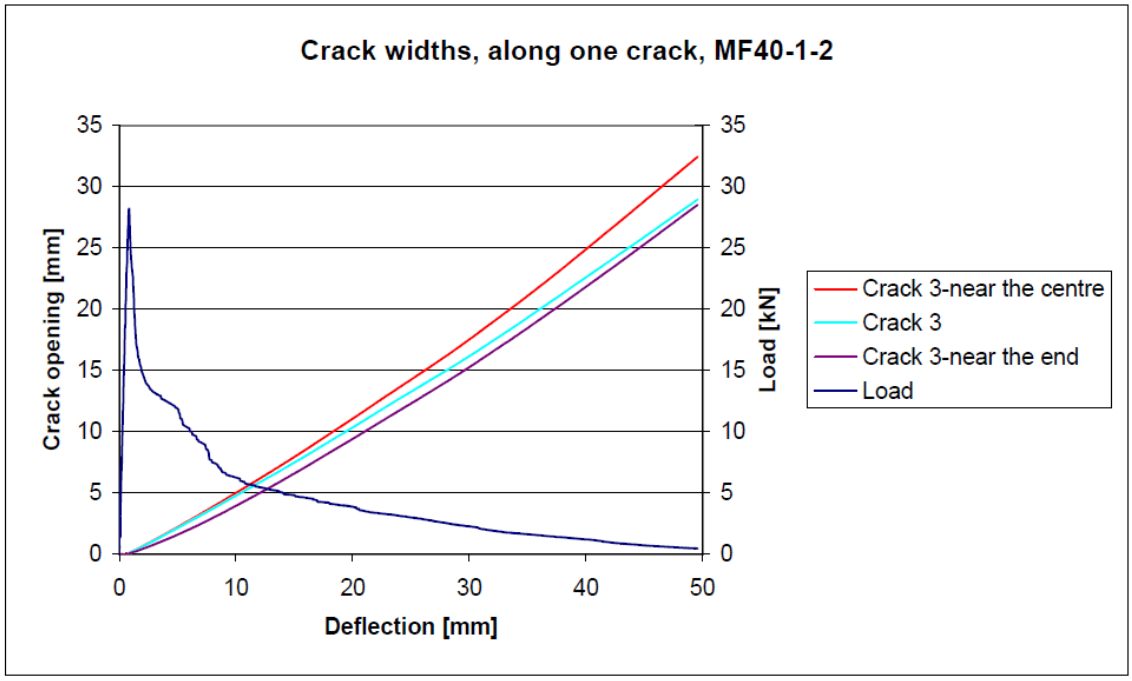

Figure 34 Crack opening along one crack, panel MF40-1-2

Comments:

- The crack growth is largest near the centre of the panel.

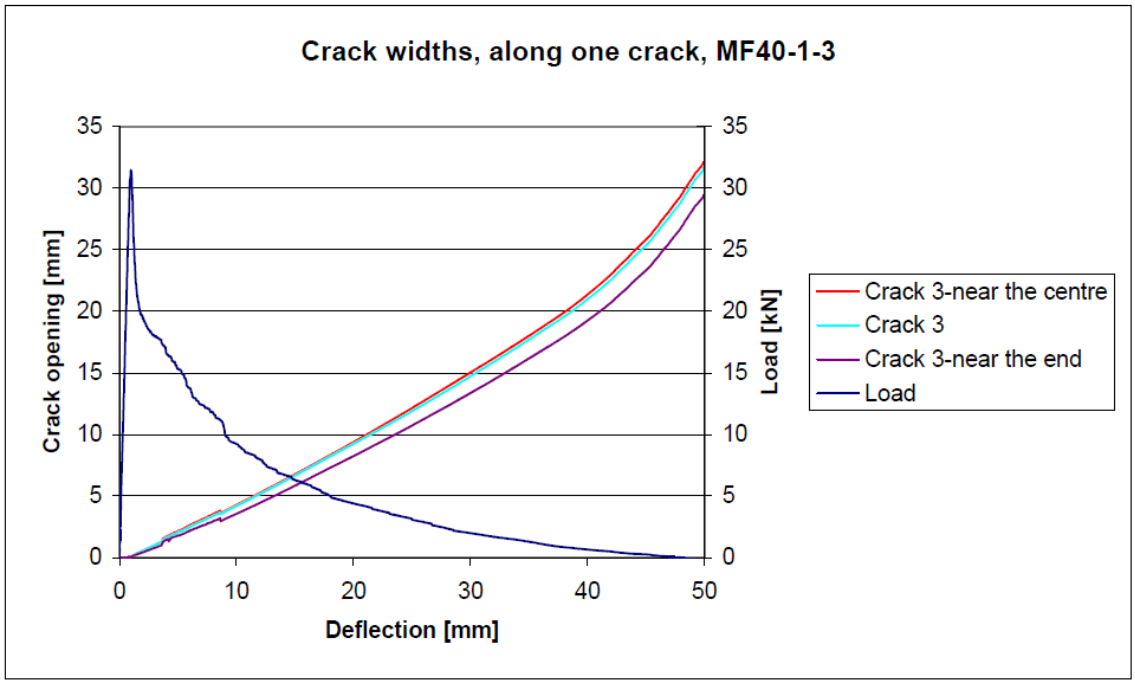

Figure 35 Crack opening along one crack, panel MF40-1-3

Comments:

- The crack growth is marginally larger near the centre of the panel.

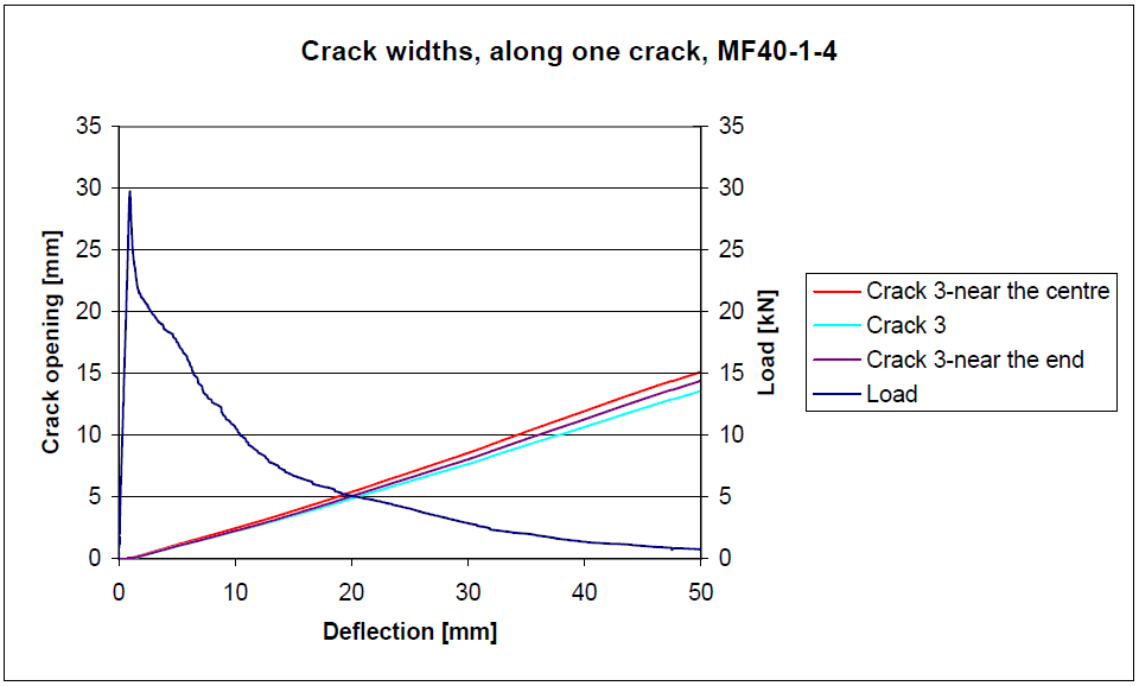

Figure 36 Crack opening along one crack, panel MF40-1-4

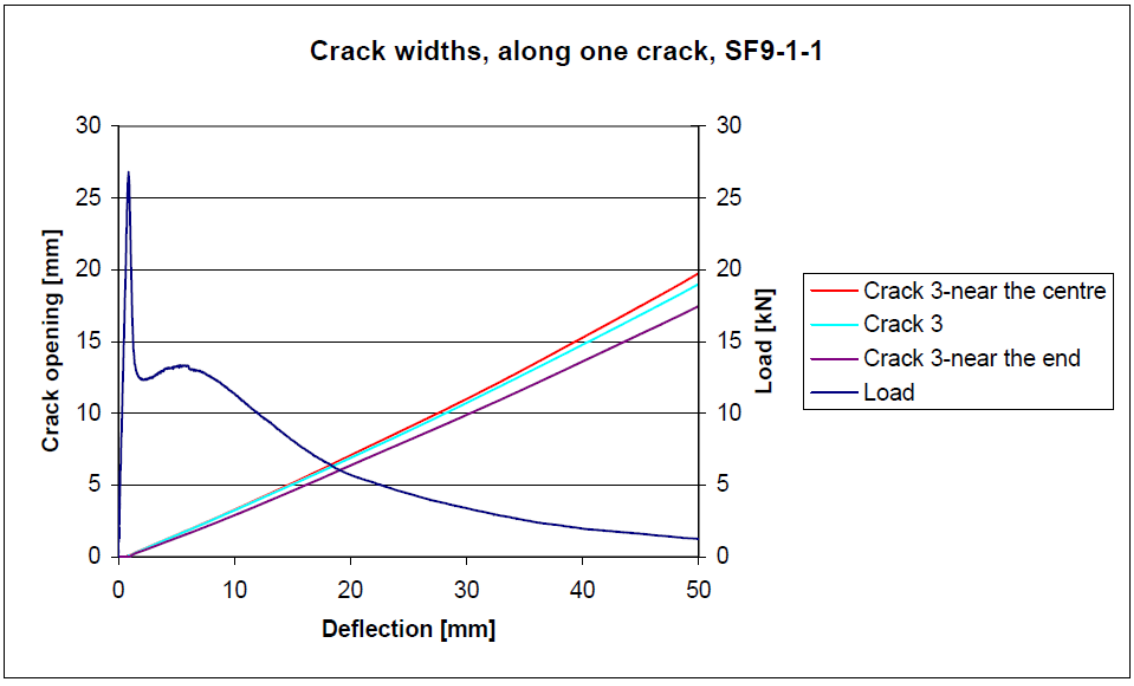

Figure 37 Crack opening along one crack, panel SF9-1-1

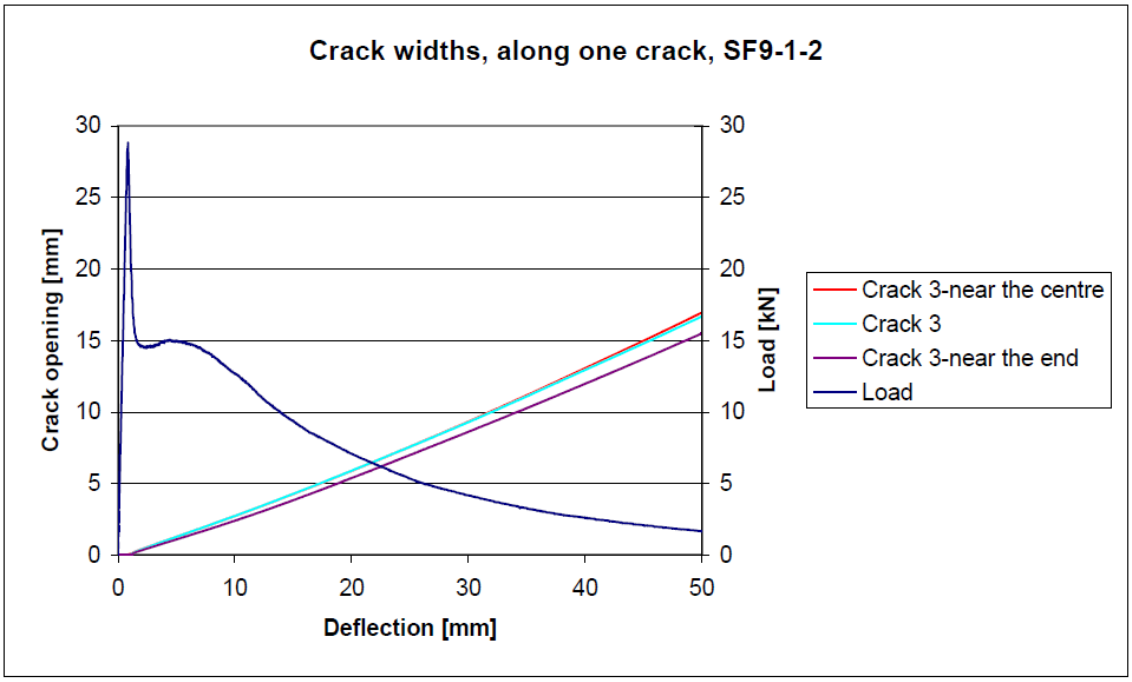

Figure 38 Crack opening along one crack, panel SF9-1-2

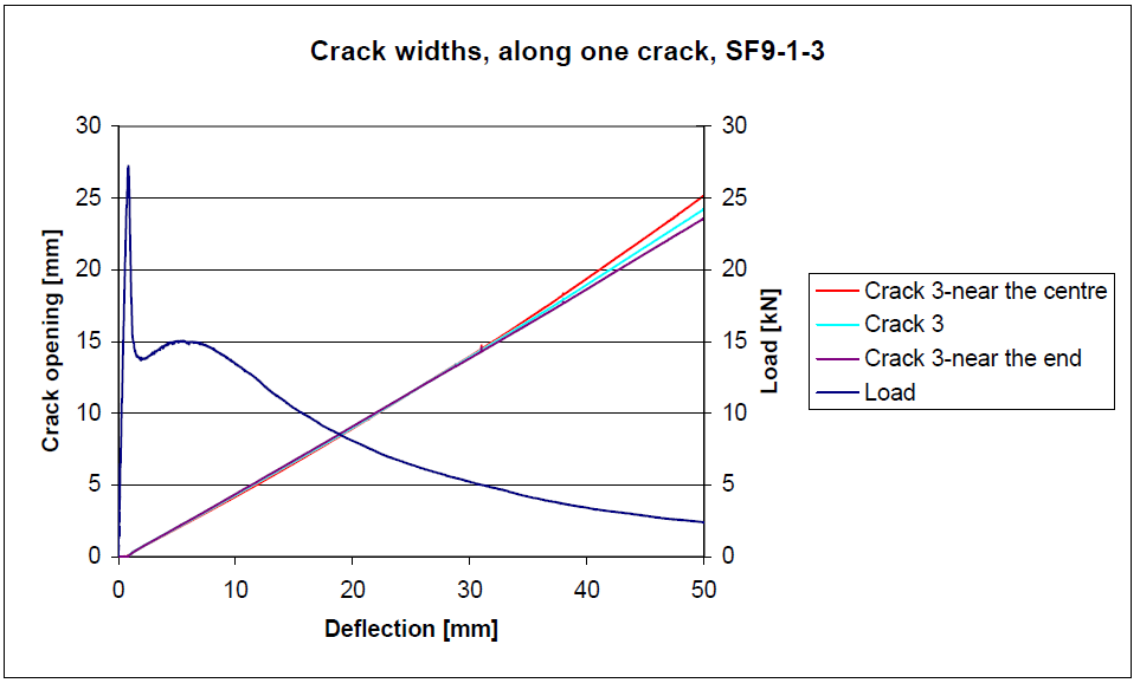

Figure 39 Crack opening along one crack, panel SF9-1-3

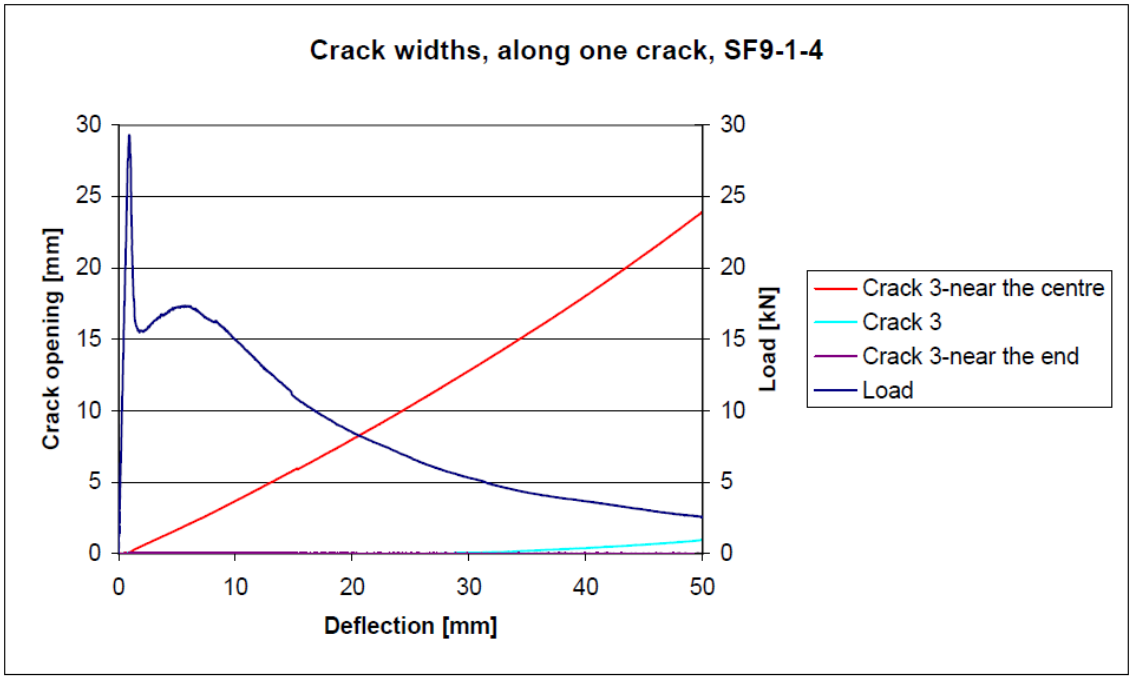

Figure 40 Crack opening along one crack, panel SF9-1-4

Comment:

- The LVDT-record from the LVDT near the mid-point of the panel and the LVDT near the end of the panel is untrustworthy.

3.2.2 BBRI panels

Figure 41 to Figure 51 show the crack opening measured three places along one crack for the BBRI-panels.

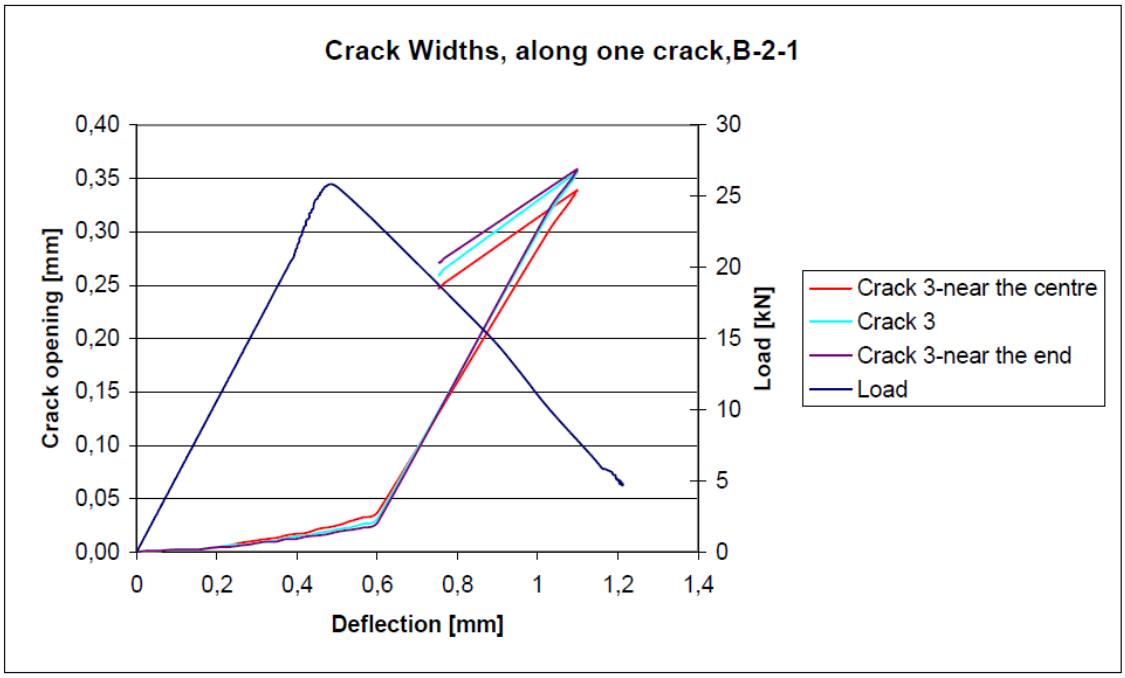

Figure 41 Crack opening along one crack, panel B-2-1

Comments: See Figure 22

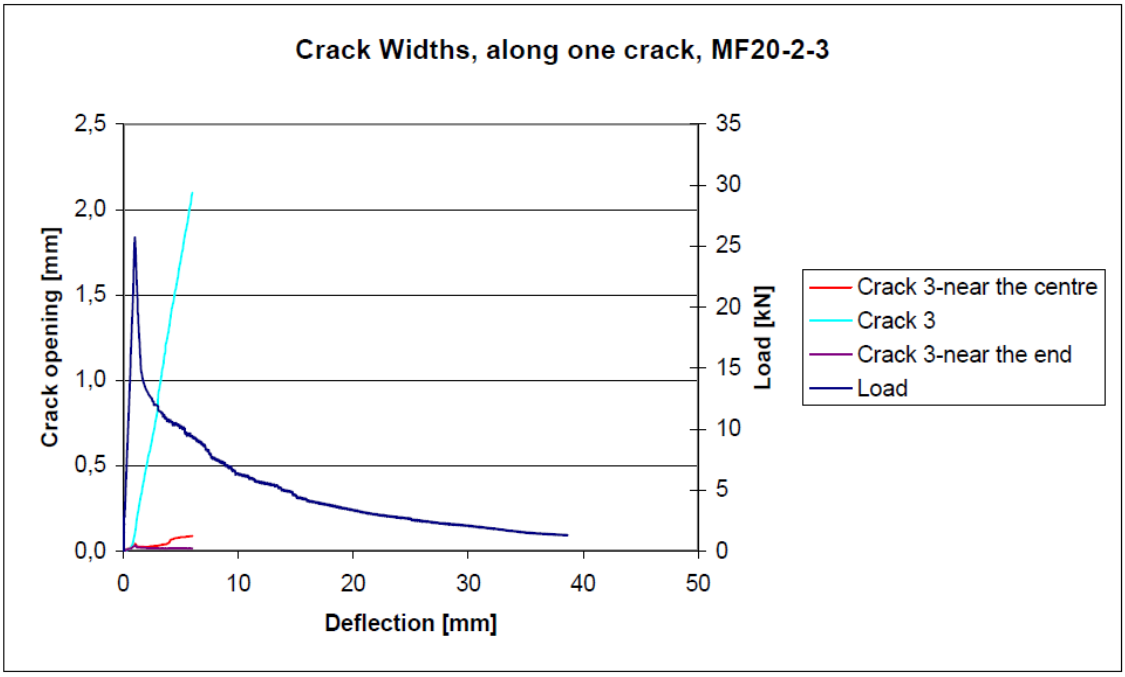

Figure 42 Crack opening along one crack, panel MF20-2-3

Comments:

- The LVDT-record has stopped at approximate 8 mm deflection.

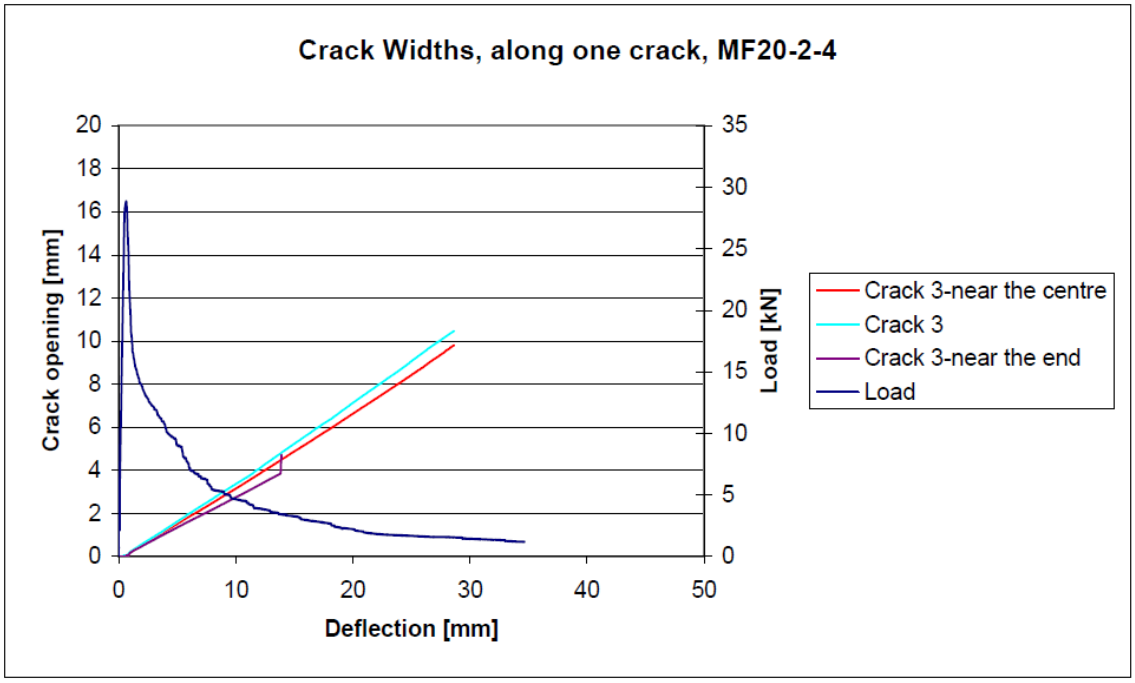

Figure 43 Crack opening along one crack, panel MF20-2-4

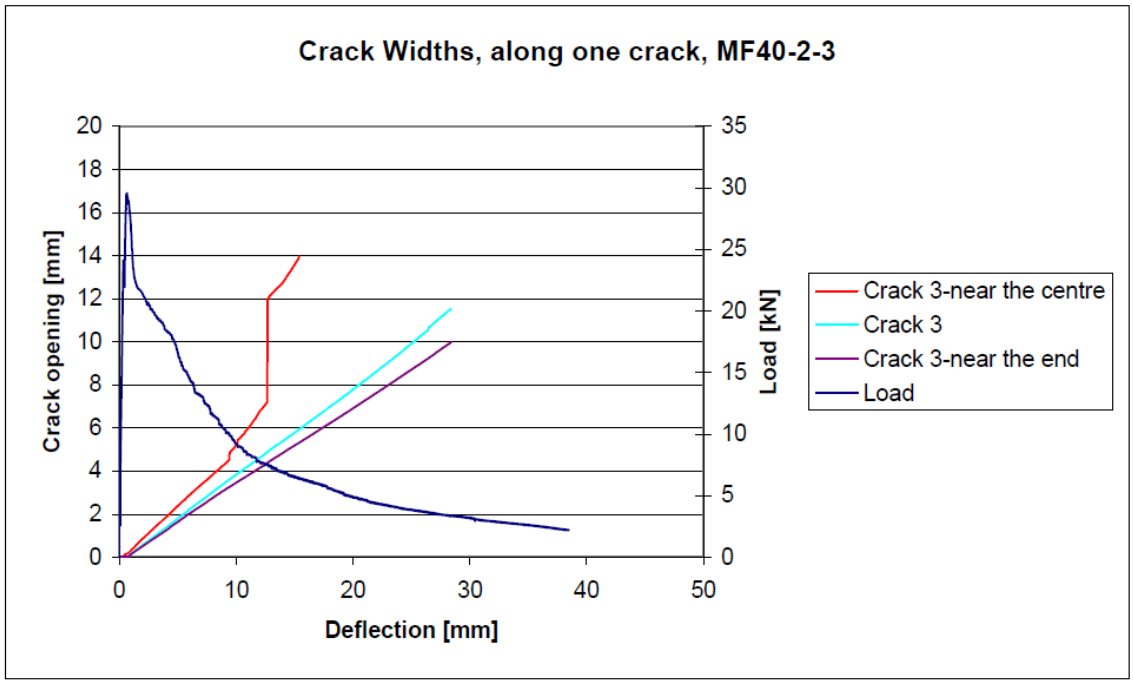

Figure 44 Crack opening along one crack, panel MF40-2-3

Comments:

- The large increase in crack opening at approximate 12 mm deflection for the measurement near the centre is most likely false.

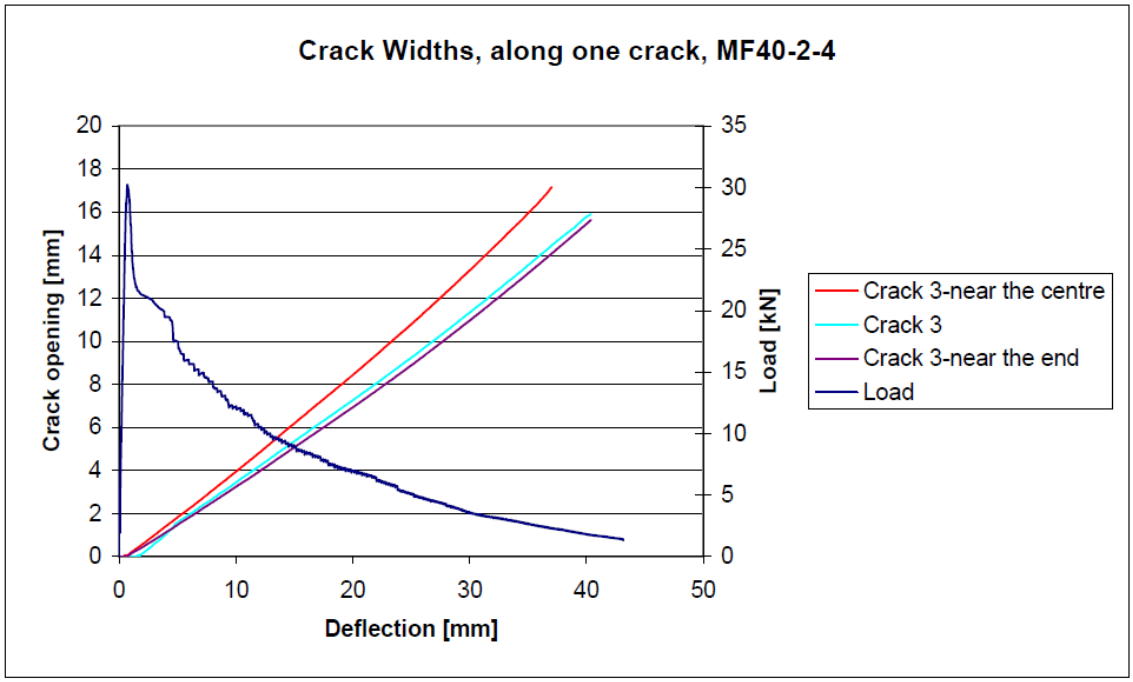

Figure 45 Crack opening along one crack, panel MF40-2-4

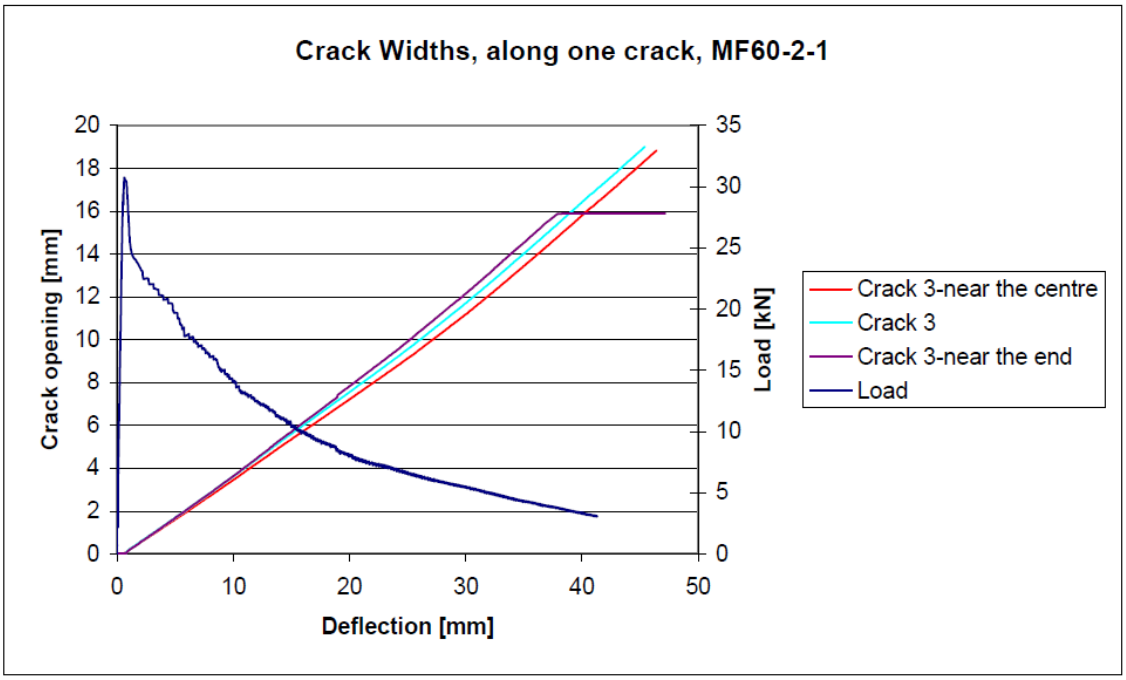

Figure 46 Crack opening along one crack, panel MF60-2-1

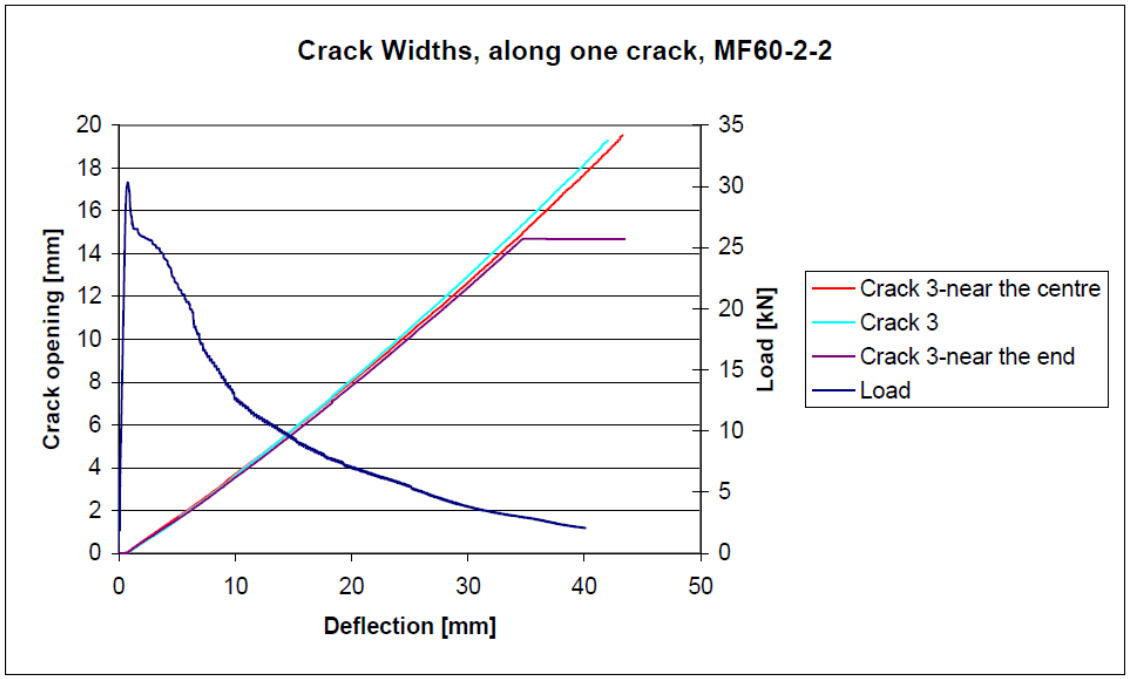

Figure 47 Crack opening along one crack, panel MF60-2-2

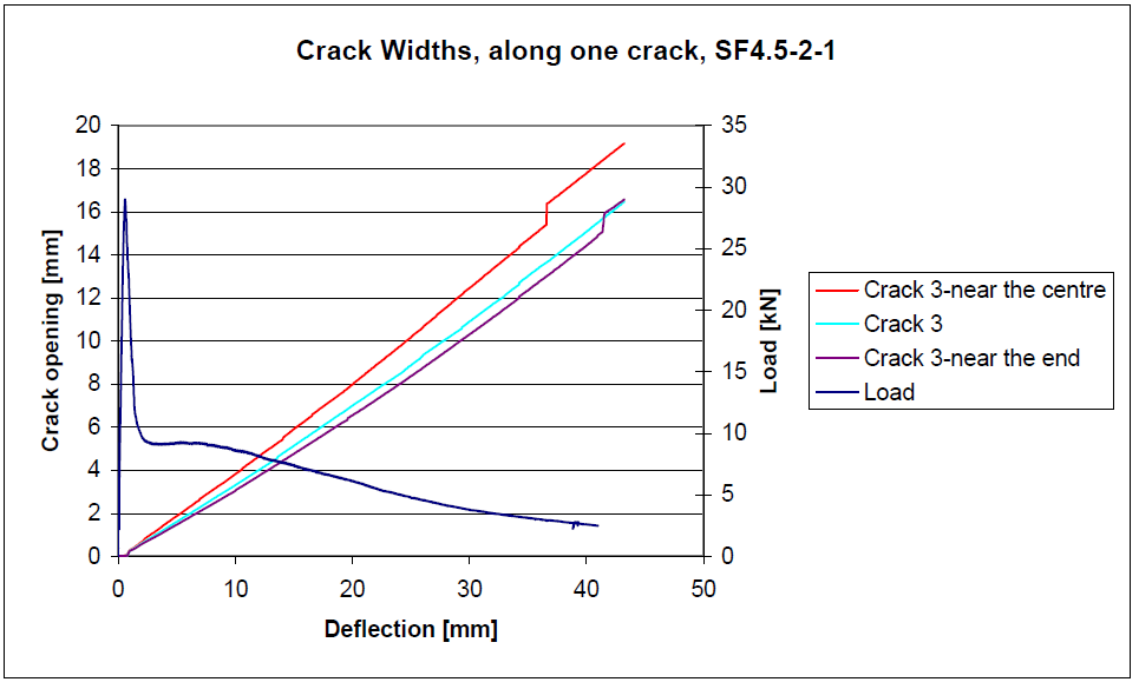

Figure 48 Crack opening along one crack, panel SF4.5-2-1

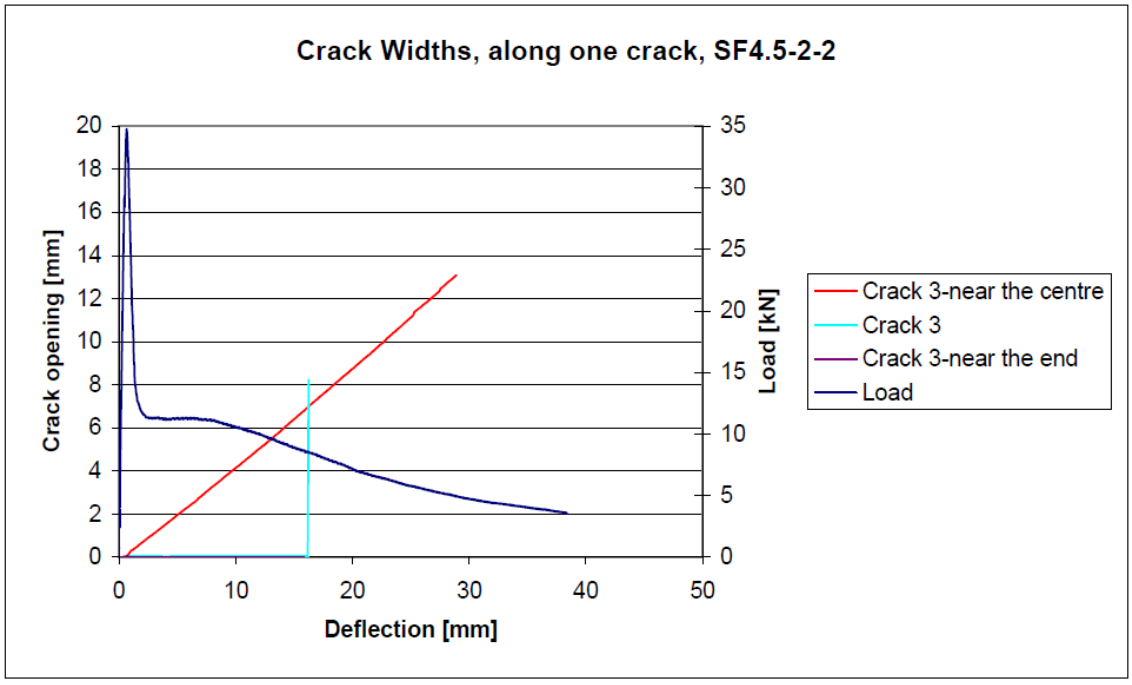

Figure 49 Crack opening along one crack, panel SF4.5-2-2

Comments:

- The only LVDT-record that is trustworthy is the "near the centre" measurement.

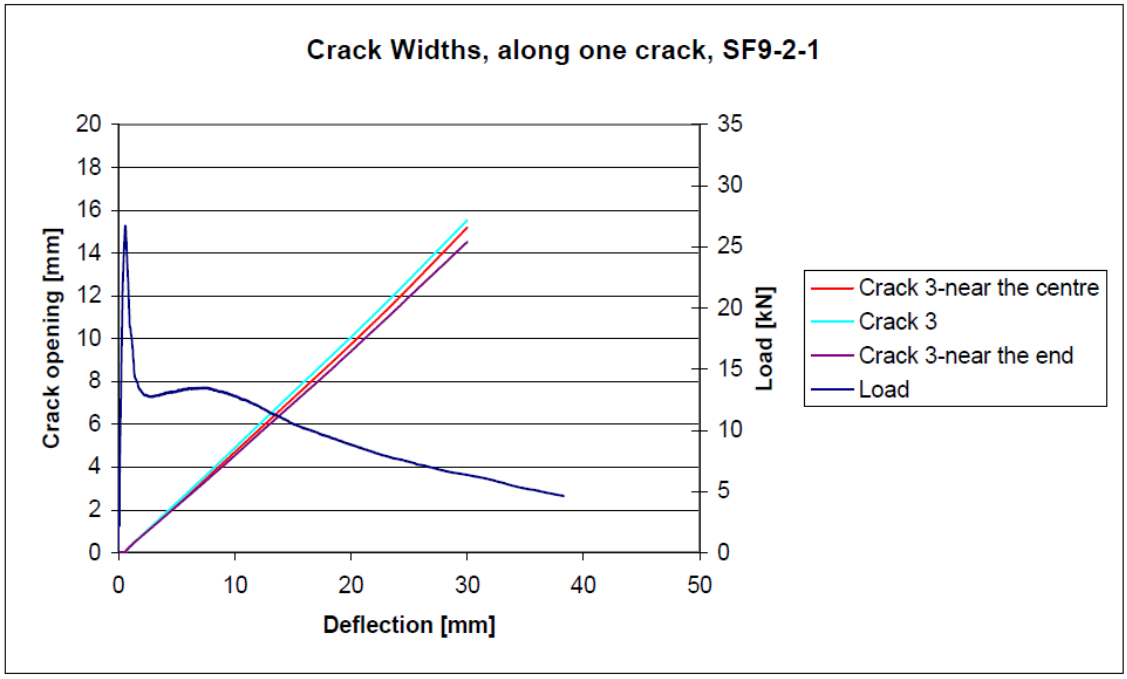

Figure 50 Crack opening along one crack, panel SF9-2-1

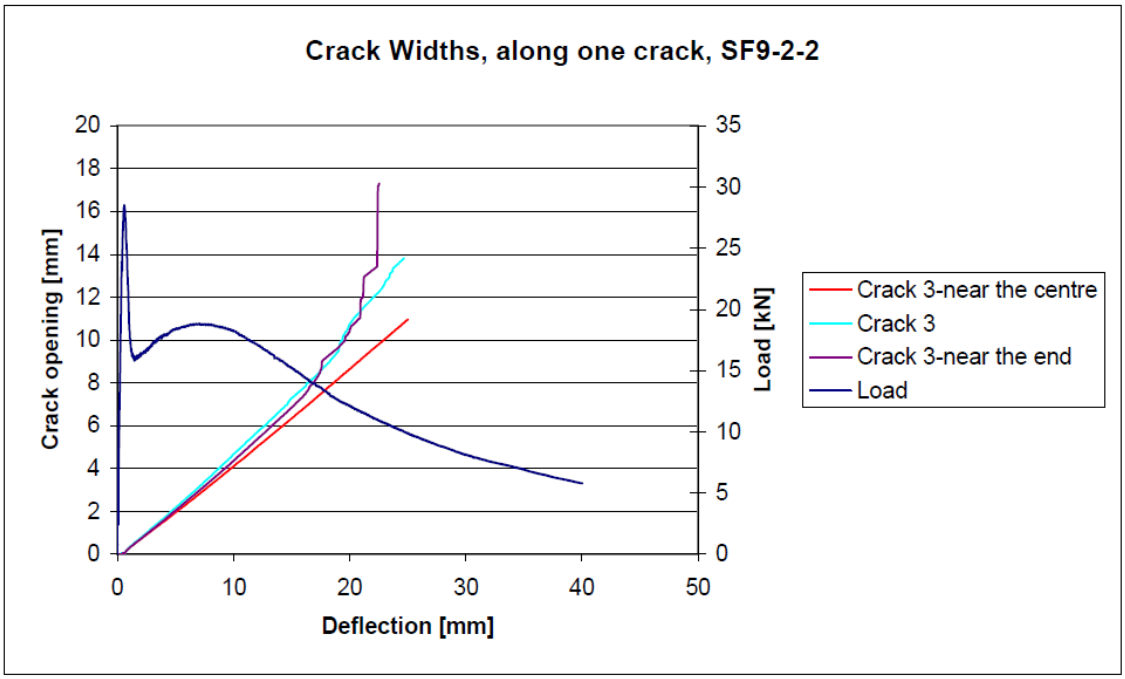

Figure 51 Crack opening along one crack, panel SF9-2-2

3.2.3 Crack opening along one crack summarized

As seen from Figure 33 to Figure 51, the trend is that the crack opening is slightly larger near the centre of the panel, and slightly less near the end of the panel, relative to the mid point of the crack. This fact indicates that the panels are influenced by friction between the support and the concrete.

4 Statistical evaluation

In order to investigate whether the results form every laboratories can be considered to be the same, hypothesis testing is performed. It is assumed that the results from each lab may be described by Gaussian distribution with an expected value μ and a variance σ^2 given by the following expressions:

$$\mu = \hat{\mu} = \overline{X} = \frac{1}{n}\sum_{i=1}^{n} X_i \tag{7}$$

$$\sigma^2 = S^2 = \frac{1}{n-1}\sum_{i=1}^{n}\left(X_i - \overline{X}\right)^2 \tag{8}$$

where n is the number of panels.

The Gaussian distribution is shown for maximum load, P_{Max}, deflection at $P_{Max\,x}$, δ_{Pmax}, and EABS summarized up to 40 mm deflection, W_{40}.

The Gaussian function is:

$$f(x) = \frac{1}{\sqrt{2\pi\sigma^2}} e^{-\frac{(x-\mu)}{2\sigma^2}} \tag{9}$$

with μ and σ as calculated according to equation 7 and equation 8, respectively. There are only 4 test results for each curve, which may be too few points to really support Gauss curves. Nevertheless, the diagrams for the Gaussian distribution give an idea of whether the results are equal or not. Further, to decide whether for instance the W_{40} is equal for all labs, a two sample Welch t-test is performed. A Welch t-test may only be used to compare one lab with another, which means that all labs are compared with each other. The Welch t-test is an adaptation of Student t-test intended for use with two samples having possibly unequal variances.

The *null hypothesis, H_0,* states that there is no difference in the mean values of the panels tested at two labs, while the *alternative hypothesis, H_1*, states that there is a difference in the mean values. The two rival hypotheses are therefore as given in the following expressions:

$$H_0 : \mu_1 = \mu_2$$

$$H_1 : \mu_1 \neq \mu_2$$

where μ_1 and μ_2 are the mean values of the four panels tested at two different labs.

The test is performed according to equation 10 and equation 11 below, for P_{Max}, δ_{Pmax}, W_{20} and W_{40}:

$$t_0 = \frac{\overline{X}_1 - \overline{X}_2}{\sqrt{\frac{S_1^2}{n_1} + \frac{S_2^2}{n_2}}} \tag{10}$$

$$v = \frac{\left(\frac{S_1^2}{n_1} + \frac{S_2^2}{n_2}\right)^2}{\frac{\left(\frac{S_1^2}{n_1}\right)^2}{n_1 - 1} + \frac{\left(\frac{S_2^2}{n_2}\right)^2}{n_2 - 1}} \tag{11}$$

where v is the degrees of freedom.

If $|t_0| < t_{\alpha/2,v}$ the H_1 hypothesis is rejected, and the two series are considered to be equal.

$\alpha/2$ is the upper percentage point of the *t*-distribution with v degrees of freedom. In all calculations the $\alpha/2$ is set to be 0.025, and the relationship between $t_{\alpha/2,v}$, $\alpha/2$ and v is shown in Table 42.

Table 42 The relationship between $t_{\alpha/2,v}$, $\alpha/2$ and v

v	$\alpha/2$			
	0.10	0.05	**0.025**	0.01
1	3.08	6.31	**12.71**	31.82
2	1.89	2.92	**4.30**	6.97
3	1.64	2.35	**3.18**	4.54
4	1.53	2.13	**2.78**	3.75
5	1.48	2.02	**2.57**	3.37
6	1.44	1.94	**2.45**	3.14

In all calculations the calculated degrees of freedom are rounded down to the nearest integer.

All statistical calculations are also performed as Student t-test, and when the two calculations give unequal conclusions it is commented.

At BBRI a student t-test based on the "Honestly Significant Difference" criterion from Tukey is performed. This method reduces the probability of making a type I error, which means to accept the alternative hypothesis when it is actually incorrect. When these calculations give unequal conclusions it is also commented.

All in all, the three different methods of performing the statistical calculations give the same conclusions.

When a statistical calculation is performed, it is important to remember that it is H_1 that is tested. It cannot be concluded that H_0 is correct even though H_1 is rejected.

4.1 Statistical evaluation of P_{Max}

Figure 52 to Figure 57 shows the Gaussian distribution for P_{Max} for every laboratory, and Table 43 to Table 48 shows the results from the statistical calculation.

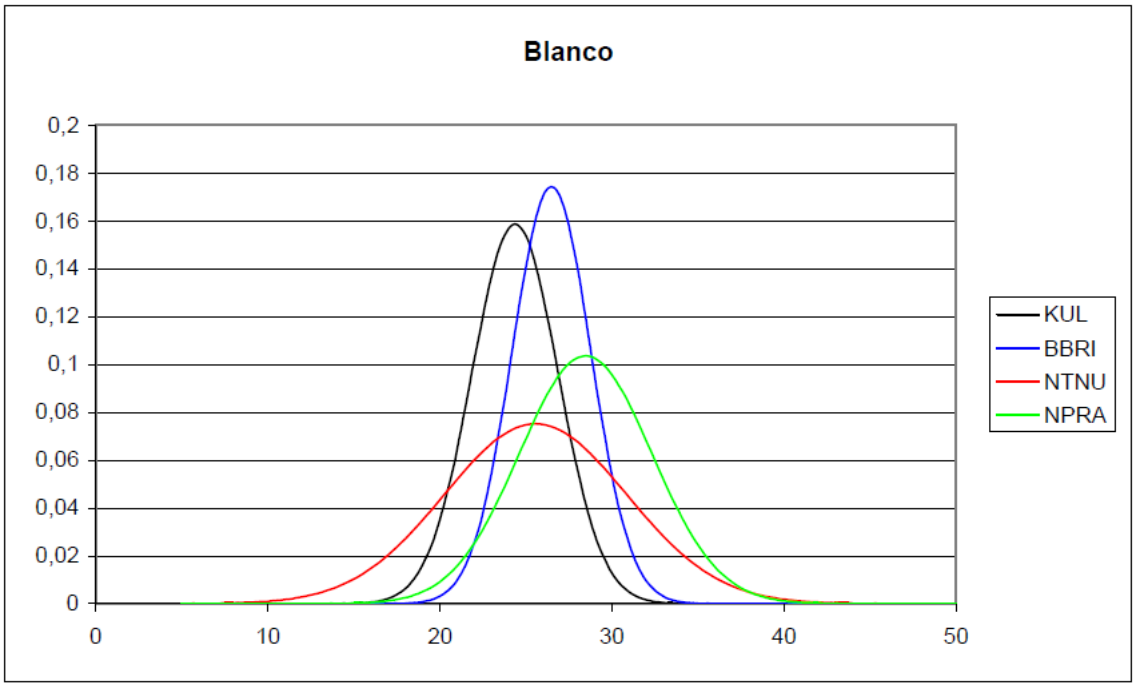

Figure 52 Gaussian distribution for P_{Max} Blanco

Table 43 Statistical inter-lab calculation of P_{Max} Blanco

	KUL vs BBRI	KUL vs NTNU	KUL vs NPRA	BBRI vs NTNU	BBRI vs NPRA	NTNU vs NPRA
$\|t_0\|$	1.25	0.36	1.78	0.28	0.89	0.80
v	5.95	2.68	5.16	2.56	4.88	3.53
$t_{\alpha/2,v}$	2.57	4.30	2.57	4.30	2.78	3.18
$\mu_1 \neq \mu_2$	NO	NO	NO	NO	NO	NO

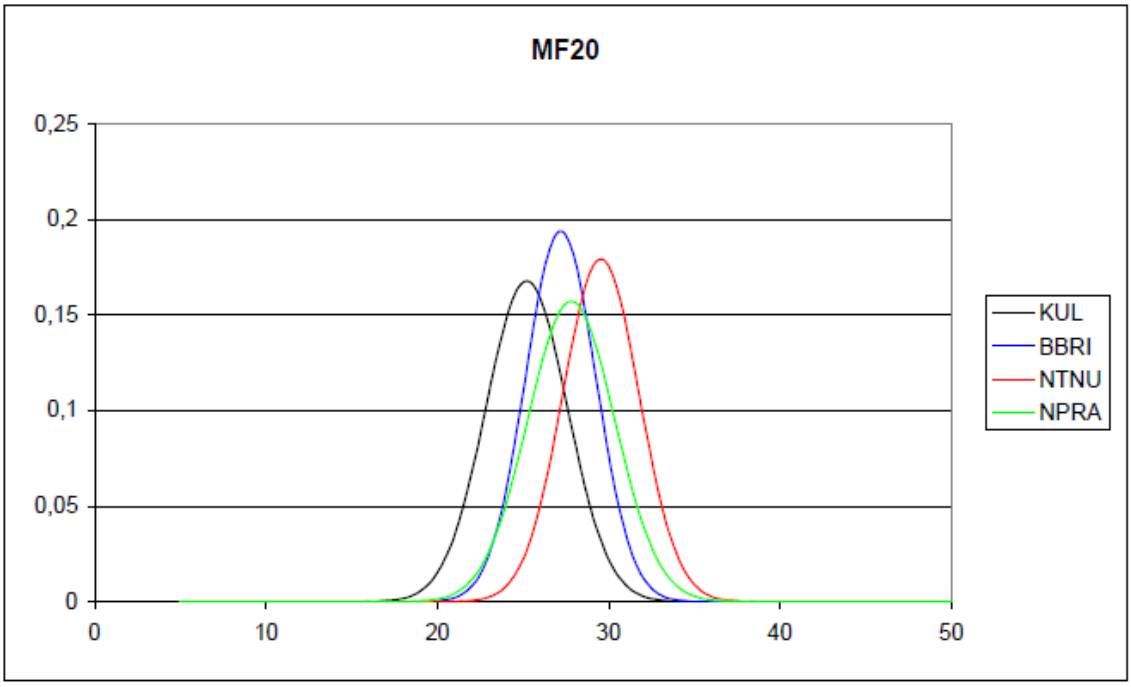

Figure 53 Gaussian distribution for P_{Max} MF20

Table 44 Statistical inter-lab calculation of P_{Max} MF20

	KUL vs BBRI	KUL vs NTNU	KUL vs NPRA	BBRI vs NTNU	BBRI vs NPRA	NTNU vs NPRA
$\|t_0\|$	1.26	2.66	1.49	1.55	0.38	1.03
v	5.88	5.97	5.97	5.96	5.75	5.90
$t_{\alpha/2,v}$	2.57	2.57	2.57	2.57	2.57	2.57
$\mu_1 \neq \mu_2$	NO	YES	NO	NO	NO	NO

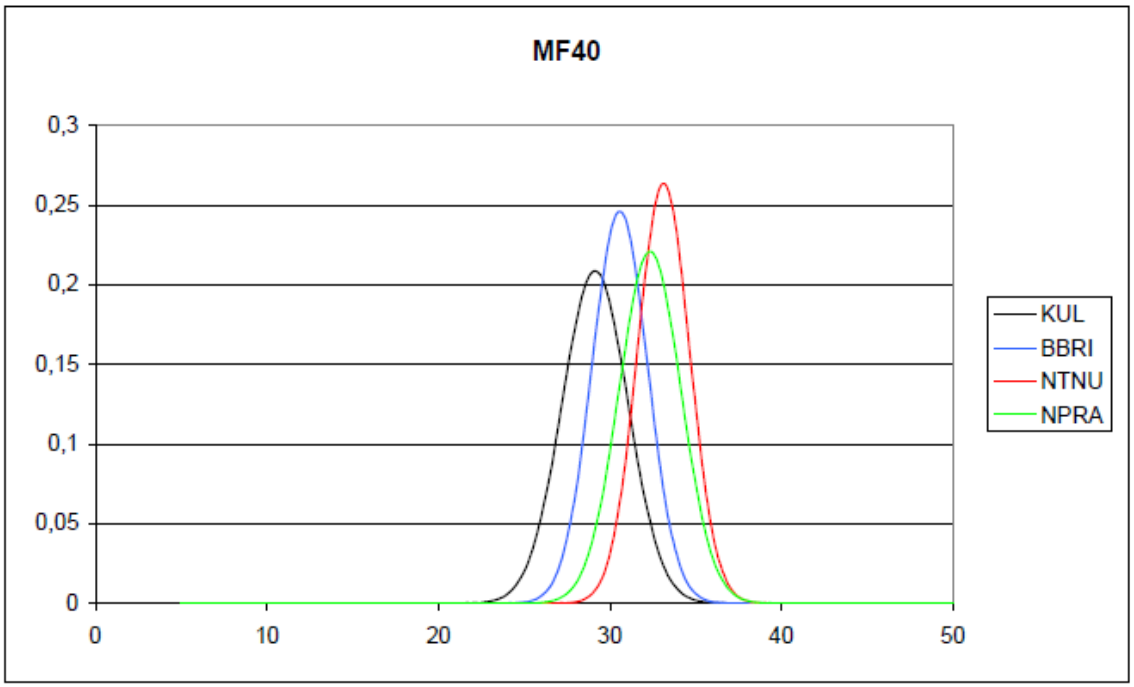

Figure 54 Gaussian distribution for P_{Max} MF40

Table 45 Statistical inter-lab calculation of P_{Max} MF40

	KUL vs BBRI	KUL vs NTNU	KUL vs NPRA	BBRI vs NTNU	BBRI vs NPRA	NTNU vs NPRA
$\|t_0\|$	1.15	3.28	2.44	2.30	1.45	0.67
v	5.84	5.70	5.98	5.97	5.93	5.82
$t_{\alpha/2,v}$	2.57	2.57	2.57	2.57	2.57	2.57
$\mu_1 \neq \mu_2$	NO	YES	NO	NO	NO	NO

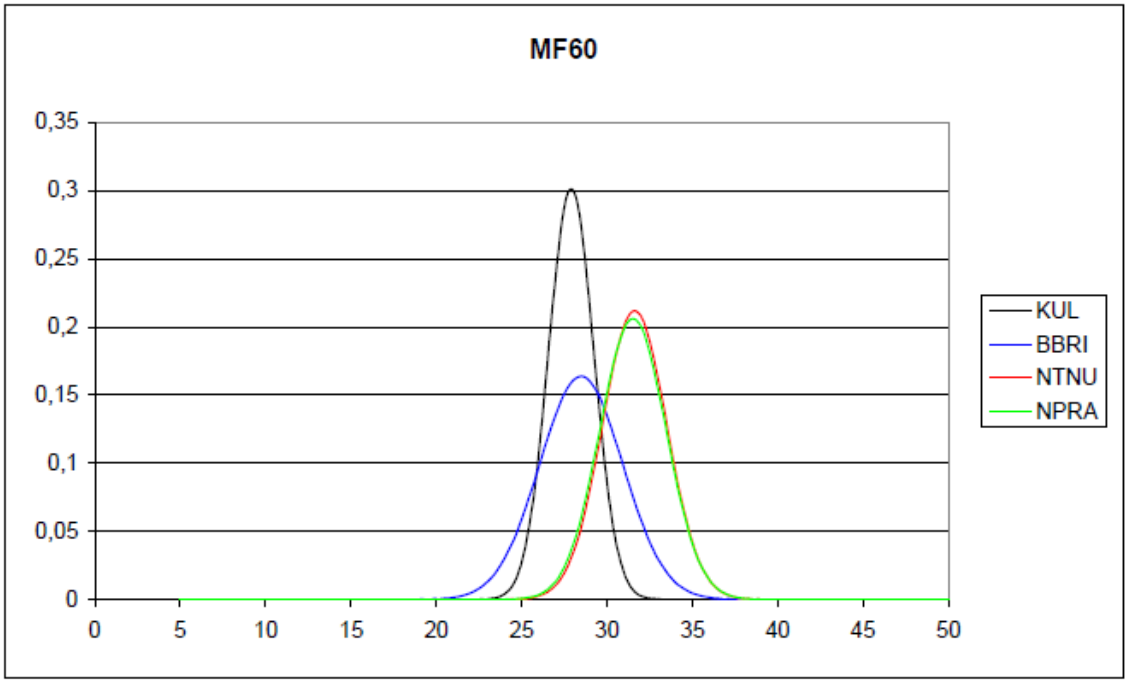

Figure 55 Gaussian distribution for P_{Max} MF60

Table 46 Statistical inter-lab calculation of P_{Max} MF60

	KUL vs BBRI	KUL vs NTNU	KUL vs NPRA	BBRI vs NTNU	BBRI vs NPRA	NTNU vs NPRA
$\|t_0\|$	0.42	3.23	3.09	2.03	1.95	0.07
ν	4.63	5.38	5.30	5.64	5.71	6.00
$t_{\alpha/2,\nu}$	2.78	2.57	2.57	2.57	2.57	2.57
$\mu_1 \neq \mu_2$	NO	YES	YES	NO	NO	NO

Comment:

- $\mu_1 \neq \mu_2$ for KUL vs NTNU and KUL vs NPRA is not confirmed with HSD.

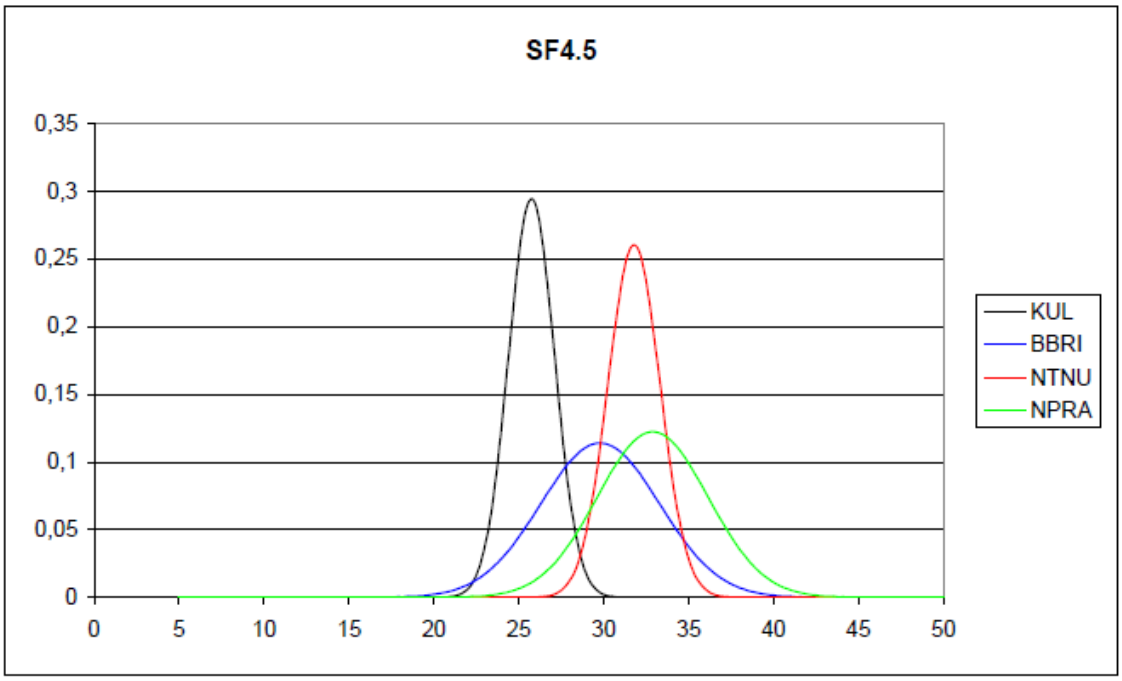

Figure 56 Gaussian distribution for P_{Max} SF4.5

Table 47 Statistical inter-lab calculation of P_{Max} SF4.5

	KUL vs BBRI	KUL vs NTNU	KUL vs NPRA	BBRI vs NTNU	BBRI vs NPRA	NTNU vs NPRA
$\|t_0\|$	2.15	5.90	4.04	1.04	1.29	0.61
ν	3.88	5.91	4.01	4.11	5.97	4.26
$t_{\alpha/2,\nu}$	3.18	2.57	2.78	2.78	2.57	2.78
$\mu_1 \neq \mu_2$	NO	YES	YES	NO	NO	NO

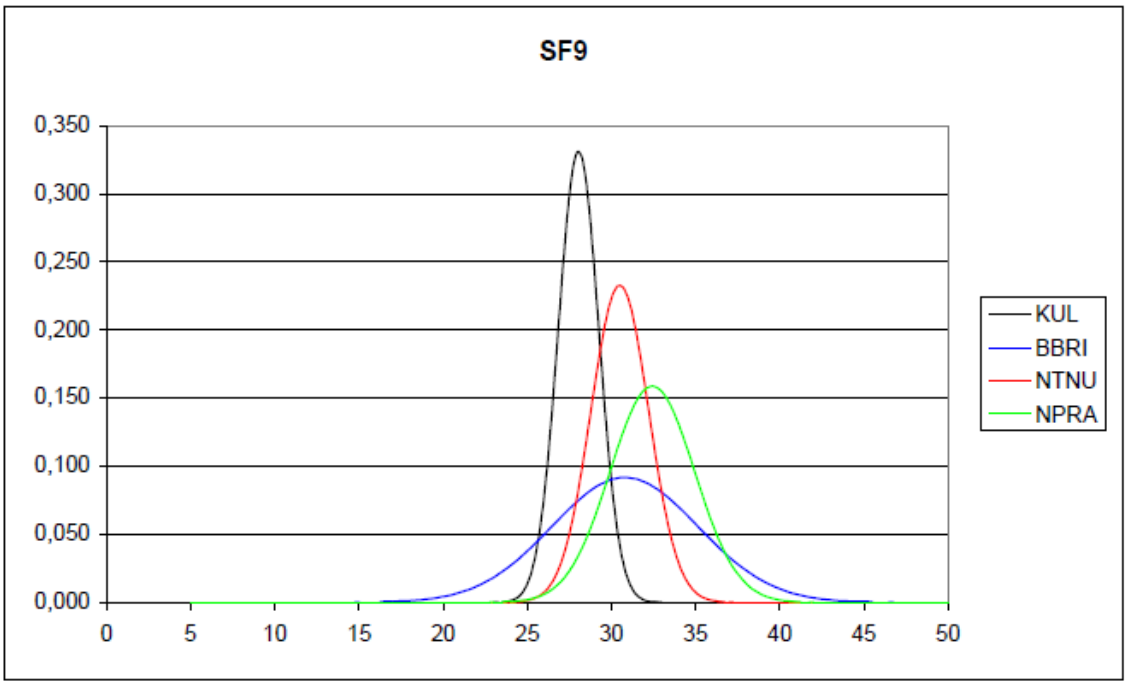

Figure 57 Gaussian distribution for P_{Max} SF9

Table 48 Statistical inter-lab calculation of P_{Max} SF9

	KUL vs BBRI	KUL vs NTNU	KUL vs NPRA	BBRI vs NTNU	BBRI vs NPRA	NTNU vs NPRA
$\|t_0\|$	1.22	2.34	3.15	0.13	0.65	1.27
v	3.46	5.38	4.31	3.91	4.80	5.29
$t_{\alpha/2,v}$	3.18	2.57	2.78	3.18	2.78	2.57
$\mu_1 \neq \mu_2$	NO	NO	YES	NO	NO	NO

Comment:

- $\mu_1 \neq \mu_2$ for KUL vs NPRA is not confirmed with HSD.

The conclusions from Table 43 to Table 48 are summarized in Table 49.

Table 49 Statistical inter-lab calculation of P_{Max} Summarized

	$\mu_1 \neq \mu_2$					
	KUL vs BBRI	KUL vs NTNU	KUL vs NPRA	BBRI vs NTNU	BBRI vs NPRA	NTNU vs NPRA
Blanco	NO	NO	NO	NO	NO	NO
MF20	NO	**YES**	NO	NO	NO	NO
MF40	NO	**YES**	NO	NO	NO	NO
MF60	NO	**YES**	**YES**	NO	NO	NO
SF4.5	NO	**YES**	**YES**	NO	NO	NO
SF9	NO	NO	**YES**	NO	NO	NO

As seen from Table 49, it can be stated that the measured P_{Max} are not equal at all laboratories at the 95% significance level. KUL vs NTNU is proven to have different maximum load in 4 of 6 series, and KUL vs NPRA is proven to have different maximum load in 3 of 6 series.

4.2 Statistical evaluation of the deflection at P_{Max}, $\delta_{P,max}$

Figure 58 to Figure 63 shows the Gaussian distribution for $\delta_{P,max}$ for every laboratory, and Table 50 to Table 55 shows the results from the statistical calculation.

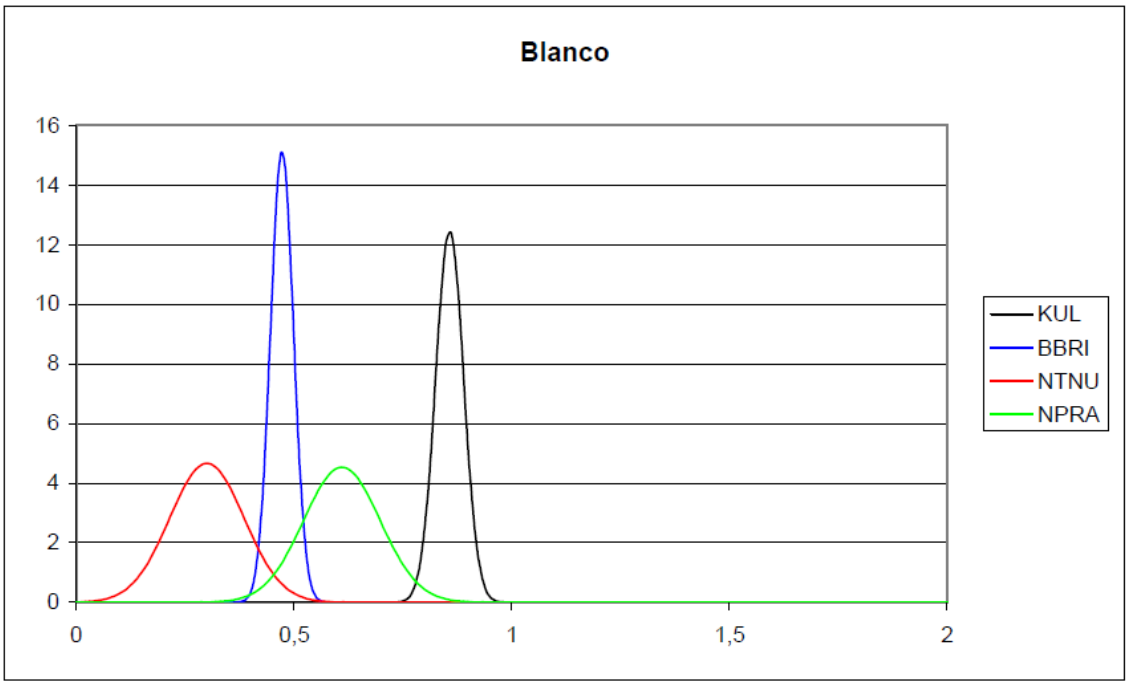

Figure 58 Gaussian distribution for $\delta_{P,max}$ Blanco

Table 50 Statistical inter-lab calculation of $\delta_{P,max}$ Blanco

	KUL vs BBRI	KUL vs NTNU	KUL vs NPRA	BBRI vs NTNU	BBRI vs NPRA	NTNU vs NPRA
$\|t_0\|$	18.58	10.75	5.29	3.38	3.00	4.69
v	5.78	2.43	3.78	2.29	3.53	4.53
$t_{\alpha/2,v}$	2.57	4.30	3.18	4.30	3.18	2.78
$\mu_1 \neq \mu_2$	YES	YES	YES	NO	NO	YES

Comment:

- Student t-test give $\mu_1 \neq \mu_2$ also for BBRI vs NTNU and BBRI vs NPRA

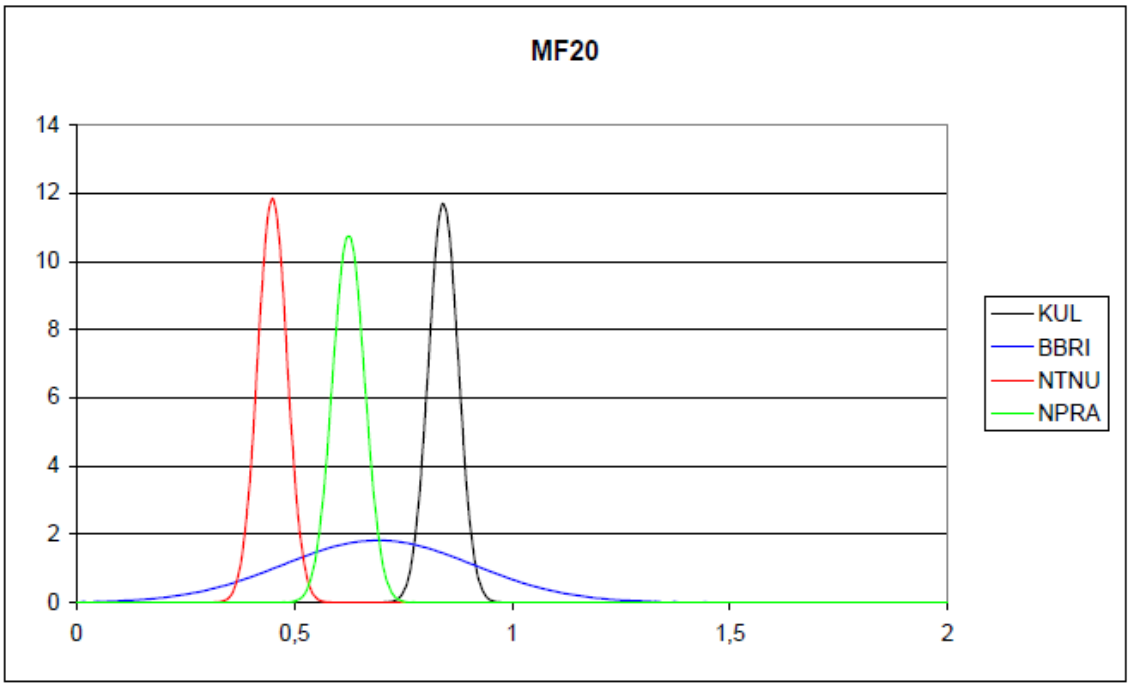

Figure 59 Gaussian distribution for $\delta_{P,max}$ MF20

Table 51 Statistical inter-lab calculation of $\delta_{P,max}$ MF20

	KUL vs BBRI	KUL vs NTNU	KUL vs NPRA	BBRI vs NTNU	BBRI vs NPRA	NTNU vs NPRA
$\|t_0\|$	1.35	16.40	8.66	2.19	0.61	7.00
v	3.15	6.00	5.96	3.14	3.17	5.95
$t_{\alpha/2,v}$	3.18	2.57	2.57	3.18	3.18	2.57
$\mu_1 \neq \mu_2$	NO	YES	YES	NO	NO	YES

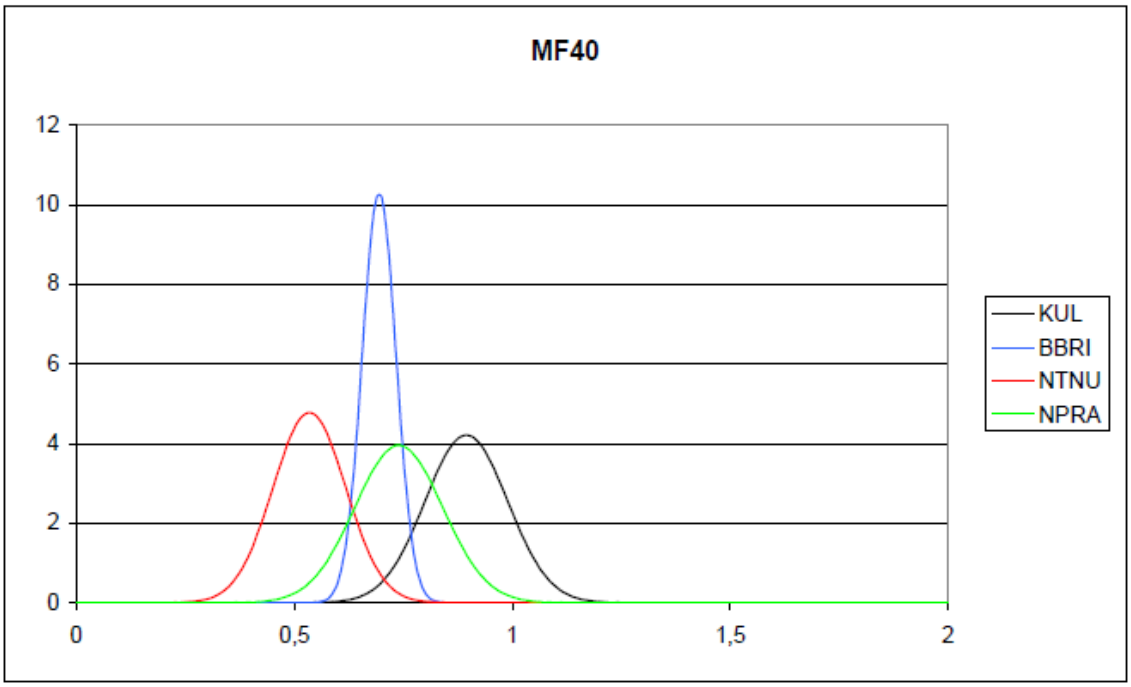

Figure 60 Gaussian distribution for $\delta_{P,max}$ MF40

Table 52 Statistical inter-lab calculation of $\delta_{P,max}$ MF40

	KUL vs BBRI	KUL vs NTNU	KUL vs NPRA	BBRI vs NTNU	BBRI vs NPRA	NTNU vs NPRA
$\|t_0\|$	3.91	5.70	2.24	3.48	0.83	4.69
v	3.98	5.91	5.98	4.23	3.86	4.53
$t_{\alpha/2,v}$	3.18	2.57	2.57	2.78	3.18	2.78
$\mu_1 \neq \mu_2$	YES	YES	NO	YES	NO	YES

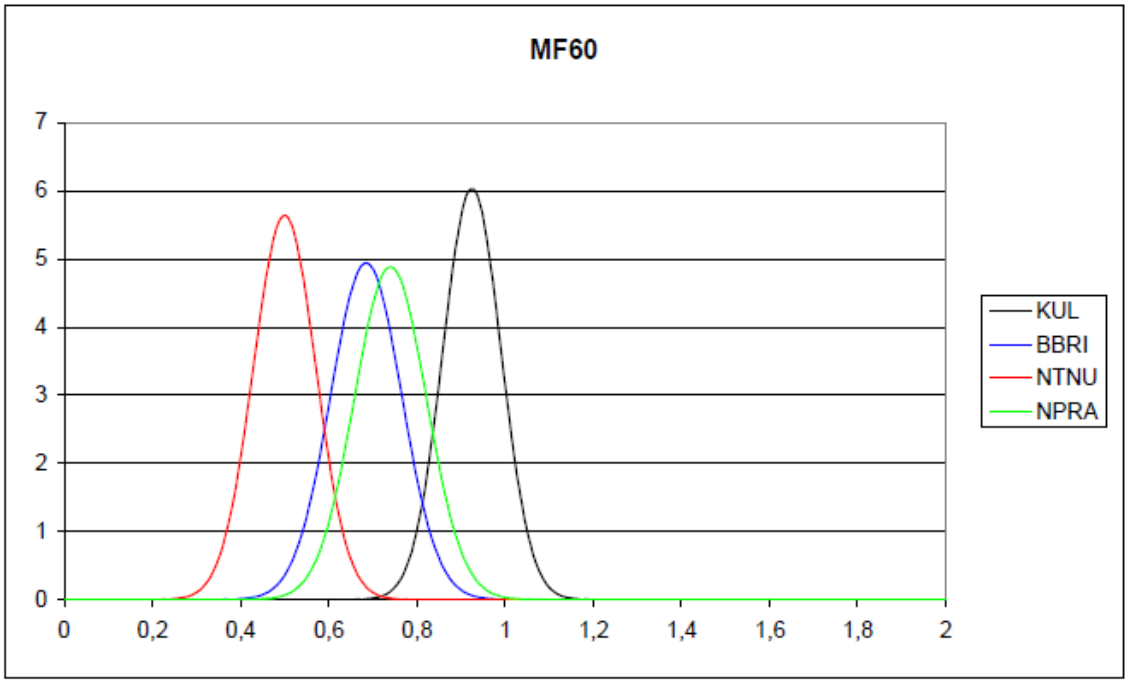

Figure 61 Gaussian distribution for $\delta_{P,max}$ MF60

Table 53 Statistical inter-lab calculation of $\delta_{P,max}$ MF60

	KUL vs BBRI	KUL vs NTNU	KUL vs NPRA	BBRI vs NTNU	BBRI vs NPRA	NTNU vs NPRA
$\|t_0\|$	4.60	8.78	3.52	3.45	0.96	4.44
v	5.78	5.97	5.75	5.90	6.00	5.88
$t_{\alpha/2,v}$	2.57	2.57	2.57	2.57	2.57	2.57
$\mu_1 \neq \mu_2$	YES	YES	YES	YES	NO	YES

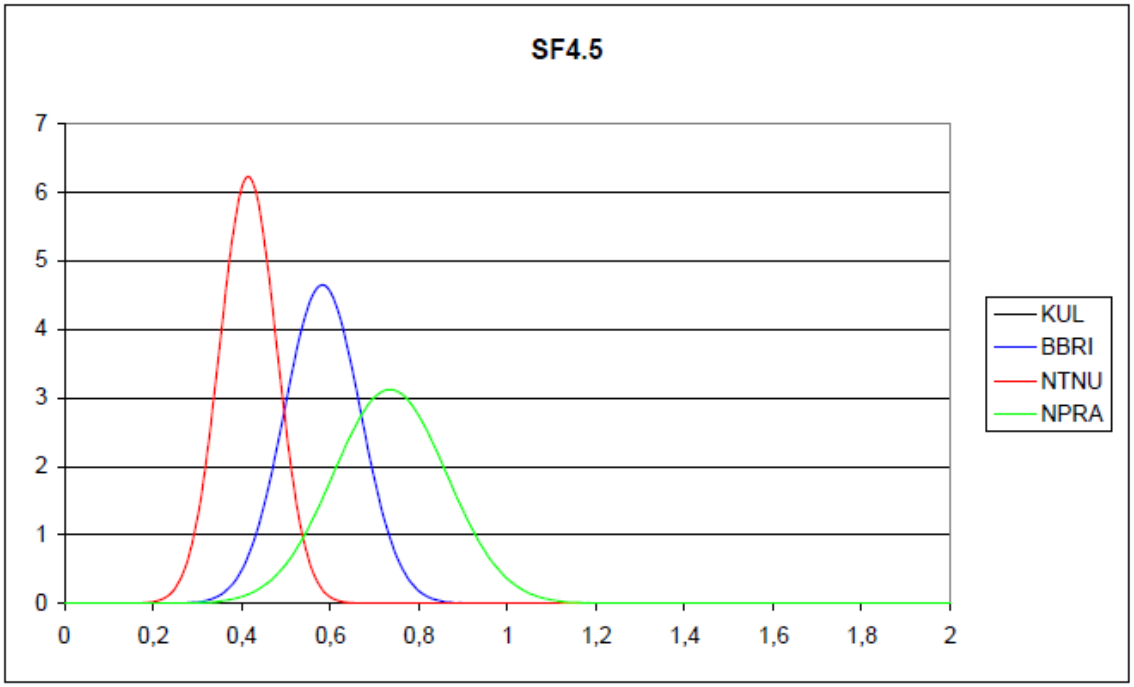

Figure 62 Gaussian distribution for $\delta_{P,max}$ SF4.5

Table 54 Statistical inter-lab calculation of $\delta_{P,max}$ SF4.5

	KUL vs BBRI	KUL vs NTNU	KUL vs NPRA	BBRI vs NTNU	BBRI vs NPRA	NTNU vs NPRA
$\|t_0\|$	-	-	-	3.13	1.98	4.48
v	-	-	-	5.55	5.25	4.42
$t_{\alpha/2,v}$	-	-	-	2.57	2.57	2.78
$\mu_1 \neq \mu_2$	-	-	-	YES	NO	YES

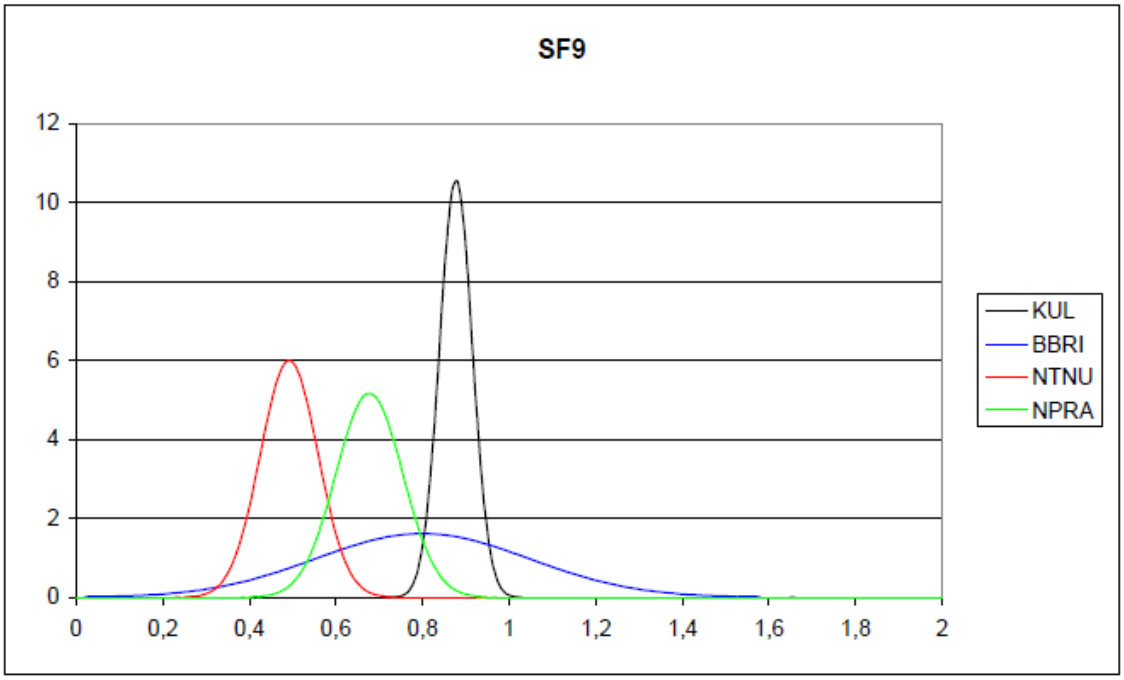

Figure 63 Gaussian distribution for $\delta_{P,max}$ SF9

Table 55 Statistical inter-lab calculation of $\delta_{P,max}$ SF9

	KUL vs BBRI	KUL vs NTNU	KUL vs NPRA	BBRI vs NTNU	BBRI vs NPRA	NTNU vs NPRA
$\|t_0\|$	0.62	10.07	4.66	2.41	0.95	3.63
v	3.14	4.75	4.36	3.43	3.58	5.87
$t_{\alpha/2,v}$	3.18	2.78	2.78	3.18	3.18	2.57
$\mu_1 \neq \mu_2$	NO	YES	YES	NO	NO	YES

The conclusions from Table 50 to Table 55 are summarized in Table 56.

Table 56 Statistical inter-lab calculation of $\delta_{P,max}$ Summarized

	$\mu_1 \neq \mu_2$					
	KUL vs BBRI	KUL vs NTNU	KUL vs NPRA	BBRI vs NTNU	BBRI vs NPRA	NTNU vs NPRA
Blanco	**YES**	**YES**	**YES**	NO	NO	**YES**
MF20	NO	**YES**	**YES**	NO	NO	**YES**
MF40	**YES**	**YES**	NO	**YES**	NO	**YES**
MF60	**YES**	**YES**	**YES**	**YES**	NO	**YES**
SF4.5	-	-	-	**YES**	NO	**YES**
SF9	NO	**YES**	**YES**	NO	NO	**YES**

As seen from Table 56, it is proven that the measured deflections at P_{Max}, $\delta_{P,max}$, are not equal at all laboratories at the 95% significance level. Only for BBRI vs NPRA it cannot be proven that $\delta_{P,max}$ are different for at least two series.

4.3 Statistical evaluation of W_{40}

Figure 64 to Figure 69 shows the Gaussian distribution for W_{40} for every laboratory, and Table 57 to Table 62 shows the results from the statistical calculation.

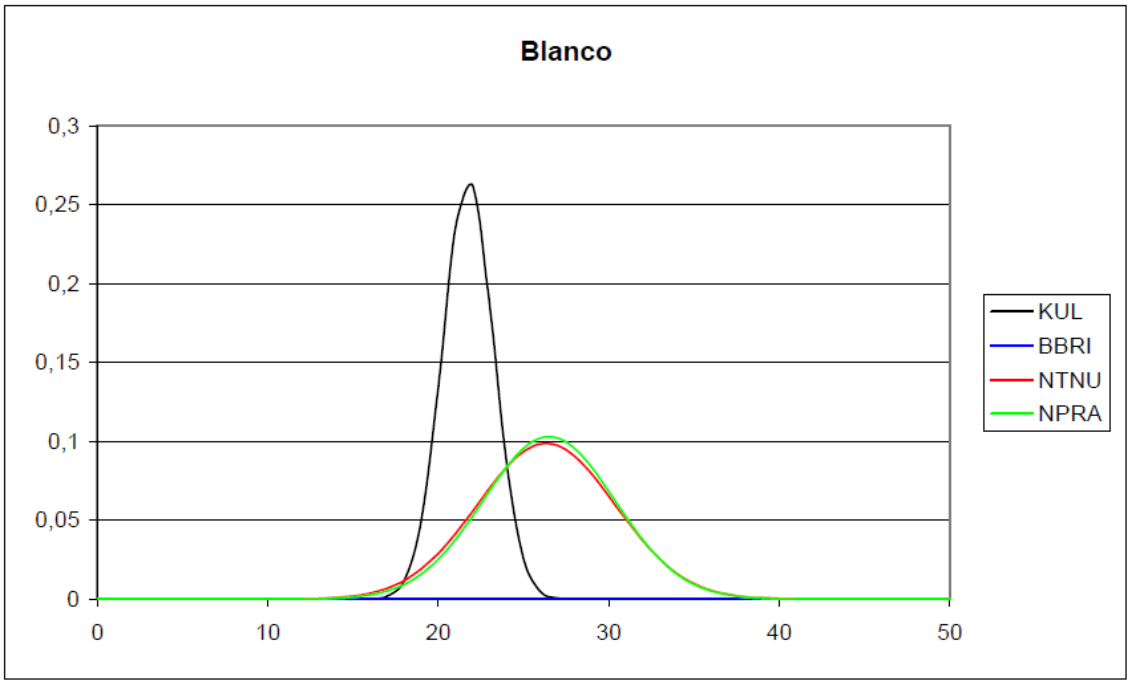

Figure 64 Gaussian distribution for W_{40} Blanco

Table 57 Statistical inter-lab calculation of W_{40} Blanco

	KUL vs BBRI	KUL vs NTNU	KUL vs NPRA	BBRI vs NTNU	BBRI vs NPRA	NTNU vs NPRA
$\|t_0\|$	-	1.87	2.29	-	-	0.05
v	-	2.42	3.88	-	-	4.33
$t_{\alpha/2,v}$	-	4.30	3.18	-	-	2.78
$\mu_1 \neq \mu_2$	-	NO	NO	-	-	NO

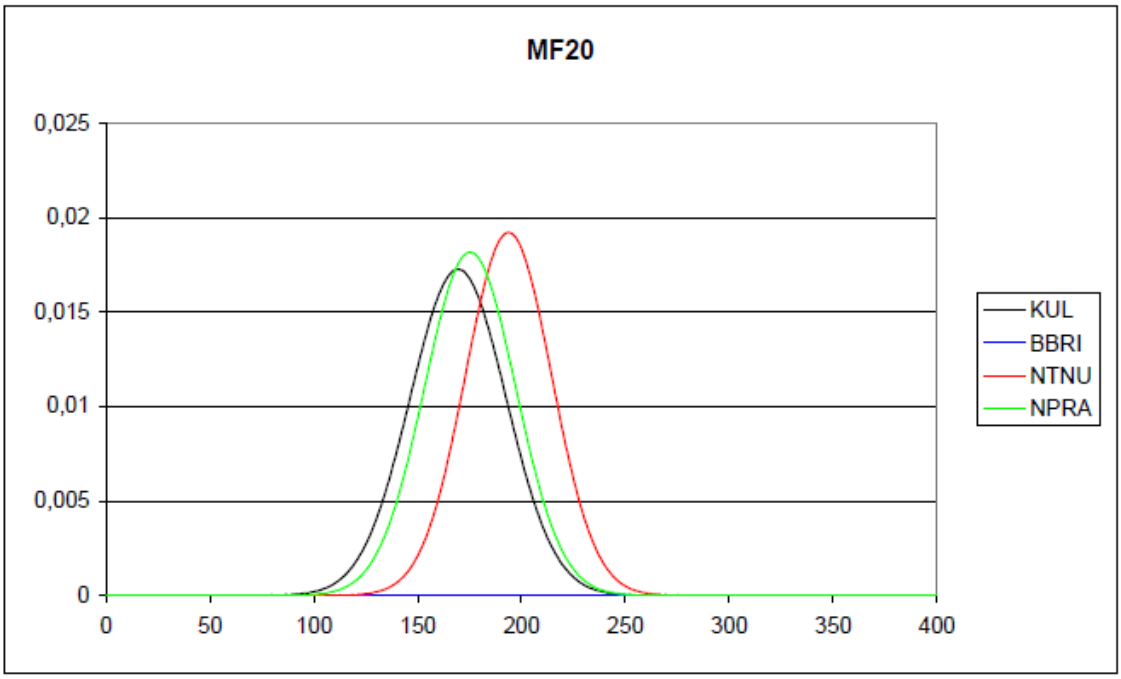

Figure 65 Gaussian distribution for W_{40} MF20

Table 58 Statistical inter-lab calculation of W_{40} MF20

	KUL vs BBRI	KUL vs NTNU	KUL vs NPRA	BBRI vs NTNU	BBRI vs NPRA	NTNU vs NPRA
$\|t_0\|$	-	1.56	0.36	-	-	1.22
ν	-	5.93	5.98	-	-	5.98
$t_{\alpha/2,\nu}$	-	2.57	2.57	-	-	2.57
$\mu_1 \neq \mu_2$	-	NO	NO	-	-	NO

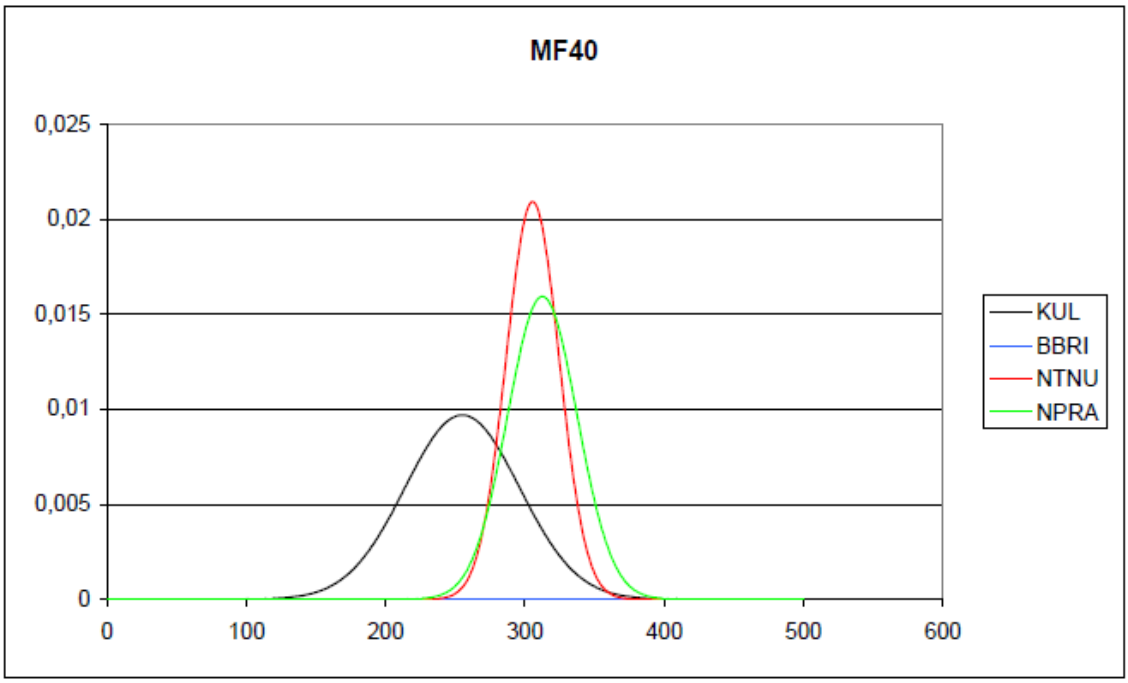

Figure 66 Gaussian distribution for W_{40} MF40

Table 59 Statistical inter-lab calculation of W_{40} MF40

	KUL vs BBRI	KUL vs NTNU	KUL vs NPRA	BBRI vs NTNU	BBRI vs NPRA	NTNU vs NPRA
$\|t_0\|$	-	2.23	2.39	-	-	0.45
v	-	4.23	4.95	-	-	5.60
$t_{\alpha/2,v}$	-	2.78	2.78	-	-	2.57
$\mu_1 \neq \mu_2$	-	NO	NO	-	-	NO

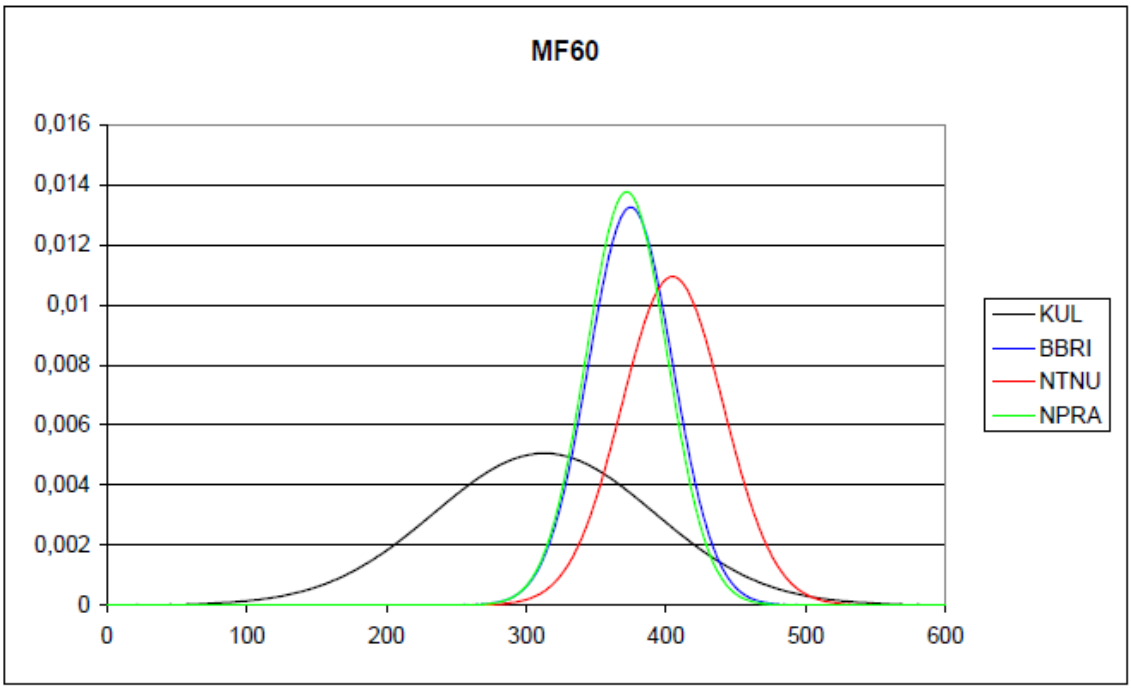

Figure 67 Gaussian distribution for W_{40} MF60

Table 60 Statistical inter-lab calculation of W_{40} MF60

	KUL vs BBRI	KUL vs NTNU	KUL vs NPRA	BBRI vs NTNU	BBRI vs NPRA	NTNU vs NPRA
$\|t_0\|$	1.46	2.11	1.40	1.27	0.13	1.41
ν	3.85	4.22	3.79	5.79	5.99	5.71
$t_{\alpha/2,\nu}$	3.18	2.78	3.18	2.57	2.57	2.57
$\mu_1 \neq \mu_2$	NO	NO	NO	NO	NO	NO

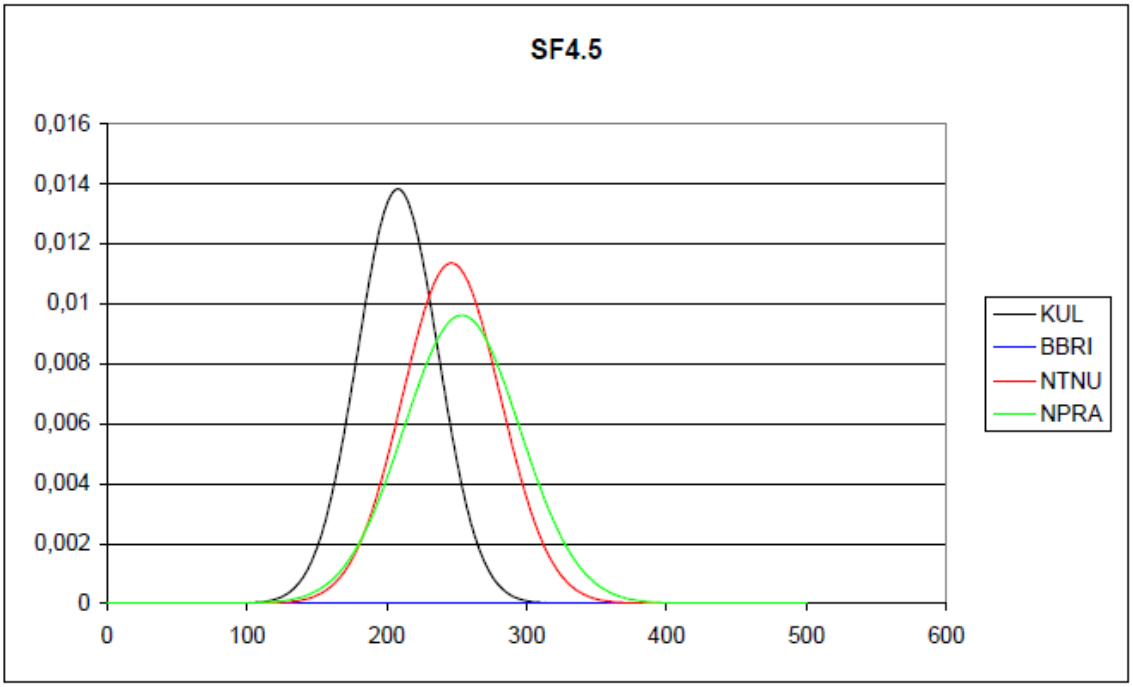

Figure 68 Gaussian distribution for W_{40} SF4.5

Table 61 Statistical inter-lab calculation of W_{40} SF4.5

	KUL vs BBRI	KUL vs NTNU	KUL vs NPRA	BBRI vs NTNU	BBRI vs NPRA	NTNU vs NPRA
$\|t_0\|$	-	1.68	1.63	-	-	0.25
v	-	5.78	3.41	-	-	3.97
$t_{\alpha/2,v}$	-	2.57	3.18	-	-	3.18
$\mu_1 \neq \mu_2$	-	NO	NO	-	-	NO

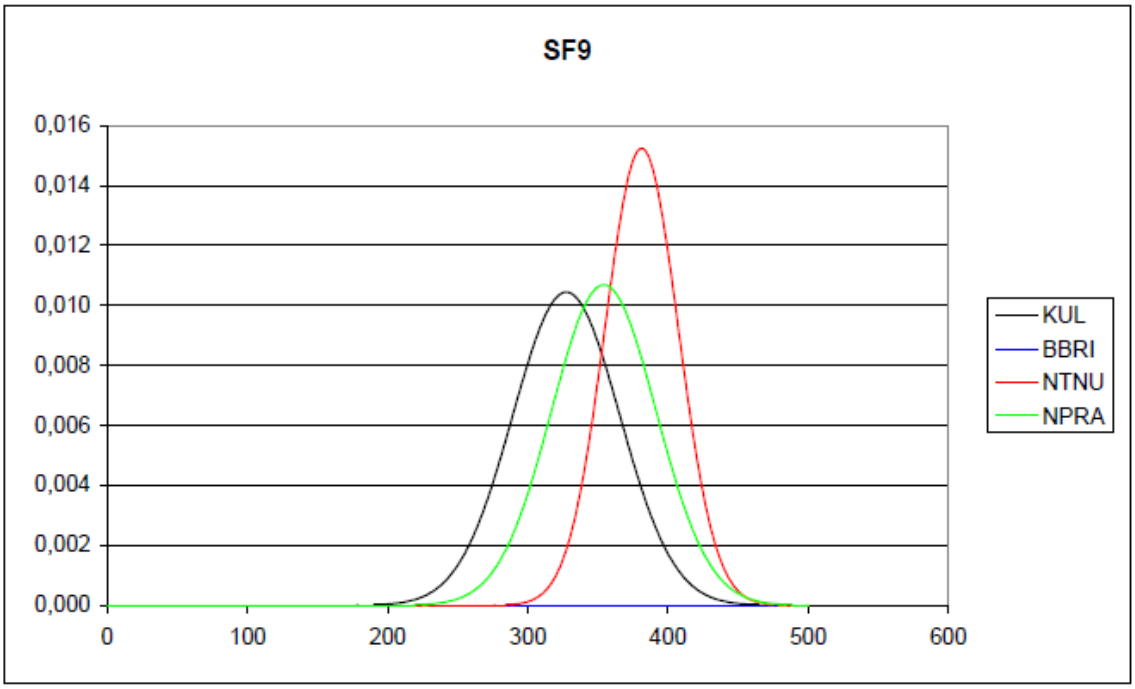

Figure 69 Gaussian distribution for W_{40} SF9

Table 62 Statistical inter-lab calculation of W_{40} SF9

	KUL vs BBRI	KUL vs NTNU	KUL vs NPRA	BBRI vs NTNU	BBRI vs NPRA	NTNU vs NPRA
$\|t_0\|$	-	2.32	1.00	-	-	1.18
v	-	5.31	6.00	-	-	5.38
$t_{\alpha/2,v}$	-	2.57	2.57	-	-	2.57
$\mu_1 \neq \mu_2$	-	NO	NO	-	-	NO

The results from Table 57 to Table 62 are summarized in Table 63.

Table 63 Statistical inter-lab calculation of W_{40} Summarized

	$\mu_1 \neq \mu_2$					
	KUL vs BBRI	KUL vs NTNU	KUL vs NPRA	BBRI vs NTNU	BBRI vs NPRA	NTNU vs NPRA
Blanco	-	NO	NO	-	-	NO
MF20	-	NO	NO	-	-	NO
MF40	-	NO	NO	-	-	NO
MF60	-	NO	NO	-	-	NO
SF4.5	-	NO	NO	-	-	NO
SF9	-	NO	NO	-	-	NO

It is impossible to investigate whether panels tested at BBRI gives equal results that panels tested at the other laboratories, due to the fact that the test was stopped before 40mm deflection was reached.

Based on the statistical calculation it cannot be concluded that there is a difference in the absorbed energy up to 40mm deflection for the panels tested at KUL, NTNU and NPRA. To include the BBRI-panels, the same statistical calculation is made for W_{20}.

4.4 Statistical evaluation of W_{20}

Figure 70 to Figure 75 shows the Gaussian distribution for W_{20} for every laboratory, and Table 64 to Table 69 shows the results from the statistical calculation.

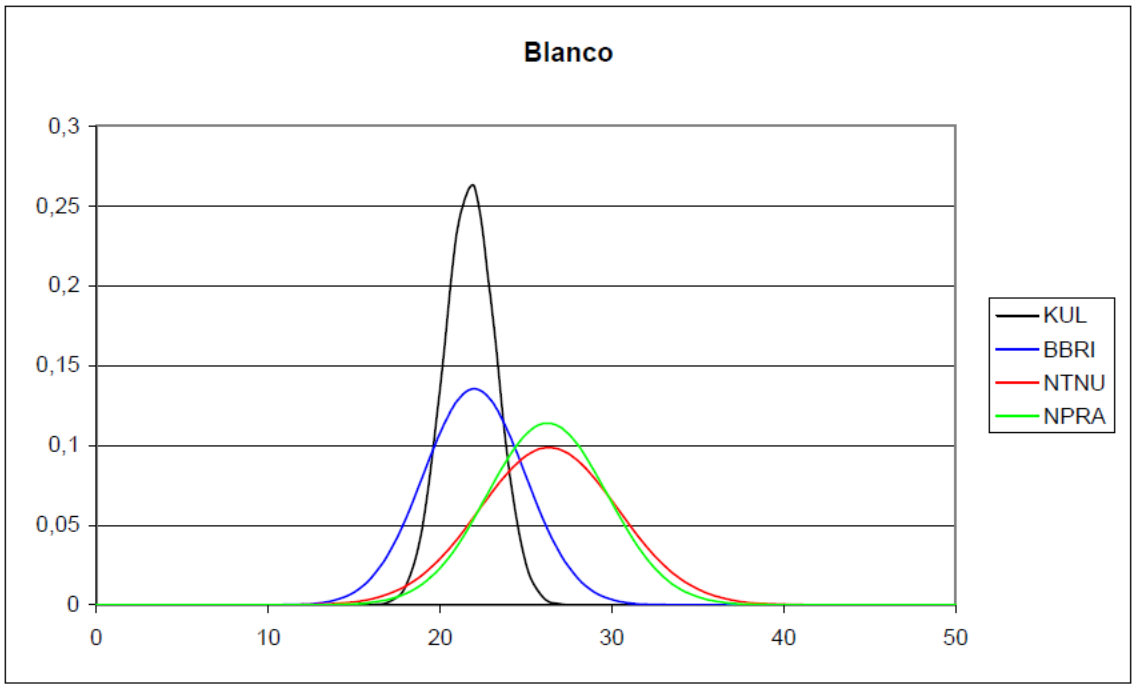

Figure 70 Gaussian distribution for W_{20} Blanco

Table 64 Statistical inter-lab calculation of W_{20} Blanco

	KUL vs BBRI	KUL vs NTNU	KUL vs NPRA	BBRI vs NTNU	BBRI vs NPRA	NTNU vs NPRA
$\|t_0\|$	0.15	1.78	2.36	1.57	1.86	0.03
ν	4.46	2.42	4.07	3.54	5.83	4.03
$t_{\alpha/2,\nu}$	2.78	4.30	2.78	3.18	2.57	2.78
$\mu_1 \neq \mu_2$	NO	NO	NO	NO	NO	NO

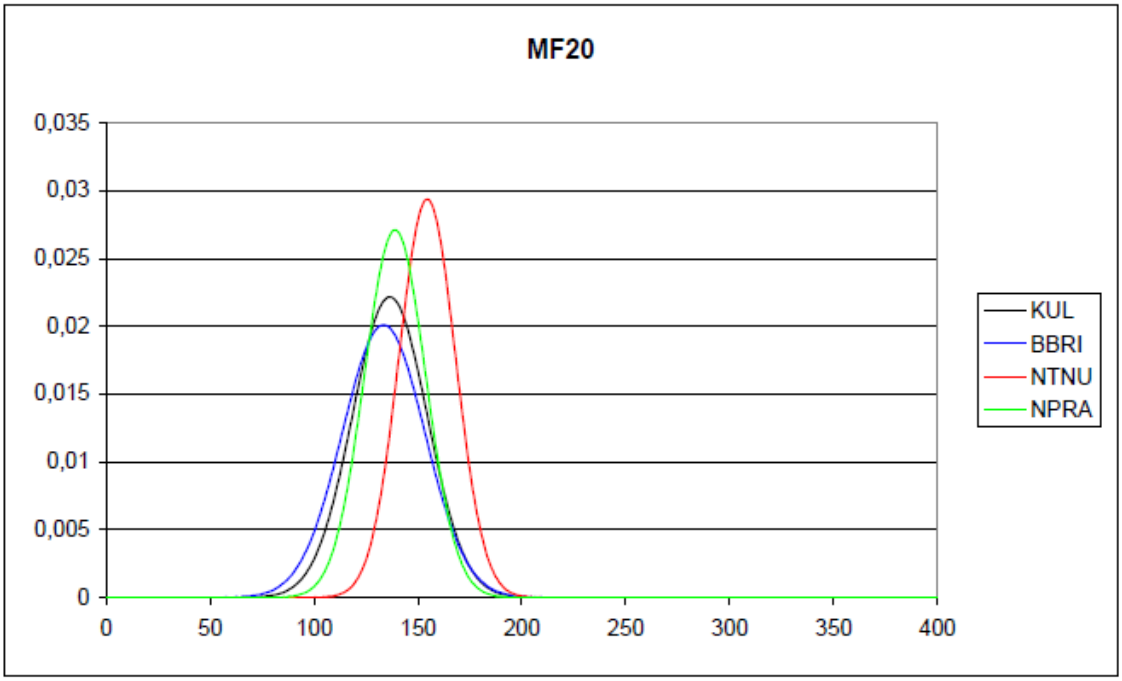

Figure 71 Gaussian distribution for W_{20} MF20

Table 65 Statistical inter-lab calculation of W_{20} MF20

	KUL vs BBRI	KUL vs NTNU	KUL vs NPRA	BBRI vs NTNU	BBRI vs NPRA	NTNU vs NPRA
$\|t_0\|$	0.22	1.60	0.22	1.75	0.45	1.55
v	5.94	5.58	5.77	5.30	5.53	5.96
$t_{\alpha/2,v}$	2.57	2.57	2.57	2.57	2.57	2.57
$\mu_1 \neq \mu_2$	NO	NO	NO	NO	NO	NO

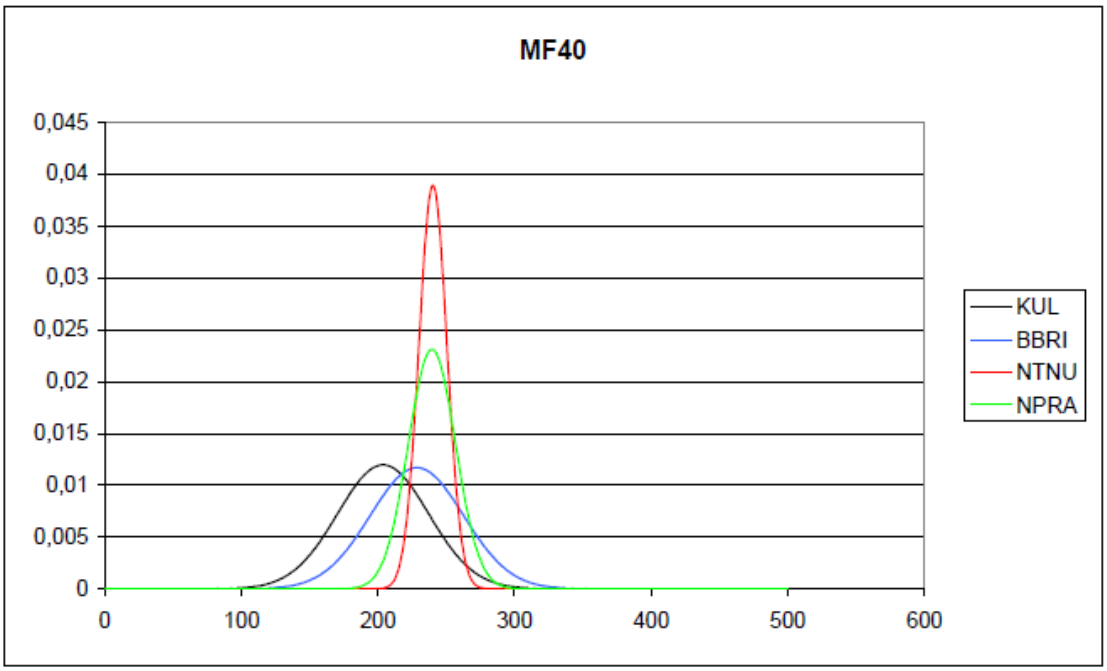

Figure 72 Gaussian distribution for W_{20} MF40

Table 66 Statistical inter-lab calculation of W_{20} MF40

	KUL vs BBRI	KUL vs NTNU	KUL vs NPRA	BBRI vs NTNU	BBRI vs NPRA	NTNU vs NPRA
$\|t_0\|$	1.04	2.09	1.90	0.66	0.58	0.07
v	6.00	3.56	4.50	3.54	4.44	4.88
$t_{\alpha/2,v}$	2.57	3.18	2.78	3.18	2.78	2.78
$\mu_1 \neq \mu_2$	NO	NO	NO	NO	NO	NO

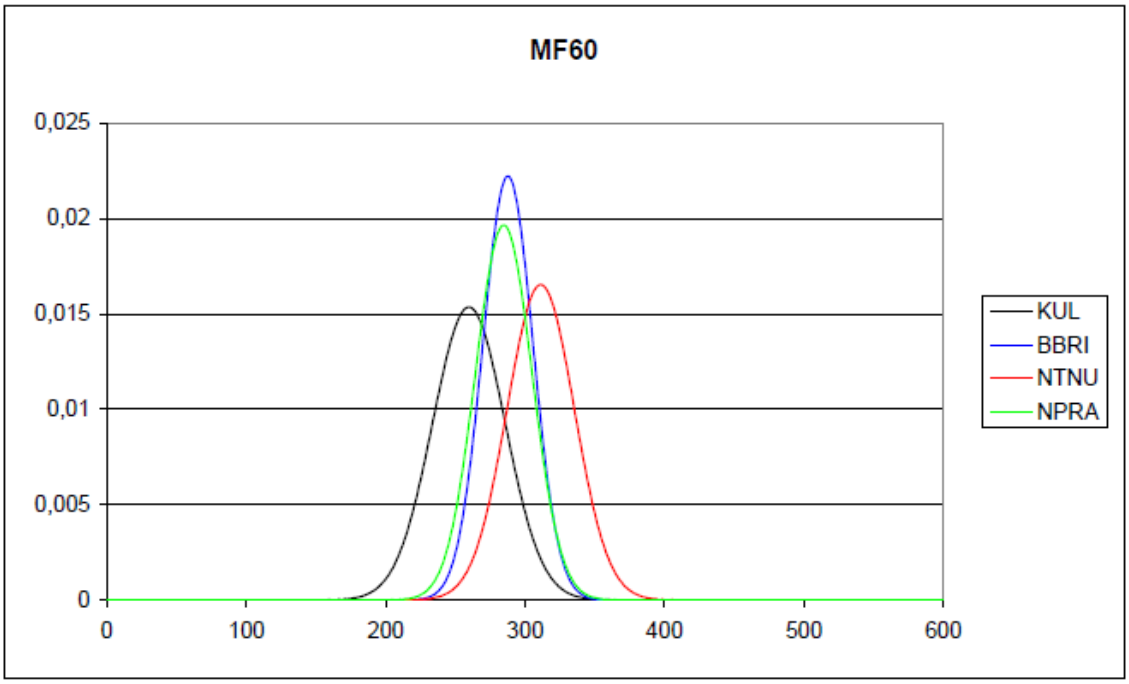

Figure 73 Gaussian distribution for W_{20} MF60

Table 67 Statistical inter-lab calculation of W_{20} MF60

	KUL vs BBRI	KUL vs NTNU	KUL vs NPRA	BBRI vs NTNU	BBRI vs NPRA	NTNU vs NPRA
$\|t_0\|$	1.77	2.91	1.52	1.56	0.22	1.68
v	5.33	5.97	5.67	5.54	5.91	5.83
$t_{\alpha/2,v}$	2.57	2.57	2.57	2.57	2.57	2.57
$\mu_1 \neq \mu_2$	NO	YES	NO	NO	NO	NO

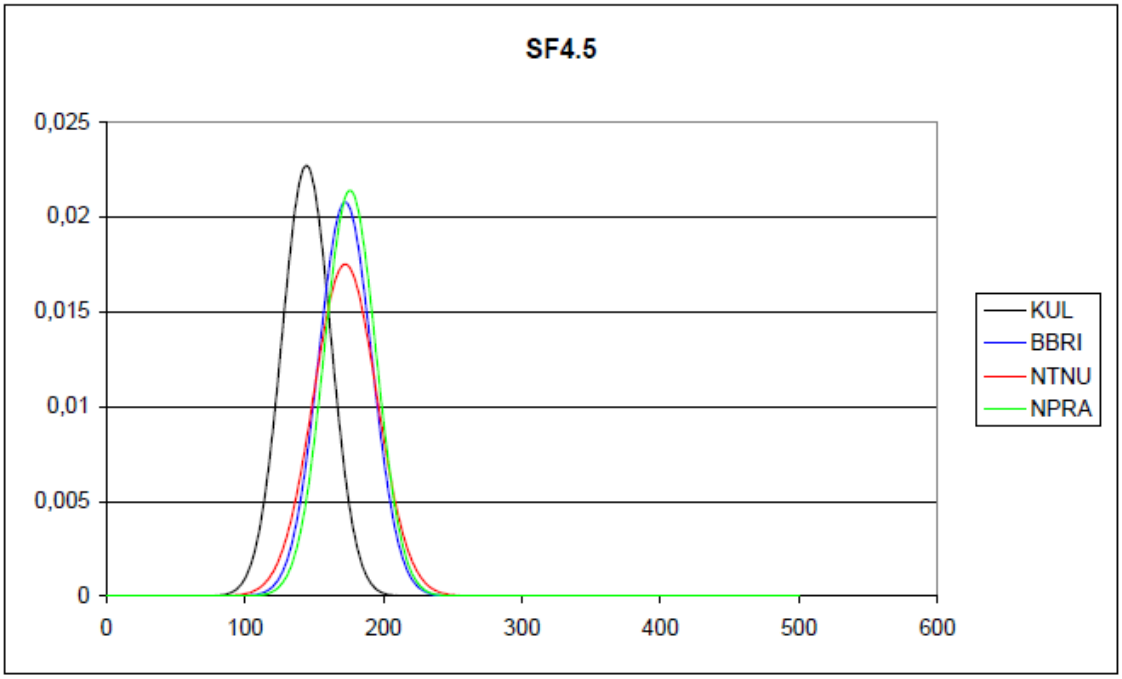

Figure 74 Gaussian distribution for W_{20} SF4.5

Table 68 Statistical inter-lab calculation of W_{20} SF4.5

	KUL vs BBRI	KUL vs NTNU	KUL vs NPRA	BBRI vs NTNU	BBRI vs NPRA	NTNU vs NPRA
$\|t_0\|$	2.15	1.95	2.46	0.00	0.26	0.24
ν	5.95	5.63	5.98	5.83	5.99	5.77
$t_{\alpha/2,\nu}$	2.57	2.57	2.57	2.57	2.57	2.57
$\mu_1 \neq \mu_2$	NO	NO	NO	NO	NO	NO

Comment:

- Student t-test give $\mu_1 \neq \mu_2$ for KUL vs NPRA

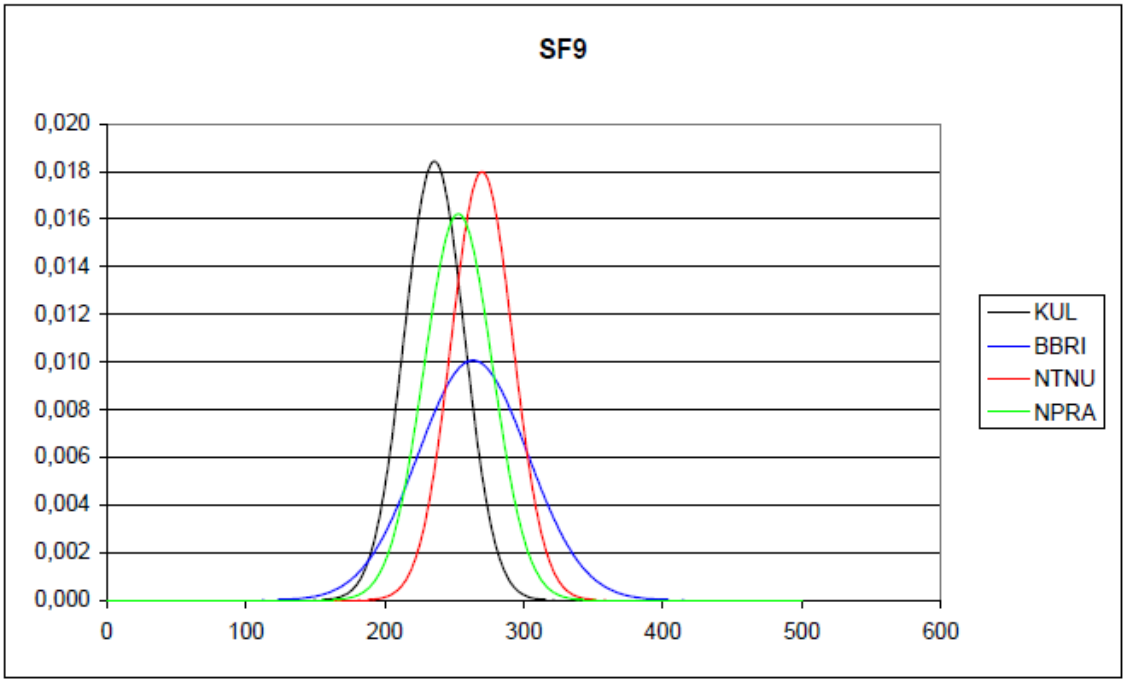

Figure 75 Gaussian distribution for W_{20} SF9

Table 69 Statistical inter-lab calculation of W_{20} SF9

	KUL vs BBRI	KUL vs NTNU	KUL vs NPRA	BBRI vs NTNU	BBRI vs NPRA	NTNU vs NPRA
$\|t_0\|$	1.23	2.21	1.05	0.29	0.45	1.03
v	4.65	6.00	5.91	4.71	5.01	5.94
$t_{\alpha/2,v}$	2.78	2.57	2.57	2.78	2.57	2.57
$\mu_1 \neq \mu_2$	NO	NO	NO	NO	NO	NO

The results from Table 64 to Table 69 are summarized in Table 70 for W_{20}.

Table 70 Statistical inter-lab calculation of W_{20} Summarized

	$\mu_1 \neq \mu_2$					
	KUL vs BBRI	KUL vs NTNU	KUL vs NPRA	BBRI vs NTNU	BBRI vs NPRA	NTNU vs NPRA
Blanco	NO	NO	NO	NO	NO	NO
MF20	NO	NO	NO	NO	NO	NO
MF40	NO	NO	NO	NO	NO	NO
MF60	NO	**YES**	NO	NO	NO	NO
SF4.5	NO	NO	NO	NO	NO	NO
SF9	NO	NO	NO	NO	NO	NO

The reason why the statistical calculation was performed also for W_{20} is that the calculation of W_{40} for the panels tested at BBRI is impossible due to the fact that the panels were not tested up to 40mm deflection.

Based on the statistical calculation it can be concluded that there is a difference in the absorbed energy up to 20mm deflection for MF60 series tested at KUL and NTNU (unlike for W_{40}). If H_1 is to be rejected also for the MF60 panels at KUL and NTNU, a $\alpha/2$-value of 0.01 has to be used.

4.5 Further evaluation of P_{Max}

Figure 76 to Figure 79 shows the Gaussian distribution of maximum load at the different laboratories.

In Table 71 to Table 74, the results from the statistical intra-lab calculation for P_{Max} are shown. *NO* means that H_1 has to be rejected; hence the expected P_{Max} cannot be proven to be unequal.

4.5.1 Panels tested at KUL

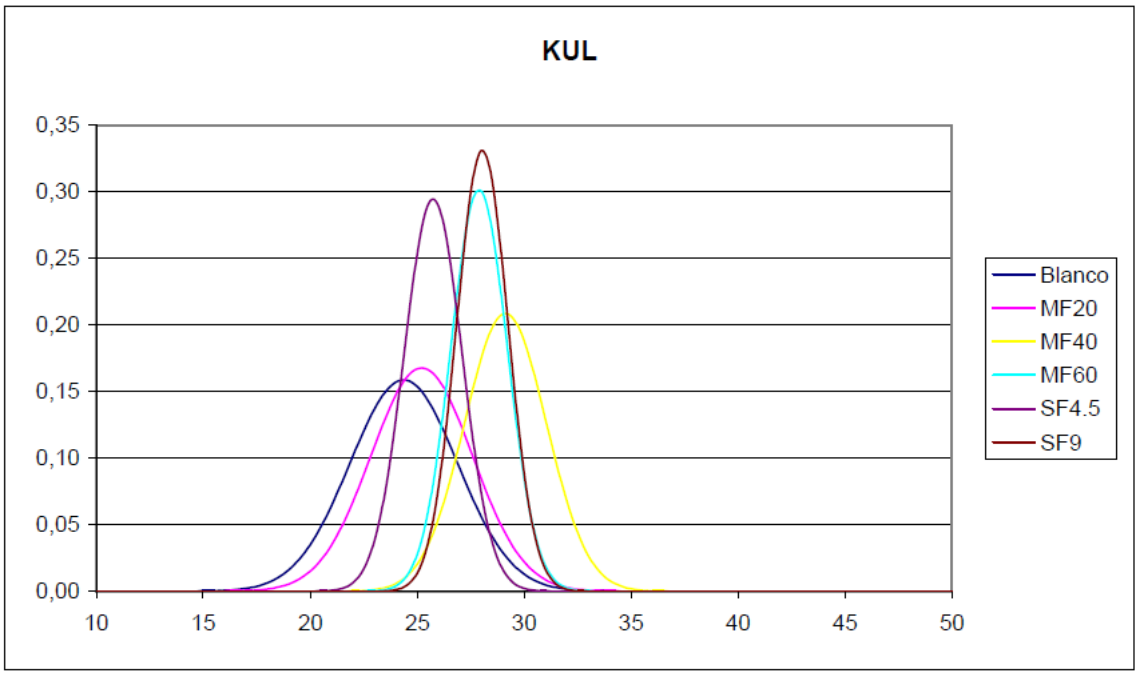

Figure 76 Gaussian distribution for maximum load, KUL

Table 71 Statistical intra-lab calculation of P_{Max} KUL

	$\mu_1 \neq \mu_2$				
	Blanco vs	MF20 vs	MF40 vs	MF60 vs	SF4.5 vs
MF20	NO				
MF40	YES	NO			
MF60	NO	NO	NO		
SF4.5	NO	NO	YES	NO	
SF9	NO	NO	NO	NO	NO

Comment:

- Student t-test give $\mu_1 \neq \mu_2$ also for Blanco vs SF9 and MF20 vs MF40

4.5.2 Panels tested at BBRI

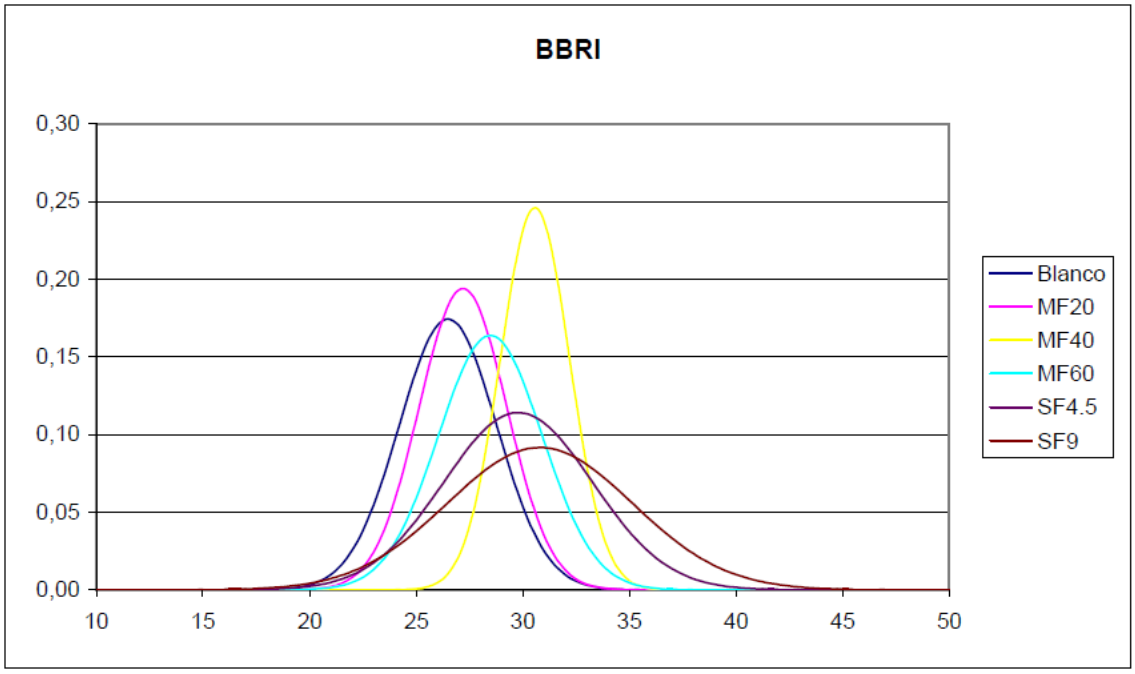

Figure 77 Gaussian distribution for maximum load, BBRI

Table 72 Statistical intra-lab calculation of P_{Max} BBRI

	$\mu_1 \neq \mu_2$				
	Blanco vs	MF20 vs	MF40 vs	MF60 vs	SF4.5 vs
MF20	NO				
MF40	YES	YES			
MF60	NO	NO	NO		
SF4.5	NO	NO	NO	NO	
SF9	NO	NO	NO	NO	NO

4.5.3 Panels tested at NTNU

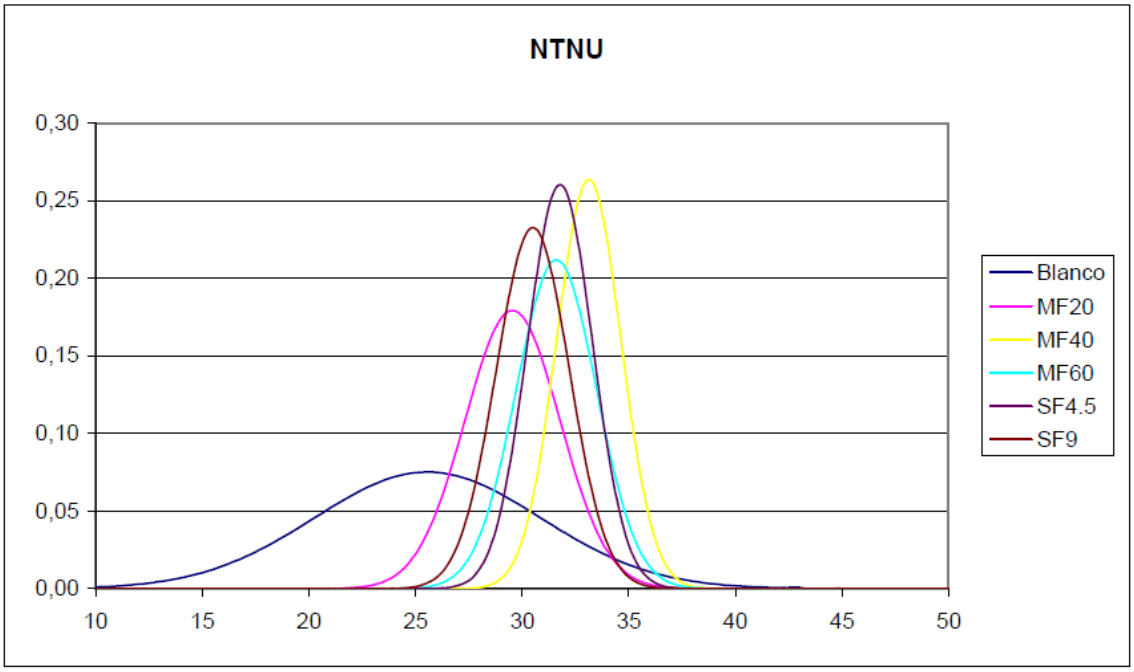

Figure 78 Gaussian distribution for maximum load, NTNU

Table 73 Statistical intra-lab calculation of P_{Max} NTNU

	$\mu_1 \neq \mu_2$				
	Blanco vs	MF20 vs	MF40 vs	MF60 vs	SF4.5 vs
MF20	NO				
MF40	NO	YES			
MF60	NO	NO	NO		
SF4.5	NO	NO	NO	NO	
SF9	NO	NO	NO	NO	NO

Comment:

- Student t-test give $\mu_1 \neq \mu_2$ also for Blanco vs MF40

4.5.4 Panels tested at NPRA

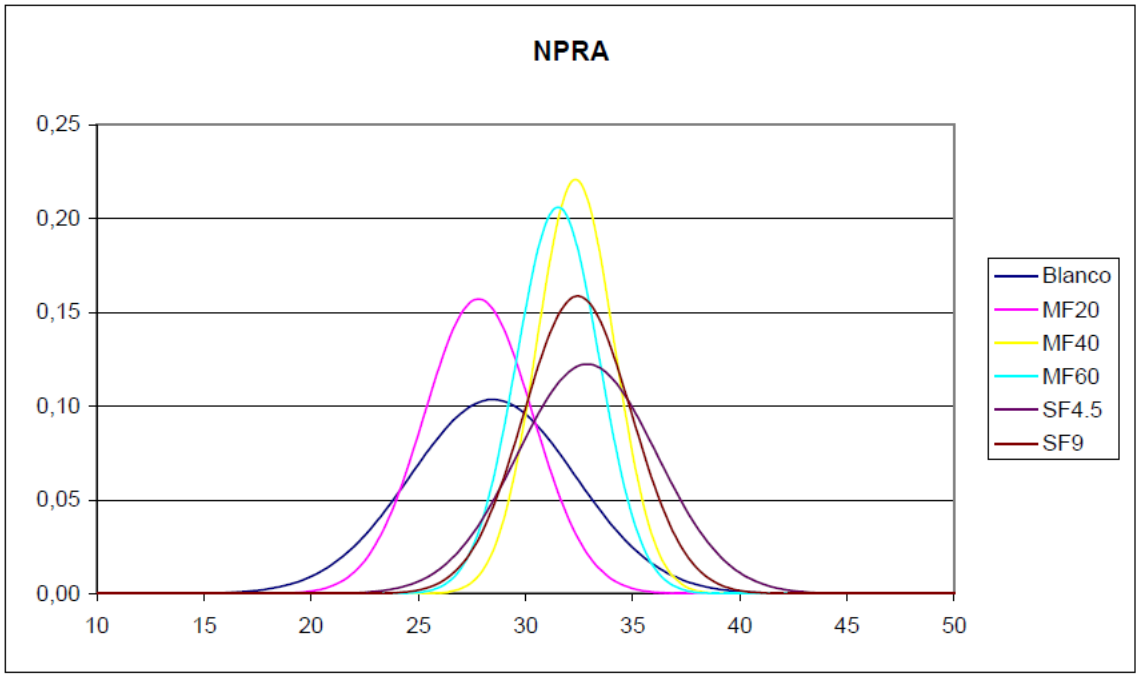

Figure 79 Gaussian distribution for maximum load, NPRA

Table 74 Statistical intra-lab calculation of P_{Max} NPRA

	$\mu_1 \neq \mu_2$				
	Blanco vs	MF20 vs	MF40 vs	MF60 vs	SF4.5 vs
MF20	NO				
MF40	NO	YES			
MF60	NO	NO	NO		
SF4.5	NO	NO	NO	NO	
SF9	NO	YES	NO	NO	NO

Comment:

- Student t-test give $\mu_1 \neq \mu_2$ also for MF20 vs SF4.5

4.5.5 Further evaluation of P_{max} summarized

Based on the results from the statistical intra-lab calculation it can be proven that P_{Max} is dependent on the fibre type and fibre dosage for some series. The following series are proven to have unequal P_{Max}:

- KUL: Blanco vs MF40 and MF40 vs SF4
- BBRI: Blanco vs MF40 and MF20 vs MF40
- NTNU: MF20 vs MF40
- NPRA: MF20 vs MF40 and MF20 vs SF9

4.6 Further evaluation of $\delta_{P,Max}$

Figure 80 to Figure 83 shows the Gaussian distribution of $\delta_{P,Max}$ at the different laboratories.

In Table 75 to Table 78, the results from the statistical intra-lab calculation for $\delta_{P,Max}$ are shown. *NO* means that H_1 has to be rejected; hence the expected $\delta_{P,Max}$ cannot be proven to be unequal.

4.6.1 Panels tested at KUL

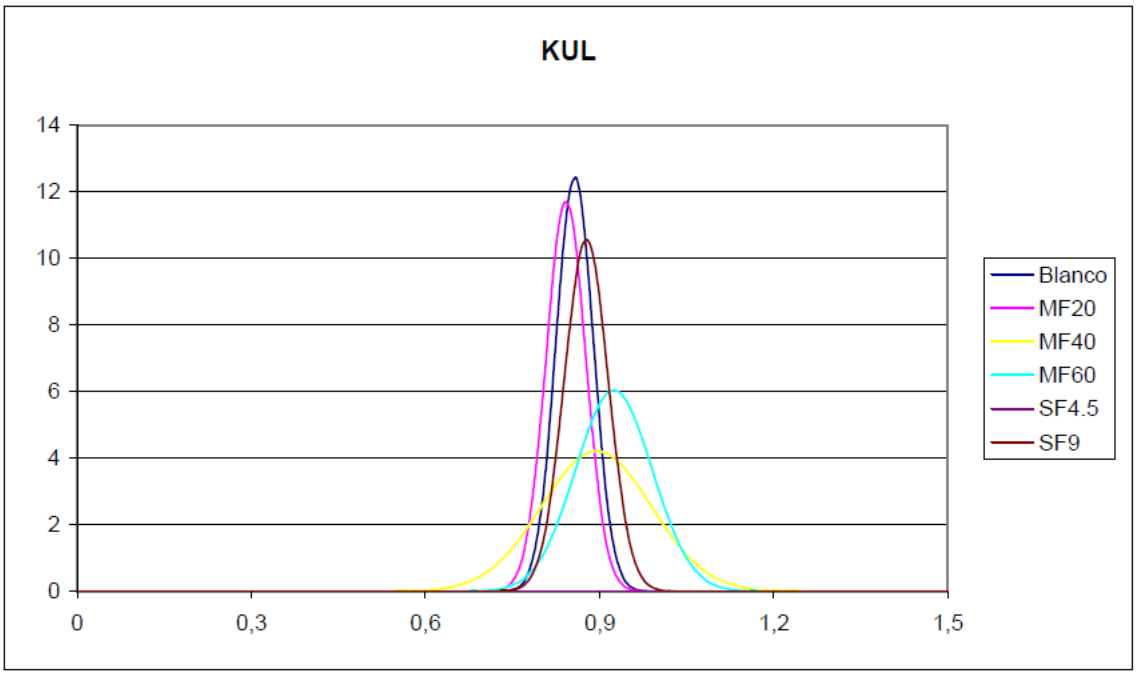

Figure 80 Gaussian distribution for deflection at maximum load, KUL

Table 75 Statistical intra-lab calculation of $\delta_{P,Max}$ KUL

	$\mu_1 \neq \mu_2$				
	Blanco vs	MF20 vs	MF40 vs	MF60 vs	SF4.5 vs
MF20	NO				
MF40	NO	NO			
MF60	NO	NO	NO		
SF4.5	-	-	-	-	
SF9	NO	NO	NO	NO	-

4.6.2 Panels tested at BBRI

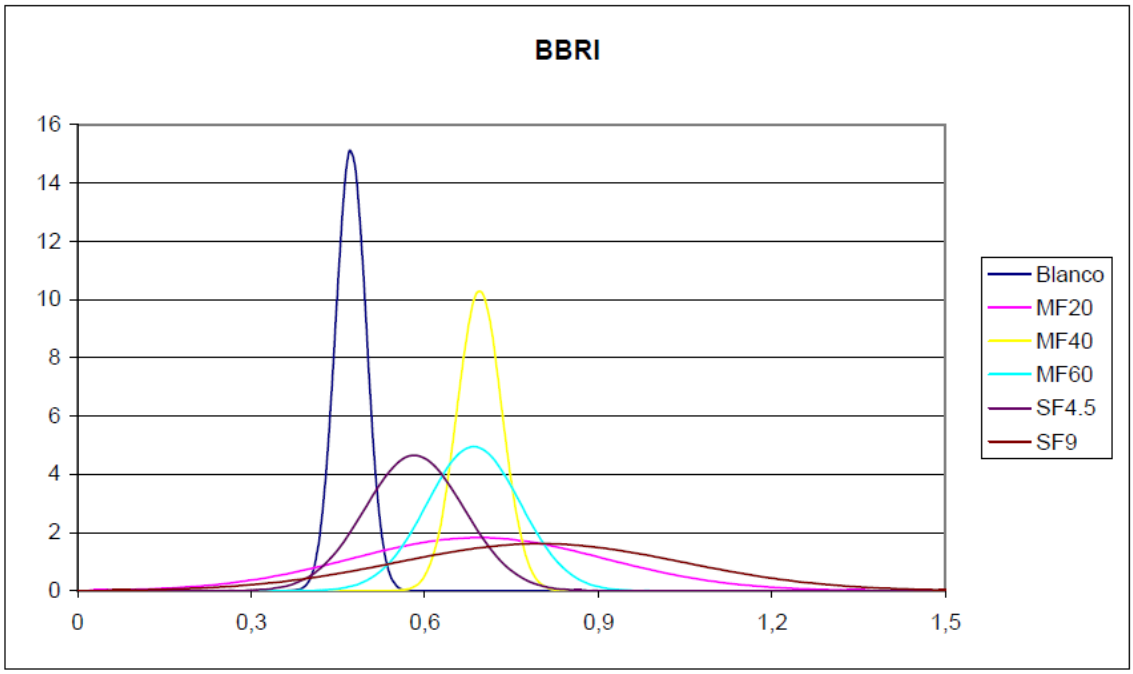

Figure 81 Gaussian distribution for deflection at maximum load, BBRI

Table 76 Statistical intra-lab calculation of $\delta_{P,Max}$ BBRI

	$\mu_1 \neq \mu_2$				
	Blanco vs	MF20 vs	MF40 vs	MF60 vs	SF4.5 vs
MF20	NO				
MF40	YES	NO			
MF60	YES	NO	NO		
SF4.5	NO	NO	NO	NO	
SF9	NO	NO	NO	NO	NO

Comment:

- Student t-test give $\mu_1 \neq \mu_2$ also for Blanco vs SF4.5 and Blanco vs SF9

4.6.3 Panels tested at NTNU

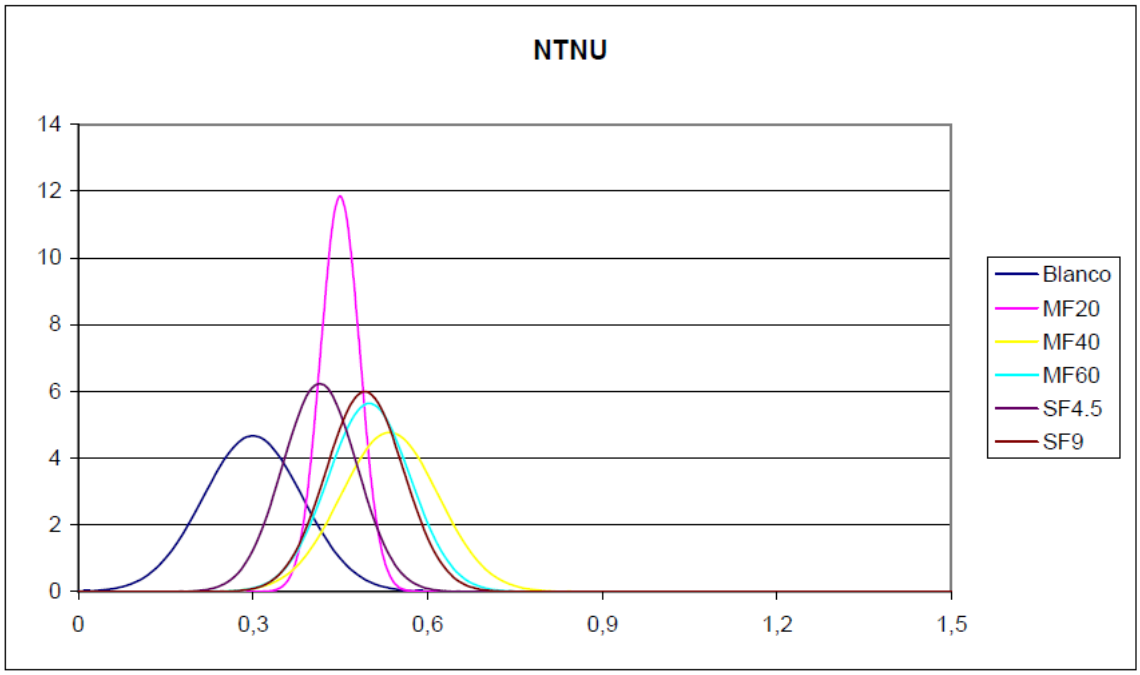

Figure 82 Gaussian distribution for deflection at maximum load, NTNU

Table 77 Statistical intra-lab calculation of $\delta_{P,Max}$ NTNU

	$\mu_1 \neq \mu_2$				
	Blanco vs	MF20 vs	MF40 vs	MF60 vs	SF4.5 vs
MF20	NO				
MF40	YES	NO			
MF60	YES	NO	NO		
SF4.5	NO	NO	NO	NO	
SF9	YES	NO	NO	NO	NO

Comment:

- Student t-test give $\mu_1 \neq \mu_2$ also for Blanco vs MF20

4.6.4 Panels tested at NPRA

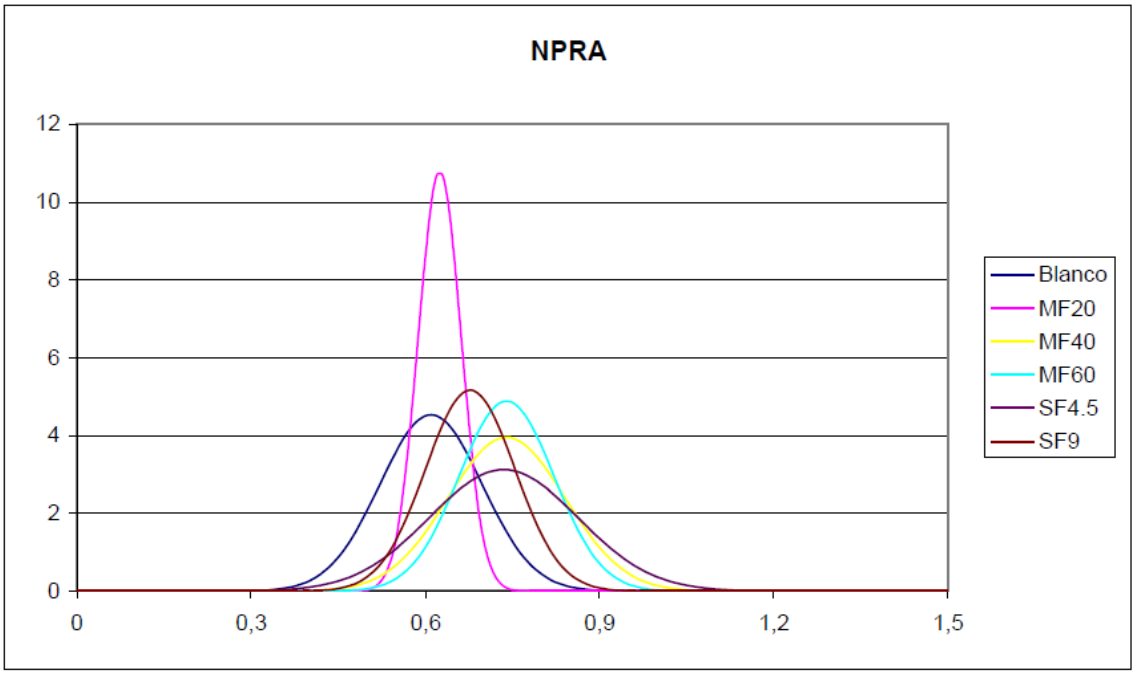

Figure 83 Gaussian distribution for deflection at maximum load, NPRA

Table 78 Statistical intra-lab calculation of $\delta_{P,Max}$ NPRA

	$\mu_1 \neq \mu_2$				
	Blanco vs	MF20 vs	MF40 vs	MF60 vs	SF4.5 vs
MF20	NO				
MF40	NO	NO			
MF60	NO	NO	NO		
SF4.5	NO	NO	NO	NO	
SF9	NO	NO	NO	NO	NO

Comment:

- Student t-test give $\mu_1 \neq \mu_2$ for MF20 vs MF60

4.6.5 Further evaluation of $\delta_{P,Max}$ summarized

The statistical calculation shows that at KUL and NPRA it cannot be concluded that adding fibres affects the deflection at maximum load.

The following series are proven to have unequal $\delta_{P,Max}$:

- BBRI: Blanco vs MF40 and Blanco vs MF60
- NTNU: Blanco vs MF40, Blanco vs MF60 and Blanco vs SF9

4.7 Conclusions from the statistical calculations

With the above mentioned conditions, the following conclusions may be drawn:

- P_{Max}
  There is a difference in the measured P_{Max} for the different laboratories. KUL vs NTNU is proven to have different maximum load in 4 of 6 series, and KUL vs NPRA is proven to have different maximum load in 3 of 6 series. Furthermore, it is proven that at each laboratory, the maximum load is dependent on the fibre type and fibre dosage fore some series.

- $\delta_{P,Max}$
  There is a difference in the measured $\delta_{P,Max}$ for the different laboratories. Only for BBRI vs NPRA it cannot be proven that the deflection at maximum is different for at least two series. Furthermore, it is proven that at BBRI $\delta_{P,Max}$ is unequal for Blanco vs MF40 and MF60. At NTNU it is proven that $\delta_{P,Max}$ is unequal for Blanco vs MF40, MF60 and SF9.

- W_{20}
  There is a difference in the calculated W_{20} between NTNU and KUL. All other series may be considered to be within one test series.

- W_{40}
  It is proven that all 16 panels within each concrete family may be considered to be within one test series. It is not possible to state that one laboratory gives different results than the other laboratories.

5 Conclusion

From the experimental work in the present report the main finding are

- There is a slight reduction in coefficient of variation of W_{40} when the amount of metallic fibre increases. The dispersion is higher for synthetic fibre reinforced concrete panels.
- The contribution to W_{40} for the synthetic fibres is larger than for the metallic fibres at large deflections (deflections above approximately 10mm). Metallic fibres are more effective at less deflection.
- Even though ASTM C 1550 describes that both the LVDT-record and the piston-record excluding the load train deformation may be used for measuring the energy absorption, the results are dependent on which method that is used.
- The relationship between crack openings and panel deflection is not linear, and the crack opening seems to be larger near the centre of the panels relative to the end of the panels. This indicates that the friction between the support and the concrete is sufficient to create tensile strain in the concrete, and that the assumption of rigid body movement is not exactly correct.
- The statistical calculation shows that
    - There may be a difference in both maximum load and deflection at maximum load measured at the different laboratories.
    - There may be a difference in W_{20} for the panels tested at the different laboratories.
    - There is NOT a significant difference in W_{40} for the panels tested at the different laboratories.

  This indicates that the difference in maximum load and corresponding deflection has minor influence on the W40-results.

References

ASTM C 1550-08 (2008): "*Standard Test Method for Flexural Toughness of Fiber Reinforced Concrete (Using Centrally Loaded Round Panel).*

Enclosure 1; Geometry of the panel

The piston-record is made at the upper side of the panel, while the LVDT-record (or laser-record) is made at the underside of the panel. This two values are identical when the deflection is small, but not at larger deflections.

In Figure 84 the deflection measured at the upper side of the panel is named Δ_{v3}, the deflection measured at the underside of the panel is named Δ_{v1}, and the rotation angle is named α. One assumption for the calculated deflections, Δ_{v1} and Δ_{v3}, is that the crack height is equal to the panel height at maximum deflection.

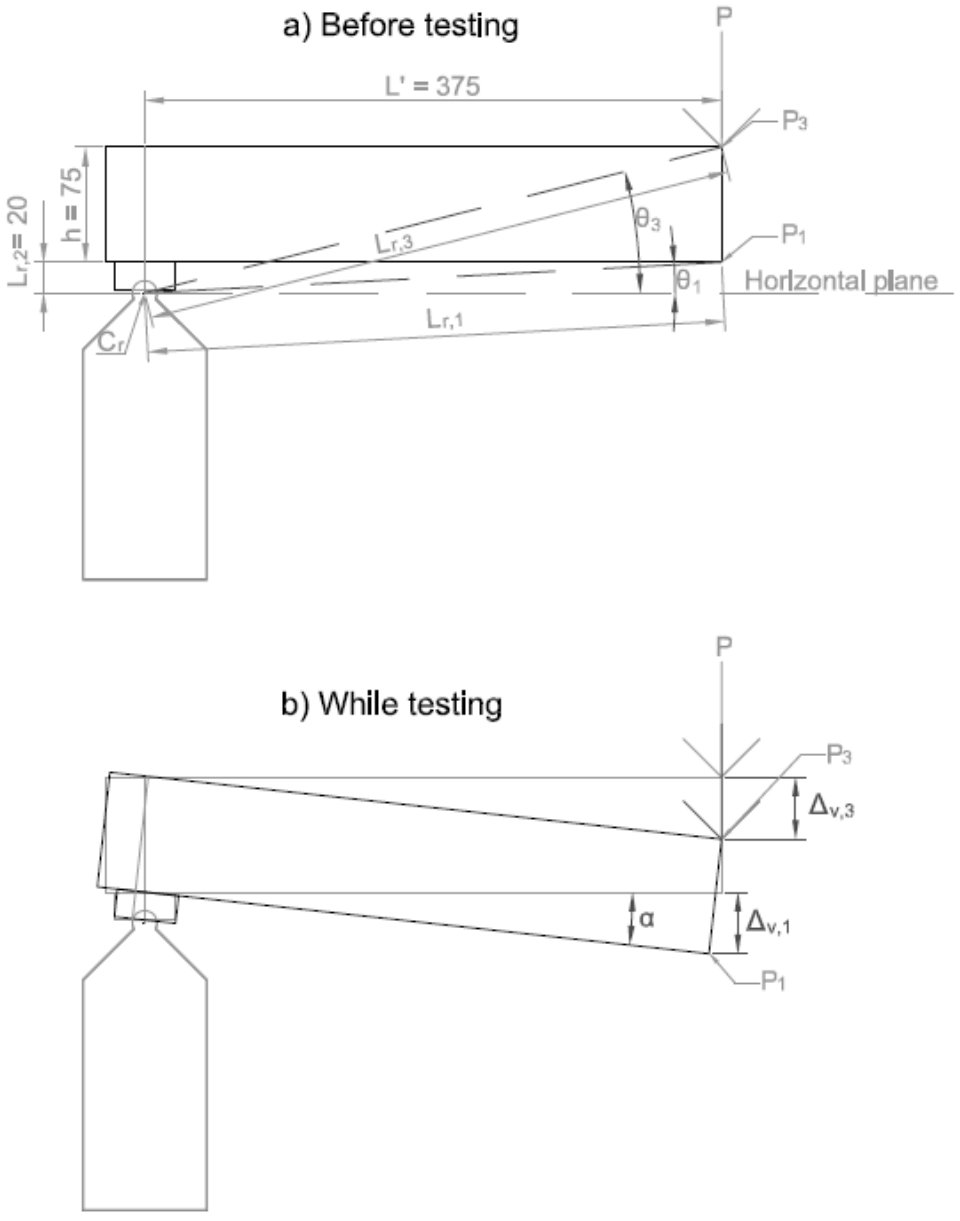

Figure 84 Difference in deflection measurement

Based on the model in Figure 84 it is possible to find the following equations for the deflections:

$$\Delta_{v3} = \frac{L'}{\cos\theta_3}\left[\sin(\theta_3 - \alpha) - \sin\theta_3 + \tan\alpha\left(\cos(\theta_3 - \alpha) - \cos\theta_3\right)\right] \quad (12)$$

$$\Delta_{v1} = L'\left[\frac{\sin(\theta_1 - \alpha) - \sin\theta_1}{\cos\theta_1} + \frac{\tan\alpha}{\cos\theta_3}\left(\cos(\theta_3 - \alpha) - \cos\theta_3\right)\right] \quad (13)$$

where

α is the rotation of the specimen
C_r is the centre of rotation
θ_1 is the angel between the horizontal plane and the line from the centre of rotation to P_1
θ_3 is the angel between the horizontal plane and the line from the centre of rotation to P_3

By require $\Delta_{v1} = 40$ mm and solving equation 13, a rotation angle $\alpha \approx 6.241°$ is found. Adding $\alpha = 6.241°$ in equation 12 gives a deflection $\Delta_{v3} \approx 40.443$ mm.

By require $\Delta_{v3} = 40$ mm and solving equation 12, a rotation angle $\alpha \approx 6.172°$ is found. Adding $\alpha = 6.172°$ in equation 13 gives a deflection $\Delta_{v1} \approx 39.56$ mm.

In Figure 84 the load is assumed to be a point load. This is off course not correct. According to ASTM C 1550 the load point shall consist of a hemispherical piston with specified dimensions. The radius of the hemispherical piston shall be 80 ± 5 mm.

Because of the hemispherical shape of the load point, the contact point between the concrete and the load will change position. The horizontal displacement of the contact point, *z*, may be calculated by the following equation:

$$z = R\tan\alpha \quad (14)$$

where:

R is the radius of the hemispherical end of the Loading Pistion [mm]

The appurtenant vertical displacement of the contact point, $\delta_{\delta y}$, may be calculated by the following equation:

$$\delta_{\delta y} = R\left(\sin\alpha - \frac{1}{\cos^2\alpha} + 1\right) \quad (15)$$

If $\alpha = 6{,}241$ and R = 80 mm, $\delta_{\delta y} = 0{,}477$ mm, which means that when the deflection is measured to be 40,00 mm at the underside of the panel, the Piston-record will be 40,443 - 0,477 = 39,966, even though the tip of the panel has moved 40,443 mm.

Even though these simplifications may not be correct, this calculations shows that it may be of no consequence if the deflection is measured at the upper side or at the underside of the panel, as long as the measurement itself is trustworthy. Uneven surface of the panels is expected, and will off course influence the placement of the contact point between the loading piston and the concrete.

SINTEF Building and Infrastructure is the third largest building research institute in Europe. Our objective is to promote environmentally friendly, cost-effective products and solutions within the built environment. SINTEF Building and Infrastructure is Norway's leading provider of research-based knowledge to the construction sector. Through our activity in research and development, we have established a unique platform for disseminating knowledge throughout a large part of the construction industry.

COIN – Concrete Innovation Center is a Center for Research based Innovation (CRI) initiated by the Research Council of Norway. The vision of COIN is creation of more attractive concrete buildings and constructions. The primary goal is to fulfill this vision by bringing the development a major leap forward by long-term research in close alliances with the industry regarding advanced materials, efficient construction techniques and new design concepts combined with more environmentally friendly material production.